Functions of the MRE11-RAD50-NBS1 complex in DNA double strand break repair

Inaugural-Disseration

zur

Erlangung des Doktorgrades

Dr. *rer. nat.*

der Fakultät für Biologie

an der

Universität Duisburg-Essen

Standort Essen

vorgelegt von

Swetlana Konkow

aus Novosibirsk, Russland

Juni, 2012

Die der vorliegenden Arbeit zugrunde liegenden Experimente wurden am Institut für Medizinische Strahlenbiologie an der Universität Duisburg-Essen, Standort Essen, durchgeführt.

1. Gutachter: Prof. Dr. Georg Iliakis

2. Gutachter: Prof. Dr. Jürgen Thomale

3. Gutachter: /

Vorsitzender des Prüfungsausschusses: Perikan Nahlband

Tag der mündlichen Prüfung: 08. August 2012

“Comparing is the end of happiness and the begin of discontent.”

Søren Aabye Kierkegaard (1813-1855)

Table of contents

Acknowledgements

I would like to thank the Helmholtz Centre for Heavy Ion Research, Darmstadt, Germany (Gesellschaft fuer Schwerionenforschung, GSI) for the stipend that supported my activities in this project. The support throughout the project of Prof. Dr. M. Durante, Drs. G. Taucher-Scholz and B. Jakob is greatly appreciated.

My profound appreciation goes to my mentor, Prof. Dr. George Iliakis. I would like to thank you very much for giving me the opportunity to be a member of your team – the best team ever, with you as the best boss! You were always there when I needed support and advice at every level of my thesis or personal life. Special thanks also to you for the critical reading of my thesis and the useful suggestions in content and form.

I am very grateful to Drs. C. Staudt and E. Mladenov. Surely, it was not always easy with me and my many questions. Yet, I greatly appreciate your patience and understanding along the way. Thank you for teaching me the very many things that made this work possible – it would certainly not be the same without you.

I am also grateful to my friends and colleagues in the lab. Thank you all for your support and thanks to you girls for the nice time we always had at work and at our cooking evenings.

Special thanks go to Profs. M. Stuschke and A. Bockisch for making possible irradiations with neutrons. I would like to thank G. Huedepohl for his help with all neutron irradiations.

And last but not least, I would like to thank my family and friends, who supported me during my thesis. You're the best… Alia, Jochen, Max, Miguel, Nadja, Patrick, Peter, Rudolf, Sara, Thomas, Tim…

List of abbreviations

<	“Less-than” sign
~	“Approximately” sign
°C	Degree Celsius
%	Percent
2-P	Two-photon laser
2-ME	2-Mercaptoethanol
53BP1	P53 Binding Protein 1
aa	Amino acid
AK	Adenylate kinase
ATLD	Ataxia-telangiectasia-like-disorder
ATM	Ataxia-telangiectasia-mutated
ATP	Adenosine triphosphate
ATR	Ataxia-telangiectasia and RAD3 related kinase
ATRIP	ATR-interacting protein
AUX	Auxiliary
BLM	Bloom syndrome protein
B-NHEJ	Backup non-homologous end-joining
bp	Base pair
BRCA1	Breast cancer susceptibility protein 1
BRCA2	Breast cancer susceptibility protein 2
BRCT	BRCA1 C-terminal domain
BSA	Bovine serum albumin
CDK1	Cyclin-dependent protein kinase 1
CHK1	Checkpoint kinase 1

CHK2	Checkpoint kinase 2
CHO	Chinese hamster ovary
CLSM	Confocal laser scanning microscopy
cm	Centimeter
cm^2	Square centimeter
CO_2	Carbon dioxide
cDNA	Complementary DNA
CTIP	C-terminal binding protein interacting protein
CSR	Class switch recombination
d	Day
Da	Dalton
DAPI	4',6-diamidino-2-phenylindole
ddH_2O	Double distilled water
DDR	DNA damage response
DEQ	Dose equivalent
DI	DNA index
DMEM	Dulbecco's modified eagle medium
DMSO	Dimethyl sulfoxide
DNA	Deoxyribonucleic acid
DNA-PKcs	DNA-dependent protein kinase, catalytic subunit
D-NHEJ	DNA-PK-dependent non-homologous end-joining
ds	Double-stranded
DSB	DNA double strand break
DTT	Dithiothreitol
EDTA	Ethylenediaminetetraacetic acid

EGTA	Ethyleneglycoltetraacetic acid
e.g.	Latin abbreviation for “exempli gratia”
et al.	Latin abbreviation for “et alii”
etc.	Latin abbreviation for “et cetera”
eV	Electronvolt
EXO1	Exonuclease 1
FACS	Fluorescence activated cell sorting
FBS	Fetal bovine serum
FDR	Fraction of DNA released
Fe	Iron
FHA	Forkhead-associated domain
fs	Femtosecond
g	Gravity
Gd	*Gallus gallus domesticus*
GeV	Gigaelectronvolt
GFP	Green fluorescent protein
GSI	Gesellschaft fuer Schwerionenforschung
Gy	Gray
h	Hour
HEPES	4-(2-hydroxyethyl)-1-piperazineethanesulfonic acid
HRR	Homologous recombination repair
HST	Histogram files
i.e.	Latin abbreviation for “id est”
Inc.	Incorporated
IR	Ionizing radiation

IRIF	Ionizing radiation-induced foci
J	Joule
k	Kilo
kDa	Kilodalton
keV	Kiloelectronvolt
kg	Kilogram
Ltd.	Limited
l	Liter
LET	Linear energy transfer
LMDS	Locally multiply damaged sites
M	Molar (mol/l)
mA	Milliampere
MDC1	Mediator of DNA damage checkpoint protein 1
MEM	Minimum essential medium
MeV	Megaelectronvolt
MHz	Megahertz
min	Minute
MIP	Maximum intensity projection
ml	Milliliter
mm	Millimeter
mM	Millimolar
mMAb	Mouse monoclonal antibody
Mn	Manganese
MP	Multiphoton
MR	MRE11-RAD50

MRN	MRE11-RAD50-NBS1 complex
Mrx	Mre11-Rad50-Xrs2 complex
ms	Millisecond
mW	Milliwatt
µm	Micrometer
ng	Nanogram
Ni	Nickel
NIR	Near-infrared
nm	Nanometer
NBS	Nijmegen breakage syndrome
NBS1	Nibrin
NLS	N-lauryl sarcosine
NHEJ	Non-homologous end-joining
NTP	Nucleotide triphosphate
OH•	Hydroxyl radical
p53	Tumor protein 53
PARP1	Poly [ADP-ribose] polymerase 1
PARP2	Poly [ADP-ribose] polymerase 2
PBG	PBS, BSA, gelatin
PBS	Phosphate-buffered saline
PCR	Polymerase chain reaction
PFA	Paraformaldehyde
PFGE	Pulsed field gel electrophoresis
PI	Propidium iodide
PIKK	Phosphoinositide-3-kinase-related protein kinase

PI-3K	Phosphatidylinositol 3-kinase
PMSF	Phenylmethanesulfonylfluoride
PMT	Photomultiplier tube
PNKP	Polynucleotide kinase 3’-phosphatase
Prof.	Professor
RAG1	Recombination activating gene 1
RAG2	Recombination activating gene 2
RBE	Relative biological effectiveness
RNA	Ribonucleic acid
ROI	Region of interest
RPA	Replication protein factor A
rPAb	Rabbit polyclonal antibody
rpm	Rounds per minute
RT	Room temperature
RT-PCR	Reverse transcription-polymerase chain reaction
s	Second
SDS	Sodium dodecyl sulfate
SDSA	Synthesis-dependent strand annealing
SDS-PAGE	Sodium dodecyl sulfate polyacrylamide gel electrophoresis
Ser	Serine
SMC	Structural maintenance of chromosomes
ss	Single-stranded
SSB	Single strand break (DNA)
SV40	Simian virus 40
TDP1	Tyrosyl-DNA phosphodiesterase 1

TDT	Deoxynucleotidyl transferase
tet	Tetracycline
Thr	Threonine
Ti	Titanium
Tris	Tris(hydroxymethyl)amino methane
Tyr	Tyrosine
UK	United Kingdom
USA	United States of America
UV	Ultraviolet light
V	Volt
W	Watt
wt	Wild-type
w/v	Weight per volume
XRCC1/2/3	X-ray repair cross-complementing group 1/2/3
YFP	Yellow fluorescent protein
Zn	Zinc

1 Introduction

1.1 Preamble

In a living organism maintenance of genomic stability and integrity is of extreme importance. Thus, any chemical change in the cellular deoxyribonucleic acid (DNA) molecule is considered as damage. Among various forms of DNA damage the DNA double stand break (DSB) is the most deleterious DNA lesion, since if misrepaired or left unrepaired it can cause loss or rearrangement of genetic material. This can lead to permanent cell cycle arrest, apoptosis, mutations, genomic instability and with that to a variety of diseases ranging from genetic disorders, chronic diseases, cancer and accelerated ageing (Ward 1988; Olive 1998; Khanna and Jackson 2001; van Gent, Hoeijmakers *et al.* 2001; d'Adda di Fagagna, Reaper *et al.* 2003).

Modifications of DNA can have different sources. They may arise naturally in a programmed fashion during cellular processes like replication (Arnaudeau, Lundin *et al.* 2001), meiotic recombination (Richardson, Horikoshi *et al.* 2004), V(D)J and class switch recombination (CSR) (Weaver 1995; Cui and Meek 2007) and DNA repair (Helleday, Lo *et al.* 2007). However, DNA changes might also derive from DNA damage induced by reactive by-products of the normal cellular metabolism, oxidative and mechanical stress (Kanaar, Hoeijmakers *et al.* 1998) or by exogenous agents like ionizing radiation (IR) (Rydberg 2001) or chemical compounds, e.g. bleomycin (Olive and Banath 1993).

To deal with these assaults, cells have evolved sophisticated mechanisms to efficiently detect, signal and repair DNA damage and thus to maintain genomic integrity (Shiloh and Lehmann 2004). Eukaryotic cells have at least two pathways to repair DSBs: (1) non-homologous end-joining (NHEJ) and (2) homologous recombination repair (HRR) (Kanaar, Hoeijmakers *et al.* 1998; Pardo, Gómez-González *et al.* 2009). In addition, an extensive signaling network, comprising several different proteins, recognizes DSBs and coordinates repair pathways with cellular checkpoint responses, commonly summarized under the term – DNA damage response (DDR).

To provide an introduction into the theoretical background of this thesis, in the following chapters we outline the basics of radiation physics and give an overview of the eukaryotic DDR system emphasizing DSB repair and the role of the MRE11-RAD50-NBS1 (MRN) complex.

1.2 Ionizing radiation and induction of DNA damage

1.2.1 Physics of ionizing radiation

In physics, radiation describes any process in which energy emitted by one body travels through a medium or through space, ultimately to be absorbed by another body, leading to excitation or ionization. There are several forms of electromagnetic radiation that are classified by the frequency of their waves. The photon is the basic "unit" of all forms of electromagnetic radiation. Electromagnetic spectrum consists of radio waves, microwaves, infrared radiation, visible light, ultraviolet (UV) radiation, x-rays and γ-rays; they all vary in their frequency and wavelength, and hence in the energy of constituting photons. Photons of high wavelength and low frequency have low energy contrary to those of low wavelength and high frequency. Some types of radiation have enough energy to ionize atoms or molecules – about 33eV are thought to be required to disrupt a chemical bond under the conditions encountered in biological systems (Hall and Giaccia 2006). Generally, this involves an electron being "kicked out" of an atom's electron shell, which will give the atom positively charged. Radiation with sufficient energy to generate this effect is then said to be ionizing radiation.

It is customary to classify ionizing radiations as either electromagnetic or particulate. X-rays or γ-rays are a form of electromagnetic radiation that do not differ in their nature or basic properties, however particulate radiations include electrons, protons, α-particles, neutrons and heavy charged particles. Moreover, radiation can be classified as directly or indirectly ionizing. Directly ionizing radiation constitutes charged particles that have sufficient kinetic energy to disrupt atomic structure of the absorber, directly producing chemical and biological changes within the absorber.

In contrast, electromagnetic radiation is considered indirectly ionizing, as it deposits the majority of its energy through the production of secondary electrons.

Radiation is measured in units of Gray (Gy) describing the amount of energy absorbed by a certain mass. The unit of 1Gy is 1J/kg (Hall and Giaccia 2006). Absorbed energy, deposited by IR, is not distributed at random but tends to localize along the tracks of directly ionizing particles in a pattern that depends on their type, energy and speed (Mothersill and Seymour 2006). One can distinguish between densely and sparsely ionizing radiation depending on the ionization patterns it generates. This property is described by the parameter linear energy transfer (LET) that is defined as the energy that an ionizing particle deposits per unit length of track (keV/µm) as it traverses matter. LET also reflects the pattern of ionizations a type of radiation generates. Sparsely ionizing radiation is of low LET, whereas highly ionizing radiation is of high LET.

It is important to note that the biological effects of a type of radiation depend strongly on its LET, frequently increasing with increasing LET. X-rays and γ-rays are mostly low LET radiations, whereas charged particles are generally high LET radiations, e.g. α-irradiation is a high LET radiation with low penetration depth (Hall and Giaccia 2006). For charged particles, the density of ionizations decreases as the particle energy increases. Fig. 1 presents track-structure segments of different ions in water.

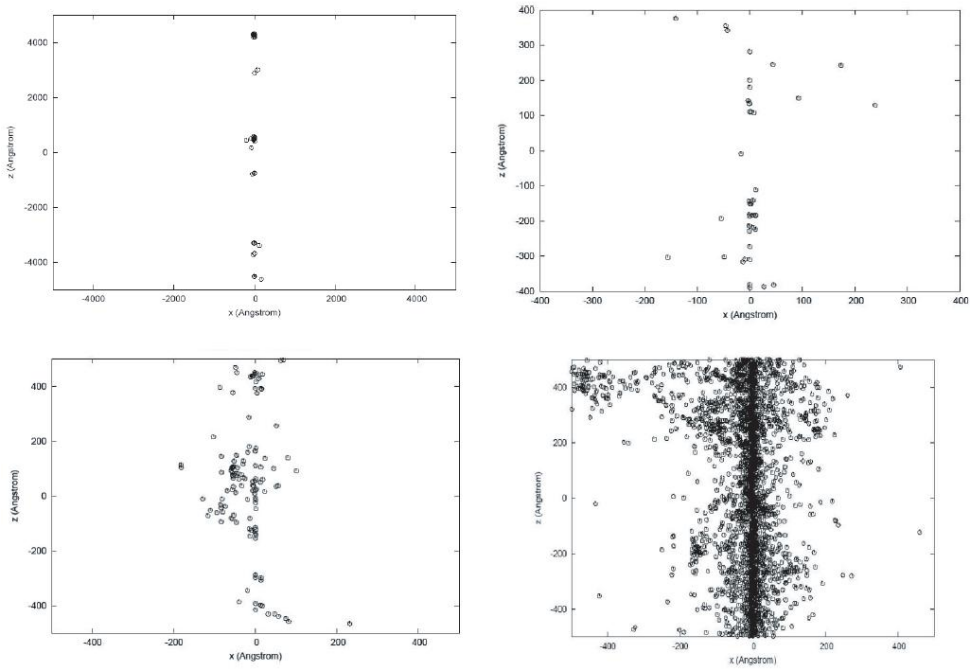

Figure 1: 2D projection of track-structure segments in liquid water for different ions with same velocity (115MeV/nucleon), as calculated with the PARTRAC code (from top to bottom and from left to right: H, He, C and Fe; note the different scale for the proton track) (Ballarini, Alloni *et al.* 2008).

Notably, each particle has a distinct track structure (i.e. distribution of ionization along its path) with randomly varying distances between the ionizations that decreases as the particles lose energy along their paths. Densely ionizing charged particles and electrons near the ends of their tracks display large increases in the density of ionizations, and as a result multiple ionizations occur in a rather small volume (Nikjoo and Goodhead 1991; Nikjoo, Charlton *et al.* 1994).

In general, at the same absorbed dose, the biological effects of high LET radiations are stronger compared to those of low LET radiations (Kadhim, Hill *et al.* 2006). It is generally assumed that this is because high LET radiation deposits most of its energy in ways producing highly accumulated damage in the DNA, other cellular structures and molecules (Goodhead and Nikjoo 1989).

1.2.2 DNA damage induction by IR

Living organisms absorb the energy of ionizing radiation, and damage in the constituting molecules is generated in return. In our studies, the principal target of radiation is considered to be the DNA, where the action of radiation can be direct or indirect. Direct radiation action is the dominant process for high LET radiations and implies that the atoms of the target itself, e.g. the DNA, are ionized. On the other hand, in the indirect action of radiation, relevant after exposure to sparsely ionizing radiation, ionization occurs in the water producing hydroxyl radicals (OH•), which can then diffuse away from the site of their production and damage the DNA (Goodhead 1994; Goodhead 1995).

Fig. 2 demonstrates a schematic illustration of direct and indirect action of IR.

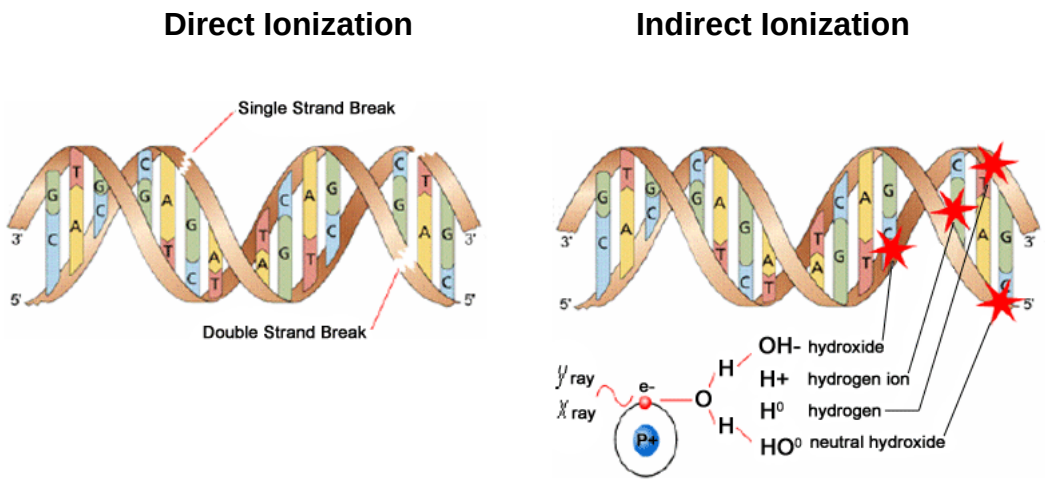

Figure 2: IR can directly or indirectly act on target molecules like the DNA. Illustration from: Canadian Nuclear Association website.

The effects of radiation are stochastic and can generate a variety of different DNA damage types, such as DNA base damages (e.g. oxybases, oxypurines and oxypyrimidines (Sutherland, Bennett *et al.* 2000) as well as regular and oxidized apurinic and apyrimidinic sites (Paap, Wilson III *et al.* 2008)), DNA backbone breaks (Sancar, Lindsey-Boltz *et al.* 2004), alkali labile lesions (Lafleur, Woldhuis *et al.* 1979) and heat labile sites (Singh, Wu *et al.* 2009).

Backbone damage includes abasic sites, single strand (ss) and double strand (ds) DNA breaks. Each Gy of low LET radiation, e.g. x-rays, is estimated to induce around 20-40 prompt DSBs, ~1000 single strand breaks (SSBs) and equal number of base damages (Ward 1990). SSBs have low biological consequences, since they can be repaired very fast with the complementary strand as template DNA. However, if breaks occur opposite one another or are separated by just a few base pairs (bp) on the opposite DNA strands, a DSB is generated that is a deleterious DNA lesion, since if left unrepaired or misrepaired it leads to severe genomic instability, cell death, carcinogenesis or mutations (Jackson 2002).

In conclusion, DNA damage produced by direct or indirect radiation action leads to DNA change of the character of the molecule, and thus impairs its function as career of genetic information. As a result, cell death, mutation and/or transformation can ensue.

1.2.2.1 Complex lesions induced by IR

It was shown that after irradiation, a high percentage (~50-80%) of DSBs is associated with further damage like base damage or additional strand breaks within the same short DNA fragment, whereas simple DSBs make up only 20% of the induced damage (Sutherland, Bennett *et al.* 2002). The so-called complex or clustered DNA damage is by definition localized in closely-spaced DNA regions and usually within 1-2 helical turns of a DNA molecule on opposite strands (Holley and Chatterjee 1996; Hada and Georgakilas 2008) as illustrated in Fig. 3. Clustered DNA lesions are considered to be highly mutagenic as they are resistant to processing by glycosylases and/or endonucleases, and are thus more difficult to repair than “simple” lesions. They are thought to persist for a long time period after irradiation (Goodhead 1994).

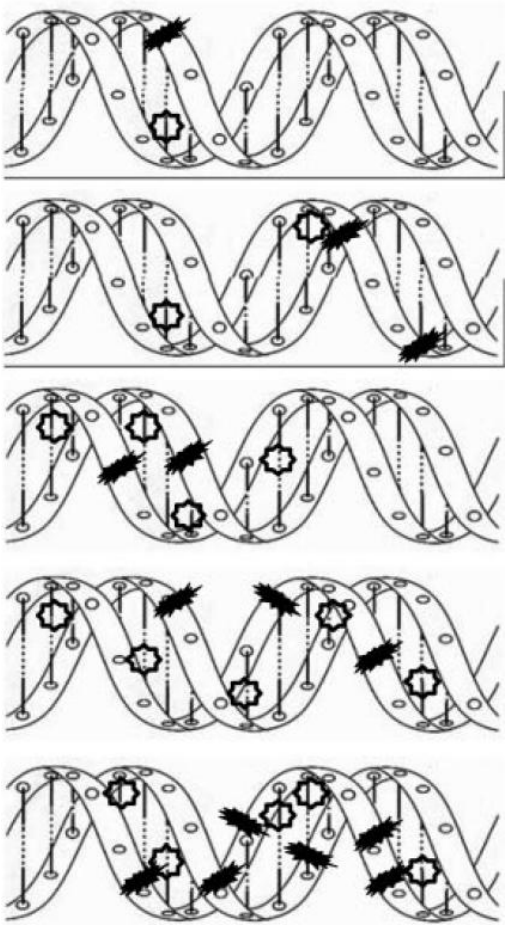

Figure 3: Clustered DNA damage is present when closely-spaced DNA lesions are generated within one or two helical turns. The schematic diagram illustrates typical examples of strand breakage (solid symbols) and also includes examples of associated base damage (open symbols) (Goodhead 2006).

Clustered DNA damage has also been termed as locally multiply damaged site (LMDS) (Hall and Giaccia 2006), and are generated more efficiently after exposure to high LET irradiation. However, LMDS are also generated after exposure to low LET radiation. Indeed, different theoretical and experimental data suggests that the induction of clustered DNA lesions, LMDSs, is the result of electrons depositing high amounts of energy in the form of multiple ionization in a small volume at the end of their tracks (Hada and Georgakilas 2008). Although clustering of DNA damage is influenced by the LET of radiation, it is also dependent on chromatin structure in the sense that after low LET irradiation clustered damage is present in small regions of the DNA and the nucleosomes, whereas after exposure to high LET irradiation, clustered damage can spread over large regions of chromatin (Rydberg 1996).

1.3 Cell cycle checkpoints, DNA damage sensing and signaling

Eukaryotic cells have evolved a complex cell cycle control system that governs proper progression through the cell cycle at regulatory transitions – the cell cycle checkpoints. Stress conditions, inside or outside the cell, activate these checkpoints, resulting in cell cycle arrest (Khanna and Jackson 2001). Cell cycle checkpoints are highly conserved in all eukaryotes (Hartwell and Weinert 1989), and include responses that enforce the right sequence in cell progression through the cell cycle, respond to and facilitate repair of DNA damage, ensure high fidelity of DNA replication and assist in proper chromosome segregation at mitosis (Niida and Nakanishi 2006). Checkpoint deficiency results in genomic instability and is associated with carcinogenesis (Hartwell and Weinert 1989).

There are three cell cycle checkpoints that control progression throughout the cell cycle; (1) at late G1, the start checkpoint or the restriction point, where the cell commits to the cell cycle and chromosome duplication, (2) at G2/M-border, where the control system checks the completion of DNA replication, and (3) at metaphase to anaphase transition, where the control system checks attachment of chromosome to the mitotic spindle, as presented in Fig. 4 (Sherr and Roberts 1995).

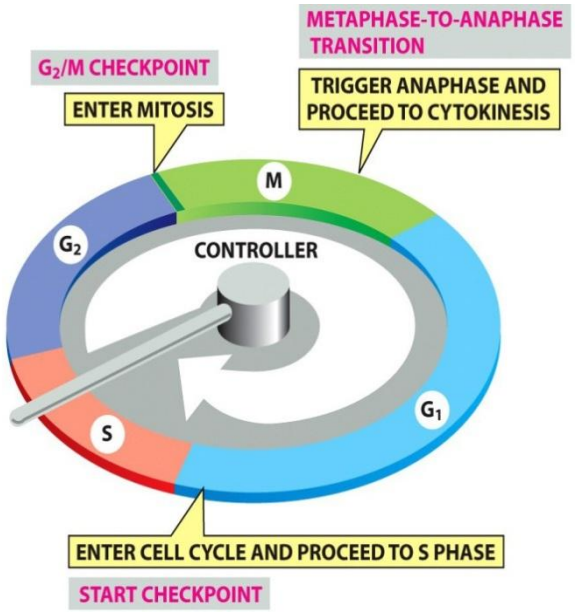

Figure 4: Cell cycle phases and checkpoint control system. The division cycle of mammalian cells consists of four distinct phases: M, G1, S and G2. Three cell cycle checkpoints are depicted in this figure; late G1, G2/M-border and M (Alberts, Johnson *et al.* 2008).

Regulation of cell cycle control system is based on a connected series of biochemical switches, each of which initiates a specific cell cycle event. Central components are the cyclin-dependent kinases (CDKs). The activity of these kinases rises and falls as the cell progresses through the cell cycle, leading to cyclical changes in the phosphorylation of specific intracellular proteins that activate and trigger major cell cycle events. This is controlled by a complex array of enzymes – the so-called cyclins, the most important CDK regulators. Cyclins undergo a cycle of synthesis and degradation in each cell cycle, while the levels of CDKs are constant throughout the cell cycle. Cyclins bind to CDKs and control their ability to phosphorylate downstream proteins, i.e. CDKs are dependent on cyclins for their activity, since unless they are complexed with a cyclin, they have no kinase activity. There are four classes of cyclins, each defined by the stage of the cell cycle at which they bind CDKs and function: G1-cyclins (cyclin D), G1/S-cyclins (cyclin E), S-cyclins (cyclin A) and G2/M-cyclins (cyclin B) (Alberts, Johnson *et al.* 2008).

In addition to the checkpoints that enforce the correct progression of the cells through the cell cycle, the cell also has checkpoints activated by DNA damage and these are described next.

1.3.1 Mechanisms of DNA damage checkpoint response

In order to maintain genomic stability, higher eukaryotic cells have evolved efficient DNA damage response mechanisms to sense, signal and repair damaged DNA as improper processing of DSBs can lead to chromosomal instability, resulting in apoptosis, carcinogenesis and mutations. Briefly, in response to different types of DNA damage or stalled replication forks, the cell activates its DNA damage checkpoint response system, which arrests normal cell cycle progression at different cell cycle phases. This process includes a step-by-step activation of several different proteins, categorized as sensors, transducers and effectors that control cell cycle progression and facilitate DNA repair (Jackson 2002; Shiloh and Lehmann 2004; Pardo, Gómez-González *et al.* 2009). Fig. 5 depicts the fundamental components of a signal-transduction pathway initiated by DNA damage that activates cell cycle checkpoints and regulates apoptosis, transcription or DNA repair.

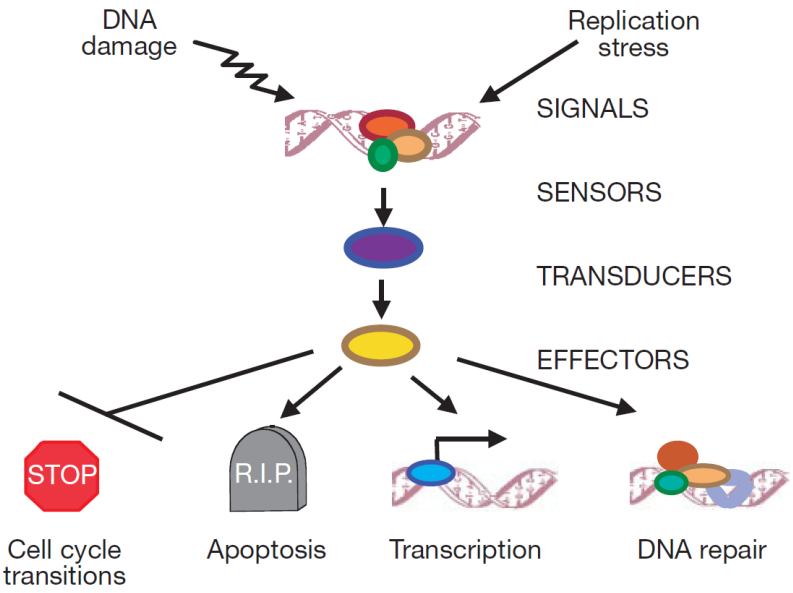

Figure 5: General outline of DDR signal-transduction pathway, consisting of signals, sensors, transducers and effectors. For simplicity, the network of interacting pathways are depicted as a linear pathway with arrowheads representing activating events, whereas inhibitory events are symbolized by perpendicular ends (Zhou and Elledge 2000).

Specifically, upon DNA damage induction, immediate cellular response to a DSB, which acts as a signal, is the initial DNA damage sensing and detection by sensor proteins, such as the MRN complex or DNA-PK. Sensor proteins activate a signal transduction cascade that involves activation of key checkpoint regulators, the DNA-damage-response transducing kinases – ataxia-telangiectasia mutated (ATM) and ataxia-telangiectasia and RAD3 related kinase (ATR) (Kastan and Lim 2000; Kastan 2001). Interestingly, for the maintenance of genomic integrity after DNA damage induction, activation of all three phosphatidylinositol 3-kinases (PI-3K), ATM, ATR and also DNA-dependent protein kinase, catalytic subunit (DNA-PKcs), is very important, as all three kinases are significant sensors of genotoxic stress (Yang, Yu *et al.* 2003). When activated, these kinases phosphorylate many downstream mediator, transducer and effector proteins, such as the checkpoint kinase 1 (CHK1) and the checkpoint kinase 2 (CHK2) (Bakkenist and Kastan 2003). These effector kinases are responsible for activation of cell cycle checkpoints that can lead to cell cycle arrest in G1- or G2-phases of the cell cycle facilitating thus DNA repair. Remarkably, there is some evidence that the DNA repair machinery can distinguish between different types of damage, which translates it into different modes of checkpoint activation in G1- and S/G2-phase cells (Barlow, Lisby *et al.* 2008).

The classical view of the DDR system is that the ATM-CHK2 pathway is activated in response to IR-induced DNA damage, acting at initial stages of DNA damage signal transduction in mammals (Canman, Lim *et al.* 1998), while the ATR-CHK1 pathway is mainly activated by UV light-induced DNA damage and/or ssDNA regions, which may evolve during processing of chromosomal lesions or result from stalled DNA replication (Ünsal-Kacmaz, Makhov *et al.* 2002). However, activation of ATR is not only restricted to S-phase cells, although the majority of replication protein factor A (RPA)-coated ssDNA is generally present during DNA replication in S-phase cells (Fanning, Klimovich *et al.* 2006). Recent studies suggest that ATR and ATM are not acting in an independent fashion during the DNA damage checkpoint response, but rather that they are co-operating to initiate and maintain the DNA damage checkpoint response (Helt, Cliby *et al.* 2005). This is also supported by the fact that ATM and ATR overlap in their substrate specificity indicating the possibility of a crosstalk between these two pathways (Tibbetts, Cortez *et al.* 2000; Yajima, Lee *et al.* 2006).

1.3.1.1 The ATM-CHK2 signaling pathway

One of the first signaling events after exposure of eukaryotic cells to IR is the activation of the ATM kinase (Canman, Lim *et al.* 1998). ATM kinase activity is thought to be required for the activation of the DNA damage checkpoints in G1/S-, intra-S- and G2/M-phases of the cell cycle (Shiloh and Kastan 2001; Shiloh 2003).

Fig. 6 shows the sequence of coordinated events involved in this activation including sensor, mediator and transducer proteins. It is generally assumed that MRN is the primary DNA damage sensor, rapidly accumulating at DSBs (Lavin 2007). MRE11 binds both, ssDNA and dsDNA, in a sequence-independent manner, hence contributing to ATM kinase activation and the fast recruitment of ATM to damaged sites (Lee and Paull 2004; You, Bailis *et al.* 2007; Borde and Cobb 2009) (Fig. 6 C). As a consequence of MRN protein retention at DNA damaged sites the local concentration of this complex at the DSB sites increases; this accumulation consists of a H2AX / mediator of DNA damage checkpoint protein 1 (MDC1)-dependent fraction on chromatin and a H2AX-independent fraction near the DSB (Bekker-Jensen, Lukas *et al.* 2006; Berkovich, Monnat Jr. *et al.* 2007).

Activation of inactive ATM dimers to active ATM monomers is known to involve intermolecular ATM autophosphorylation events at different Ser-residues including Ser-1981, Ser-367 and Ser-1893 (O'Neill, Dwyer *et al.* 2000; Bakkenist and Kastan 2003); these events cause dimer dissociation and initiate ATM monomer formation. It was shown that ATM autophosphorylation at Ser-1981 is necessary for both, its monomerization and the binding to regions flanking DSBs (Berkovich, Monnat Jr. *et al.* 2007). Activated ATM molecules phosphorylate various downstream ATM substrates such as NBS1 (Gatei, Young *et al.* 2000), MRE11 (Dong, Zhong *et al.* 1999), MDC1 (Goldberg, Stucki *et al.* 2003), breast cancer susceptibility protein 1 (BRCA1) (Cortez, Wang *et al.* 1999), CHK2 (Matsuoka, Rotman *et al.* 2000), tumor protein 53 (p53) (Banin, Moyal *et al.* 1998), RPA (Wang, Guan *et al.* 2001), RAD17 and the H2A histone variant, H2AX at its conserved C-terminus on Ser-139 (Burma, Chen *et al.* 2001; Stiff, O'Driscoll *et al.* 2004), hence initiating a cellular DNA damage signal.

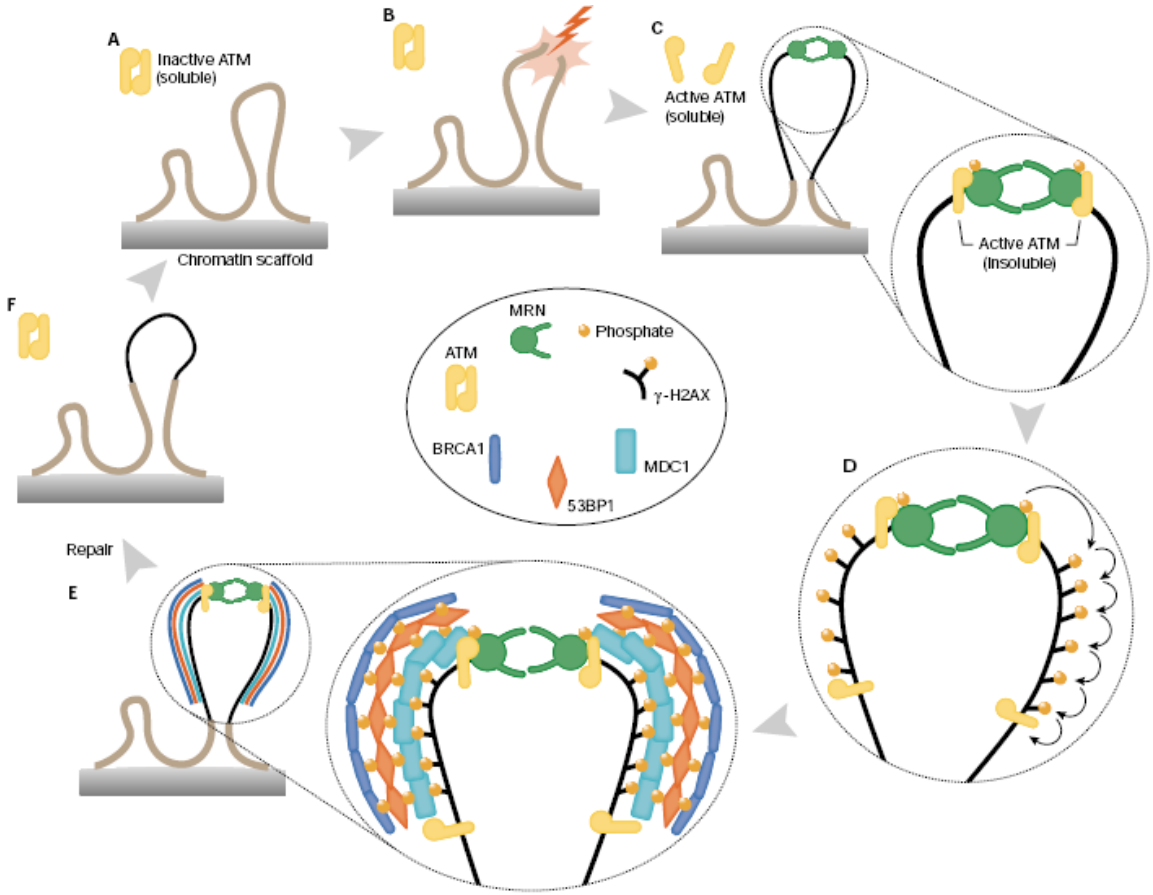

Figure 6: A model of the cellular DSB response cycle. (A) Undamaged section of a chromosome, showing two chromatin loops and an inactive ATM dimer. (B, C) Induction of a DSB, modification of chromatin, ATM activation and recruitment of both ATM and MRN complex to the DSB. The thin black line indicates modified chromatin. (D, E) A wave of H2AX phosphorylation is followed by recruitment and ATM-dependent phosphorylation of mediator proteins, such as MDC1, p53 Binding Protein 1 (53BP1) and BRCA1 to the growing focus. (F) Disassembly of the focus, ATM inactivation and chromatin remodeling. Note that MRN complex is also a component of the growing focus but, for clarity, has been excluded here (van den Bosch, Bree *et al.* 2003).

Phosphorylation of H2AX (the phosphorylated form of H2AX is termed γ-H2AX) is MRN-dependent, since MRE11-depletion abrogates H2AX phosphorylation (Rogakou, Pilch *et al.* 1998; Kinner, Wu *et al.* 2008; Di Virgilio, Ying *et al.* 2009). MRN-regulated phosphorylation of H2AX marks DSB sites, and provides at the same time a phosphorylation-regulated recruitment and retention platform for the γ-H2AX-dependent assembly of further mediator proteins (Stucki, Clapperton *et al.* 2005; Lou, Minter-Dykhouse *et al.* 2006). Interestingly, the primary migration of factors to DSBs has no need of γ-H2AX (Celeste, Fernandez-Capetillo *et al.* 2003; Kim, Minter-Dykhouse *et al.* 2006).

Amplification of the initial DNA damage signal in mammalian cells is facilitated by molecular recognition modes involving direct binding of the phosphorylated γ-H2AX tail to the BRCA1 C-terminal (BRCT)-domain of MDC1. Localization of MDC1 to the vicinity of a DSB initiates the recruitment of additional, activated ATM molecules that allow further phosphorylation and spreading of γ-H2AX on chromatin (Rogakou, Pilch *et al.* 1998). This ATM-dependent γ-H2AX expansion, occurring at megabase regions surrounding the break (Fig. 6 D), facilitates the recruitment of other scaffolding and enzymatic repair factors, e.g. 53BP1 and BRCA1, to chromatin regions distal to the breaks. Such protein accumulation processes at sites of DSBs lead to the formation of large protein foci (Fig. 6 E), which can be microscopically visualized by immunofluorescence staining. After completion of repair proteins that have accumulated at the site dissociate from chromatin and the protein focus disappears (Fig. 6 F).

In summary, upon DNA damage induction, MRN activates ATM, MDC1 enhances kinase activity of ATM, which then transduces the genotoxic stress signal by activating its downstream substrates, particularly the effector kinase, CHK2. This kinase is essential for the entire DNA damage response as it phosphorylates several cell-cycle proteins, and thus initiates the activation of cellular DNA damage checkpoints (Chaturvedi, Eng *et al.* 1999; Matsuoka, Rotman *et al.* 2000).

In general, cellular DNA damage, in particular DSBs can be removed by two major repair pathways. After completion of repair and restoration of DNA integrity, imposed cell cycle brakes in the form of checkpoints are released and cell cycle progression resumes (Hartwell and Weinert 1989; Niida and Nakanishi 2006). In case of irreparable DNA lesions apoptosis is initiated (Rich, Allen *et al.* 2000). The next chapters describe in detail DSB repair by different pathways and review the current status of understanding regarding the regulation of repair pathway choice.

1.4 Eukaryotic DSB repair and its regulation

Higher eukaryotic cells remove DNA damage by two main repair pathways – NHEJ and HRR. The fundamental difference between these two repair pathways is that HRR requires a homologous template whereas NHEJ does not (Essers, van Steeg *et al.* 2000). Consequently, HRR ensures accurate DNA repair by using either an undamaged sister chromatid or a homologous chromosome as a repair template (Khanna and Jackson 2001), whereas NHEJ rejoins two DNA ends without any needs for homology (Karran 2000), thus the term “non-homologous end-joining” (Weterings and Chen 2008). Repair of DSBs by NHEJ is accompanied with limited or extensive additions or deletions of nucleotides at the generated junction generated during the process of producing ligatable ends. The result is an altered sequence of the repaired DNA molecule due to the fact that NHEJ does not restore sequence information in the damaged DNA molecule, although it restores its molecular integrity (Iliakis, Wang *et al.* 2004; Lieber 2010). Thus, DSB repair by NHEJ is considered as error-prone.

The relative contribution of the two repair pathways is likely to be determined by the phase of the cell cycle and the abundance of repetitive DNA, although the importance and usage of NHEJ varies greatly among species (Karran 2000). As NHEJ has no need for a DNA template, it can operate throughout the cell cycle, although it is thought to dominate repair in the G1-phase of the cell cycle, where HRR cannot operate. In contrast, HRR is restricted to S- and G2-phases of the cell cycle, where a sister chromatid is available that can be used as a repair template (Krüger, Rothkamm *et al.* 2004; Moynahan and Jasin 2010). Fig. 7 presents the function of the two DSB repair pathways throughout the cell cycle with their dependency on DNA template.

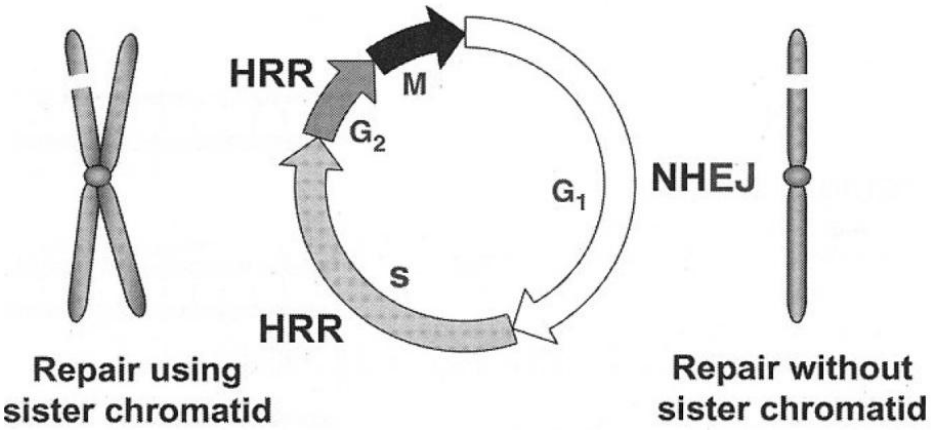

Figure 7: Illustration shows two major DSB repair pathways with its dependency on DNA template and their occurrence in different cell cycle phases (Hall and Giaccia 2006).

In theory, HRR could also occur in diploid G1-phase cells, using existing copy of the chromosome as a template for repair. However, homologous chromosomes are usually not directly available due to nuclear chromosome compartmentalization. It is therefore believed that NHEJ is the prevailing repair pathway during G1/G0- and M-phases of the cell cycle (Lee, Mitchell *et al.* 1997), whereas HRR is the main repair pathway during S- and G2-phases of the cell cycle. In the next section are described the processes of HRR and NHEJ in detail.

1.4.1 Homologous recombination repair

As mentioned above, DSB repair by HRR utilizes a homologous sequence either on the same DNA molecule, on a sister chromatid or on a homologous chromosome (Krüger, Rothkamm *et al.* 2004), hence the term “homologous recombination repair”. This template-dependent process is relatively slow but provides the mammalian genome a high-fidelity mechanism for repairing DNA damages including DNA gaps, DSBs and DNA interstrand crosslinks in an error-free manner. In addition to these repair mechanisms, HRR is also implicated in several other biological processes such as meiotic crossover during allelic rearrangement in gametes, proper chromosome segregation, mating type switching in yeast as well as epitope immunoglobulin class switching in many organisms.

The basic HRR machinery and its regulation are greatly conserved among eukaryotes. Interestingly, null mutations in core HRR genes, e.g. *RAD51*, *BRCA1* and *breast cancer susceptibility protein 2 (BRCA2)* are lethal (Thompson and Schild 2002), and cells with mutated HRR genes present reduced HR levels, resulting in high levels of chromosomal aberrations and miss-segregation at mitosis (Pierce, Johnson *et al.* 1999; Griffin, Simpson *et al.* 2000), elevated radiosensitivity to killing and increased tumorigenesis (Pierce, Stark *et al.* 2001). In yeast and bacteria, HRR is the primary mechanism of DSB repair (San Filippo, Sung *et al.* 2008).

In general, HRR involves the following distinct steps: (1) processing of DNA ends, (2) search for homology, strand invasion and formation of holiday junction, (3) DNA synthesis, branch migration and final resolution of synapsed DNA molecules (Kinner, Wu *et al.* 2008). Fig. 8 shows the key steps of HRR with its main players.

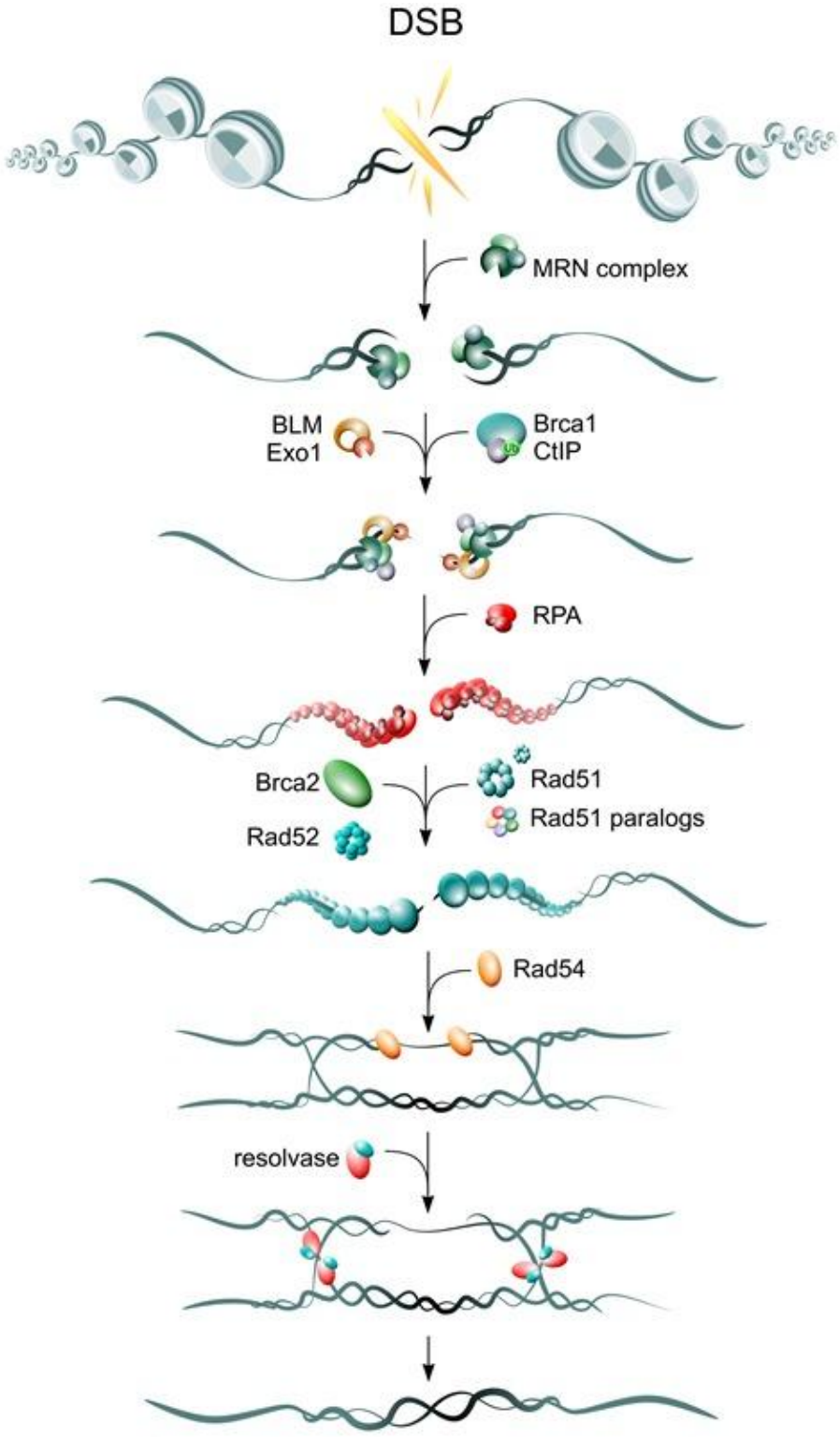

Figure 8: Outline of main HRR repair players. Illustration courtesy: Emil Mladenov, Institute of Medical Radiation Biology, Medical School, University of Duisburg-Essen, Germany.

Initial DNA damage sensing by MRN and its binding to damaged DNA initiates an intracellular DNA damage signal leading to the recruitment of different proteins to damaged DNA ends, e.g. BRCA1, Bloom syndrome helicase (BLM), C-terminal binding interacting protein (CTIP) and the nucleases – exonuclease 1 (EXO1) and DNA2 (Stucki, Clapperton *et al.* 2005; Lou, Minter-Dykhouse *et al.* 2006). MRN, CTIP and activated EXO1 and DNA2 nucleases promote resection of DSBs to form recombinogenic 3'-ssDNA overhangs (Sartori, Lukas *et al.* 2007; Takeda, Nakamura *et al.* 2007; Bolderson, Tomimatsu *et al.* 2010). The resulting 3'-ssDNA tails are then coated by RPA, hence protecting the ends from degradation and preventing the formation of secondary structures (Wold 1997). Interestingly, formation of 3'-ssDNA tails might also determine the switch from NHEJ to HRR, particularly as NHEJ preferentially utilizes unprocessed DNA ends for ligation (Zhu, Chung *et al.* 2008; Yun and Hiom 2009). Accordingly, ssDNA ends activate the ATR-CHK1 pathway that might also promote DSB repair by HRR (Sorensen, Hansen *et al.* 2005).

With the aid of RAD52 epistasis group members like RAD54, RAD51 paralogs (RAD51B, RAD51C, RAD51D, XRCC2 and XRCC3) and BRCA2 (Symington 2002; Sy, Huen *et al.* 2009), the DNA strand exchange protein, RAD51 displaces RPA from ssDNA tails, consequently generating a RAD51 nucleoprotein filament that can be composed of thousands RAD51 monomers. This RAD51 nucleoprotein filament is bound to ssDNA and searches for homology by invading homologous duplex DNA segments for polymerase-mediated DNA synthesis (West 2003; Mazin, Mazina *et al.* 2010). The 3'-end from the invading end is used to prime a leading strand DNA synthesis templated by the donor duplex. The other end of the break interacts with the displaced strand from the donor duplex, forming a so-called Holiday Junction, thus priming DNA synthesis from the other end of the break. Resolution of Holiday Junctions may result in crossover or non-crossover products, although crossing over is a seldom event during somatic HRR (Richardson, Moynahan *et al.* 1998; Nagaraju, Odate *et al.* 2006). In the process of synthesis-dependent strand annealing (SDSA), the invading strand, previously being extended by DNA synthesis, is extended by branch migration and then leaves the template chromatid. This extended strand anneals to complementary DNA sequences exposed by 5'-3'-resection of the other site of the break, and the molecule is completed by filling remaining gaps by DNA

synthesis by polymerase δ and/or ε and LIG1-mediated sealing of the nicks (Mimitou and Symington 2009). In the case of Holiday Junction resolution, HRR is completed by separation of the synapsed DNA molecule through resolvases.

1.4.2 Non-homologous end-joining

Cells of higher eukaryotes rejoin DSBs in their DNA predominantly by NHEJ, comprising four general steps: A set of enzymes (1) recognizes and (2) mediates the capture of both ends of the broken DNA molecule; (3) formation of a molecular bridge between the two DNA ends and (4) finally re-ligation of the broken DNA molecule.

In general, NHEJ utilizes proteins like DNA-PKcs, KU, ARTEMIS, LIG4, XRCC4, XLF/CERNUNNOS, as well as DNA polymerase λ. Here, this pathway will be termed as DNA-PK-dependent non-homologous end-joining (D-NHEJ), stressing its dependence on DNA-PK, where KU and DNA-PKcs act in a coordinated manner to direct the DNA end-joining process towards the D-NHEJ pathway (Perrault, Wang *et al.* 2004; Lieber and Wilson 2010).

Interestingly, D-NHEJ mutants remove a large proportion of DSBs from their genome using an alternative pathway of end-joining (Wang, Perrault *et al.* 2003). This repair pathway may therefore have a backup function becoming active whenever D-NHEJ is inactivated (Wang, Rosidi *et al.* 2005). In order to differentiate it from D-NHEJ, and to indicate its putative backup function, we term it here as backup NHEJ (B-NHEJ) (Iliakis 2009). Both end-joining pathways are described in detail below.

1.4.2.1 D-NHEJ

As briefly discussed in 1.4, D-NHEJ repair pathway is error-prone but is extremely efficient in removing DSBs from the genome, with half times of 15-30min. Many components involved in D-NHEJ are conserved from yeast to humans with the difference that mammals utilize DNA-PKcs for DSB repair by NHEJ, while a homolog of this enzyme in yeast as well as in lower eukaryotes has not been found (Critchlow and Jackson 1998).

Moreover, it is proposed, that the high speed of D-NHEJ is an evolutionary development in higher eukaryotes orchestrated around the newly evolved DNA-PKcs protein and pre-existing factors. Within a few minutes it achieves restoration of chromosome integrity through an optimized synapsis mechanism operating by a sequence of protein-protein interactions in the context of chromatin and nuclear matrix (Iliakis, Wang *et al.* 2004). In addition, D-NHEJ is indispensable in processing DSB intermediates generated during V(D)J recombination (Karran 2000; Weterings and Chen 2008), where defects in D-NHEJ lead to chromosomal aberrations, immunodeficiency and sensitivity against IR (Couedel, Mills *et al.* 2004).

The heterodimeric KU70/80 complex, consisting of 70kDa and 80kDa subunits (Walker, Corpina *et al.* 2001), is one of the most abundant cellular proteins with about 300,000 molecules per cell (Lieber, Grawunder *et al.* 1997). In an early stage of D-NHEJ-mediated DSB repair, DNA ends are recognized by the KU heterodimer that captures DNA ends (blunt, 5'- or 3'-overhangs). Through its asymmetric ring structure, that wraps around the DNA helix (Walker, Corpina *et al.* 2001), it recruits DNA-PKcs to DNA ends (Lees-Miller and Meek 2003), thus activating its kinase activity. DNA-PKcs forms a synaptic complex and brings both DNA ends together. Moreover, it undergoes conformational changes, and probably dimerizes to generate a platform for subsequent processing of non-ligatable DNA termini before final re-ligation (Meek, Gupta *et al.* 2004). Once the two DNA ends have been captured and tethered by DNA-PK (complex of KU70/80 and DNA-PKcs), the D-NHEJ repair process is initiated, thus enabling the phosphorylation of various downstream substrate proteins, e.g. RPA2, WRN helicase, ARTEMIS, XLF/CERNUNNOS, DNA LIG4 and XRCC4, as well as autophosphorylation of DNA-PKcs itself (Chen, Trujillo *et al.* 2000; Jeggo and Löbrich 2005; Otsuki, Seki *et al.* 2007; Cruet-Hennequart, Glynn *et al.* 2008; Kinner, Wu *et al.* 2008; Yu, Mahaney *et al.* 2008). Fig. 9 depicts DSB repair by D-NHEJ and the main proteins involved.

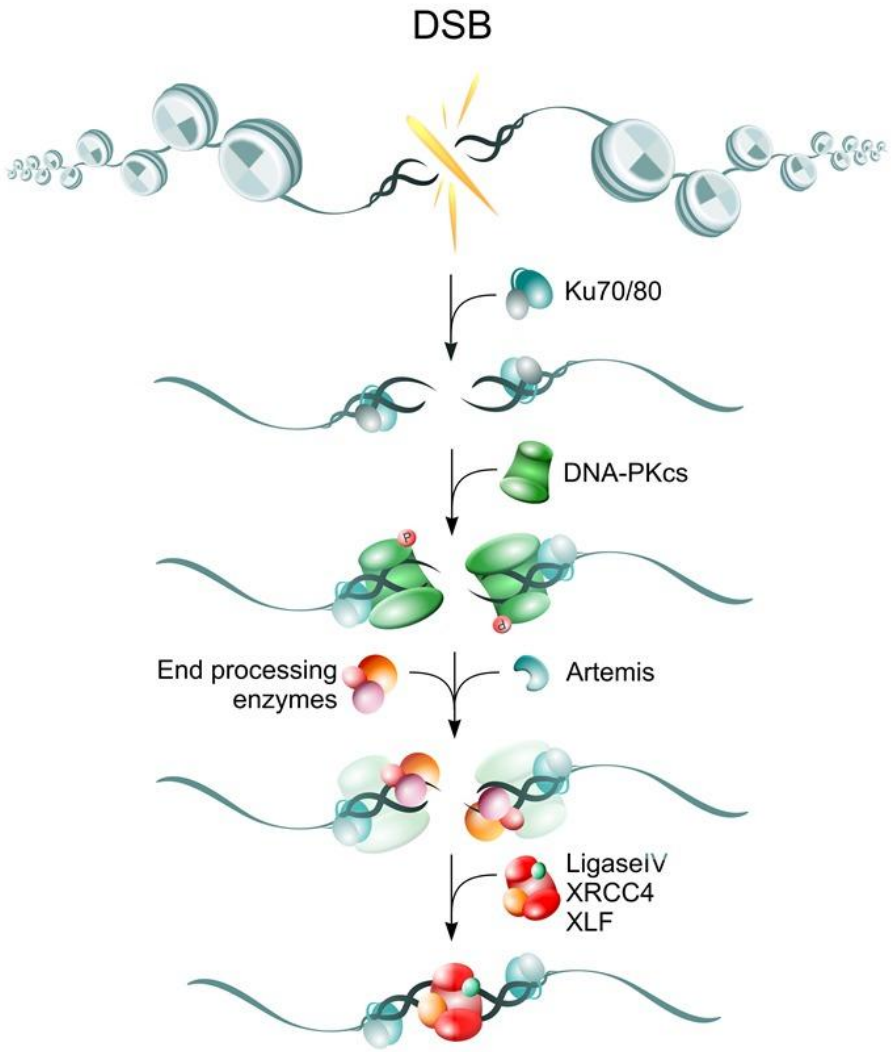

Figure 9: Outline of the main players in the different D-NHEJ steps. D-NHEJ efficiently restores genomic integrity without ensuring sequence restoration. Association of KU to DNA ends facilitates recruitment of DNA-PKcs, which is activated by the DNA ends, thus regulating the efficiency of this repair pathway. DNA-PKcs promotes end-processing by the ARTEMIS nuclease, and subsequent rejoining of broken DNA ends utilizing the LIG4/XRCC4/XLF complex (Mladenov and Iliakis 2011).

Several enzymes have been identified, like tyrosyl-DNA phosphodiesterase (TDP1), polynucleotide kinase 3'-phosphatase (PNKP), terminal deoxynucleotidyl transferase (TDT), nucleases like ARTEMIS or polymerases, that are able to either remove or fill-in ss and non-compatible overhangs. During this step of D-NHEJ process, occasional loss of nucleotides is possible (Valerie and Povirk 2003). Finally and after release of DNA-PK from DNA ends, LIG4/XRCC4/XLF complex catalyzes/coordinates the ligation of processed DNA ends by the help of polymerase μ or λ (Mahajan, McElhinny *et al.* 2002; Capp, Boudsocq *et al.* 2006; Wu, Frit *et al.* 2007).

Interestingly, it is believed that dissociation of NHEJ proteins from repaired damage sites is facilitated by its autophosphorylation; in yeast, it also depends on MRX and the ATPase functions of RAD50 (Wu, Topper *et al.* 2008).

1.4.2.2 B-NHEJ

As pointed out above, cells with mutations in components of D-NHEJ, or when D-NHEJ components are either absent from the vicinity of the break or are genetically or chemically compromised, are still capable of repairing the majority of IR-induced DSBs, utilizing an alternative repair pathway, which is, rather surprisingly, not sensitive to mutations in HRR genes (Feldmann, Schmiemann *et al.* 2000; Wang, Zeng *et al.* 2001; Wang, Zhao-Chong *et al.* 2001). This alternative pathway is a distinct form of end-joining, and is likely to be an evolutionarily older pathway with less optimized synapsis mechanisms, rejoining DNA ends with slower kinetics with half-times of 2-10h. It is thought that the rapid DNA end-joining of D-NHEJ kinetically suppresses this slower alternative pathway (DiBiase, Zeng *et al.* 2000). However, alternative end-joining pathways (B-NHEJ) are expected to contribute significantly to genome maintenance and stability, playing an important role in the overall repair of DSBs.

Interestingly, B-NHEJ has a strong growth-state dependency (Windhofer, Wu *et al.* 2007). Its activity is markedly reduced in plateau and G1-phase cells, but is significantly elevated during the G2-phase of the cell cycle, suggesting that suppression of growth signaling significantly compromises DSB repair by B-NHEJ (Wu, Wang *et al.* 2008). Moreover, B-NHEJ is implicated in telomere maintenance (Rai, Zheng *et al.* 2010), but it can also robustly substitute for D-NHEJ in CSR in LIG4-deficient mice (Soulas-Sprauel, Le Guyader *et al.* 2007; Yan, Boboila *et al.* 2007), and is likewise found to substitute for V(D)J recombination in D-NHEJ-deficient cells, where mutations in recombination activating genes (*RAG1*/*RAG2)* lead to proteins able to generate DNA ends but unable to hold them (Lee, Neiditch *et al.* 2004; Iliakis, Rosidi *et al.* 2005; Jones and Simkus 2009).

However, the slow kinetics and suboptimal synapsis mechanisms of B-NHEJ allow more time for exchanges through the joining of incorrect DNA ends, consequently leading to formation of chromosome aberrations during the repair of IR-induced DSBs in wild-type and D-NHEJ mutant cells. This error-prone nature of B-NHEJ (Virsik-Köpp, Rave-Fränk *et al.* 2003) could also be demonstrated for other endpoints, as in XRCC4- and LIG4-deficient mice chromosome abnormalities included translocations at the immunoglobulin heavy locus chain (IgH) that give rise to lymphoid malignancies (Soulas-Sprauel, Le Guyader *et al.* 2007; Yan, Boboila *et al.* 2007), hence B-NHEJ is placed at the center of carcinogenesis.

Despite the potential consequences of B-NHEJ function, little is known about the underlying mechanism, its regulation, integration into the cellular DSB processing apparatus, and its interaction with components of D-NHEJ and HRR. Genetic and biochemical experiments have shown that proteins like poly [ADP-ribose] polymerase 1 and 2 (PARP1, PARP2), MRN, Werner syndrome (WRN), histone H1, LIG3 and X-ray repair cross-complementing protein 1 (XRCC1), are implicated in B-NHEJ (Wang, Zhao-Chong *et al.* 2001; Haince, McDonald *et al.* 2008; Rosidi, Wang *et al.* 2008; Sallmyr, Tomkinson *et al.* 2008; Davies and Chen 2010; Della-Maria, Zhou *et al.* 2011). Fig. 10 illustrates the characterized B-NHEJ repair pathway steps and the proteins involved.

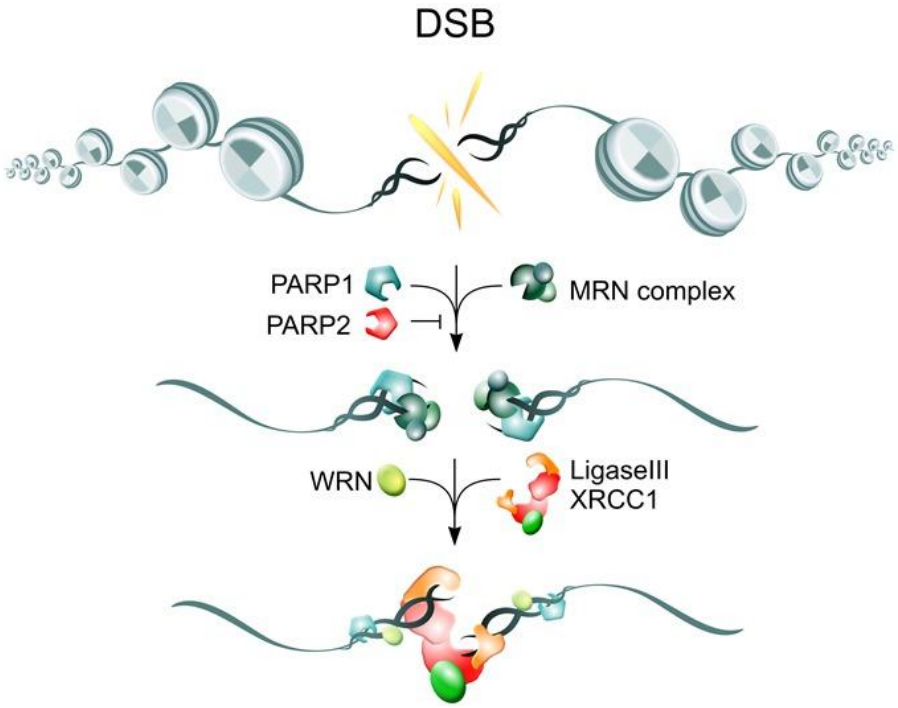

Figure 10 Outline of B-NHEJ key steps with its main players (Mladenov and Iliakis 2011).

Upon DNA damage induction, proteins such as MRN, PARP1 and PARP2 are recruited to DSBs. Prior to ligation, H1 helps to align the DNA ends (Rosidi, Wang *et al.* 2008). Remarkably, MRN seems to be essential for end-joining by B-NHEJ, as its inhibition in D-NHEJ mutants decreases end-joining frequency (Rass, Grabarz *et al.* 2009); LIG3 functions in a complex with XRCC1 being regulated by PARP1 (Robert, Dantzer *et al.* 2009). Interestingly, PARP1 might compete with KU for DNA ends, where particularly KU's much higher affinity for DNA ends provides a kinetics basis for the backup character of B-NHEJ. Another cause for this backup character might be the fact that other forms of lesions, like SSBs or base damages, also compete for PARP1, and LIG3 as the PARP1/XRCC1/LIG3 complex is likewise involved in the repair of SSBs and base damages (Audebert, Salles *et al.* 2004; Wang, Wu *et al.* 2006).

1.4.3 Regulation of DSB repair pathway choice

Notably, in the field of DNA repair a central and largely unanswered question is how and when a cell selects which pathway to use for the repair of a certain DSB. This is because the regulatory mechanisms of DSB repair pathway choice are still unknown. Thus, it remains open whether the decision for pathway choice is determined by the nature of the DSB, or whether it is regulated by a global regulatory network responding to uncharacterized signals and physiological conditions. In the remaining of this section, several models of DSB repair pathway choice and its coordination are discussed.

It is widely assumed that in higher eukaryotes NHEJ is the main DSB repair pathway, and that HRR has only a minimal contributing function in DSB repair, restricted to G2-phase of the cell cycle (1.4.1, 1.4.2) (Jeggo and Löbrich 2005; Beucher, Birraux *et al.* 2009). This is supported by the observation that in higher eukaryotes gene targeting is inefficient, whereas random integration is very efficient (Fattah, Lichter *et al.* 2008). In line with this, HRR-deficient mutants have comparable DSB processing activity as wild-type cells throughout the cell cycle (Wang, Zeng *et al.* 2001). However, other results suggest a substantial contribution of HRR to DSB processing, as mutants defective in HRR components, are radiosensitive, and have highly compromised HRR of site-specific DSBs (Pierce, Stark *et al.* 2001). When analyzing the DSB repair capability of HRR mutants by measuring γ-H2AX foci decay, a relatively small but clearly visible defect in removing DSBs is measurable (Rothkamm, Krüger *et al.* 2003). Thus, it can be assumed that HRR has an important role in DSB repair. Clearly, further investigations are needed to unravel the contribution of different repair pathways in DSB repair.

For instance, one theory suggests that D-NHEJ and HRR compete for the recruitment of DSBs. It was shown that transfected plasmid DNA could be repaired in mammalian cells by both pathways, and that both D-NHEJ and HRR proteins bind to broken DNA ends. According to this model, pathway choice reflects the outcome of this competition and may have a stochastic component. In apparent agreement with this passive competition model, cells with defects in D-NHEJ have increased HRR (Allen, Kurimasa *et al.* 2002). Specifically, inactivation of D-NHEJ by eliminating DNA-PKcs resulted in elevated HRR (Delacote, Han *et al.* 2002; Shrivastav, Miller *et*

al. 2009). In contrast to this observation, chemical inhibition or functionally compromised DNA-PKcs leads to reduced HRR, implicating that non-functional DNA-PKcs has a dominant negative effect; it abolishes alternative DSB processing by capturing DNA ends, hence blocking access to other repair factors (Wang, Perrault *et al.* 2003; Perrault, Wang *et al.* 2004; Cui, Yu *et al.* 2005). In line with this competition model, two groups reported that Mre11-Rad50-Xrs2 (Mrx) complex (homolog for MRN in yeast) and Ku compete for DNA end binding (Taylor, Cecillon *et al.* 2009). In the absence of Ku, Mre11 binding to DNA ends was increased in G1-phase cells, leading to a higher number of DNA ends being processed by HRR. Conversely, over-expression of Ku can inhibit Mre11 binding to DSBs, and with that the initiation of DNA end resection in G2-phase cells. Similarly, EXO1 can also compete with KU for DNA end binding and, if present at high concentrations it can process DNA ends for HRR (Barlow, Lisby *et al.* 2008). Also, Ku can prevent Exo1 and Sgs1-dependent resection of DNA ends in the absence of a functional Mrx or Sae2 (Mimitou and Symington 2010), inhibiting HRR, and promoting DSB repair towards D-NHEJ. In addition, KU can also inhibit B-NHEJ throughout the genome as well as HR at telomeres (Fattah, Lee *et al.* 2010). However, other results indicate that differences in the DSB binding properties of MRE11 and KU determine different efficiencies of HRR and NHEJ, at least for the repair of high LET radiation-induced DSBs (Wang, Zhang *et al.* 2010).

In opposition to this competition model, other studies revealed no competition between HRR and NHEJ, when repair of IR-induced DSBs was followed in different repair mutants. After all, HRR deficient mutants presented no evident defects in removing DSBs, whereas D-NHEJ mutants showed strong repair defects – although they rejoined the majority of DSBs with slower kinetics using B-NHEJ (DiBiase, Zeng *et al.* 2000). More importantly, it was shown that this rejoining capability is not HRR-dependent (Wang, Zeng *et al.* 2001) as one would expect, based on a competition model. However, in view of the fact that higher eukaryotes predominantly use NHEJ for DSB repair, a simple competition model appears to be incompatible with all available facts, and we hypothesize the existence of determinants that mediate selection while at the same time allowing D-NHEJ to dominate. Of course, all these

models of pathway selection will be valid only in S- and G2-phases of the cell cycle, where HRR can operate.

There is evidence that pathway choice might be controlled by the expression or post-translational modification of repair proteins such as CTIP, BRCA1 or MRN (Esashi, Christ *et al.* 2005; You and Bailis 2010), as well as by the ability of cyclin-dependent protein kinase 1 (CDK1) activity to promote and regulate DSB end resection (Aylon, Liefshitz *et al.* 2004). For instance, it has been reported that loss of MRE11 affects both D-NHEJ and B-NHEJ, thus decreasing end-joining frequencies in experimental systems, whereas MRE11 overexpression activates resection of ssDNA leading to increased DSB repair by B-NHEJ, particularly as MRE11 nuclease activity was found to be an essential factor favoring B-NHEJ (Xie, Kwok *et al.* 2009).

Other results report that dissociation of NHEJ proteins from repaired damage sites depends on Mrx complex and the ATPase activity of Rad50, indicating that Mrx may be the critical factor in repair pathway switching, at least at DNA ends that failed D-NHEJ (Wu, Topper *et al.* 2008). The most obvious mechanism for this dissociation would be the formation of recombinogenic ss-3'-tails, by nucleases like MRE11, CTIP, EXO1 and DNA2, presumably because D-NHEJ mostly uses unresected DNA ends for ligation (Zhu, Chung *et al.* 2008; Mimitou and Symington 2009; Yun and Hiom 2009; Cejka, Cannavo *et al.* 2010; Rupnik, Lowndes *et al.* 2010). In DNA end resection, CTIP is directly implicated in the cell cycle specific HRR activities of MRN, and functional interactions between MRN and CTIP have been observed. Similar observations were also made in yeast, where the major task of Sae2 (CTIP homologue in yeast) is to control Mrx' activity, and thus to regulate the balance between HRR and NHEJ.

Interestingly, Sae2 was identified as one target of CDK1-dependent control of DNA end resection (Huertas, Cortes-Ledesma *et al.* 2008). Recently, it was proposed that MRN can initiate different forms of DNA damage and checkpoint signaling depending on the type of DNA ends it is bound to; two-ended DSBs, which generally arise in chromatin after IR, cause ATM activation, whereas one-ended DSB that arise from stalled replication forks lead to ATR activation. Through such mechanisms MRN can control repair pathway choice at a DSB, with ATM and ATR activation resulting in

replication fork rescue and leading to DSB repair by HRR (Williams, Lees-Miller *et al.* 2010).

However, activation of ATR-CHK1 pathway by ssDNA is also implicated in HRR (Sorensen, Hansen *et al.* 2005), possibly because CHK1 phosphorylates RAD51 that in turn attenuates its interaction with BRCA2 (Sorensen, Hansen *et al.* 2005). Post-translational modifications of MRN like phosphorylation, methylation and acetylation are clearly involved in regulating MRN activities (Olson, Nievera *et al.* 2007; Zhuang, Jiang *et al.* 2009; Bennetzen, Larsen *et al.* 2010; Olsen, Vermeulen *et al.* 2010), even though the effects of these post-translational modifications on MRE11, RAD50 and NBS1 activities are not well understood. Thus, it is still unknown, whether processes like the formation of ss-3'-DNA ends, reflect coordinating functions or are themselves the result of overarching coordination.

1.5 The MRN complex

In the context of DSB repair pathway utilization and coordination, the early function of MRN complex, immediately upon generation of DSBs, places this complex at the interface of DSB repair pathway choice, although its precise functional significance in diverse aspects of the response to DNA damage, DSB repair and pathway choice remains to be elucidated. The reported MRE11 and KU heterodimer interaction (Goedecke, Eijpe *et al.* 1999; Wu, Topper *et al.* 2008) is compatible with the roles proposed for these proteins in NHEJ, particularly when considering that they are the earliest players in the choice of the repair pathway that will remove a DSB. In the following, we give an overview of MRN, and its biochemical and structural characteristics, its involvement in DDR signaling and its contribution to different DSB repair pathways. This information forms the framework for arguments and interpretations of results obtained in the experiments described in the following section.

Eukaryotic MRN is composed of three subunits: MRE11, RAD50 and NBS1. MRE11 and RAD50 are highly conserved from archaea to humans, whereas NBS1 (homolog of Xrs2 in yeast) is a less conserved eukaryotic-specific protein (D'Amours and Jackson 2002; Williams, Williams *et al.* 2007). MRN has different enzymatic activities, and is thus considered as a cornerstone complex, rather than a simple component within a linear pathway. It is involved in DNA damage sensing (Lee and Paull 2007), DNA repair (Tauchi, Kobayashi *et al.* 2002; Buis, Wu *et al.* 2008), DNA replication (Tittel-Elmer, Alabert *et al.* 2009), meiosis (Ajimura, Leem *et al.* 1993), mitosis (Mimitou and Symington 2009), telomere maintenance (Dimitrova and de Lange 2009) and apoptosis (Stracker, Morales *et al.* 2007). MRN is also required for V(D)J recombination (Saidi, Li *et al.* 2010), and the programmed DSB induction during CSR (Dinkelmann, Spehalski *et al.* 2009).

Cells with deficiencies in MRN components have phenotypes similar to ATM-deficient cells including impaired IR-induced cell cycle checkpoint activation, ineffective DNA repair, dramatic reduction of targeted integration of exogenous DNA, gene conversion, sister chromatid exchanges, impaired ss-annealing and apoptosis. However, in contrast with ATM loss, which is not embryonically lethal, null mutations

in any of these three proteins leads to embryonic lethality (Demuth, Frappart *et al.* 2004).

Links between defects in the MRN complex and tumorigenesis in humans, and the recognition that defects in MRN subunits, cause cancer-prone diseases like Nijmegen breakage syndrome (NBS) or Ataxia Telangiectasia like disorder (ATLD) (Stewart, Maser *et al.* 1999; Tauchi, Matsuura *et al.* 2002; McKinnon 2004; Taylor, Grom *et al.* 2004; Uchisaka, Takahashi *et al.* 2009) underscore the importance of MRN in cellular functions. To date, mutations in RAD50 gene have been reported in only a few cases of patients, and have not yet been associated with a defined human phenotype (Heikkinen, Rapakko *et al.* 2006; Tommiska, Seal *et al.* 2006). However, recent results report a patient with heterozygous mutations in *RAD50* gene with low levels of unstable RAD50 protein. Cells from this patient were characterized with a RAD50 deficiency resulting in a phenotype that can be classified as NBS (Waltes, Kalb *et al.* 2009). All three disorders share similar clinical and cellular phenotypes, such as immunodeficiency, cerebellar degeneration, defects in DNA damage-induced checkpoint activation, failure to form DNA damage-induced MRN foci, increased chromosome instability, radio-resistant DNA synthesis, radiation sensitivity and premature ageing (Matsuura, Tauchi *et al.* 1998; Varon, Vissinga *et al.* 1998; Petrini 2000; Waltes, Kalb *et al.* 2009).

1.5.1 Structural and functional characteristics of the MRN complex

1.5.1.1 MRE11

MRE11 is composed of 708 amino acids (aa), and is the central 80kDa protein-nucleic acid and protein-protein interaction core component of the MRN complex (Hopfner, Karcher *et al.* 2001; Williams, Williams *et al.* 2007). MRE11 comprises several protein domains involved in different functions. The amino-terminal end has four conserved phosphoesterase motifs and a NBS1-binding site, whereas its C-terminus includes a RAD50-binding site and two DNA binding domains, enabling binding of duplexed as well as ssDNA-ends (Borde and Cobb 2009). The protein domains of MRE11 are presented in Fig. 11.

Figure 11: Scheme of MRE11 protein domains. Regions important for the NBS1 and RAD50 interactions are indicated, blue regions show the relative position of four phosphoesterase motifs, whereas the DNA binding domains are shown in orange (Borde and Cobb 2009).

The nuclease domain of MRE11 is responsible for different enzymatic activities including ssDNA endonuclease activity on 5'-overhangs, 3'-flaps and 3'-branches, as well as the double-stranded (ds) DNA 3'-5'-exonuclease activity that is manganese-(Mn^{2+}), ATM- and NBS1-dependent. Furthermore, the protein has DNA annealing, as well as DNA unwinding activities that are regulated through interactions with RAD50 and NBS1 (Paull and Gellert 1998; Buis, Wu *et al.* 2008; Jazayeri, Balestrini *et al.* 2008). Moreover, MRE11 is known to homodimerize via poorly characterized mechanisms that is required for basic MRN functions, such as MRE11-DNA-binding *in vitro* and MRE11 repair *in vivo* activities (Williams, Moncalian *et al.* 2008).

Because MRE11's nuclease activity does not seem to be required for resection of clean DSBs but rather for processing of DNA ends with covalent adducts, such as those created by IR (Llorente and Symington 2004), it is likely that MRE11 is necessary for 5'-3' resection of DNA ends suitable for HRR (Mimitou and Symington 2009). However, structural and biochemical data suggest that generation of 3'-tails for HRR *in vivo* requires additional factors with reverse nuclease directionality compared to MRE11, such as CTIP or EXO1 (Schaetzlein, Kodandaramireddy *et al.* 2007). Thus, one possible mechanism for DNA end resection might be a two-step mechanism, involving a helicase, e.g. BLM, in conjunction with a ss-specific endo- or exonuclease for resection of DSBs (Mimitou and Symington 2008; Mimitou and Symington 2009). There is some evidence, that in yeast the first step depends on Mrx and Sae2, resulting in endonucleolytic removal of about 50-100 nucleotides from the 5'-end, which gives rise to an intermediate with short 3'-ssDNA tails that is rapidly processed in a second step by a ss-specific nuclease, like Exo1 or Sgs1 (BLM orthologue in yeast) (Niu, Raynard *et al.* 2009). Interestingly, it was shown that the nuclease acting with Sgs1 is Dna2, a conserved endonuclease implicated in Okazaki

fragment and DSB processing in post-replication repair pathways. In yeast Mrx and Sae2 initiate DSB resection, and either Sgs1 with Dna2 or Exo1 rapidly degrade 5'-strands to expose long 3'-ssDNA tails. Thus, it appears that Sgs1 and Dna2 function in a parallel pathway to Exo1 (Zhu, Chung *et al.* 2008).

1.5.1.2 RAD50

RAD50 is a 150kDa ATP-dependent subunit of MRN belonging to the structural maintenance of chromosome (SMC) group of proteins. At each end of the protein, Walker A and B nucleotide triphosphate (NTP)-binding motifs are separated by two long heptad-repeat regions bearing two MRE11 binding sites and a central conserved zinc-hook structure (CXXC motif) that are depicted in Fig. 12 (Alani, Subbiah *et al.* 1989; Hopfner, Karcher *et al.* 2000).

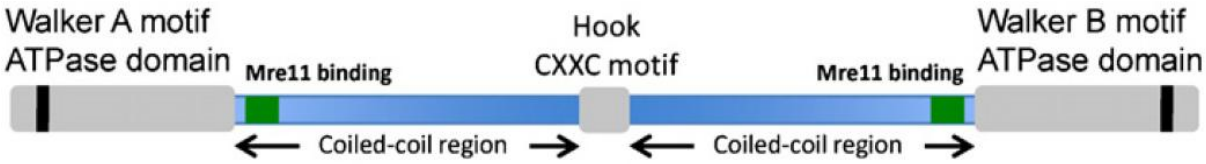

Figure 12: The domain structure of RAD50 shows Walker A and B motifs at each end of the protein, MRE11 binding sites, adjacent to ATPase domains are shown in green. Coiled-coil regions meet at the hook region in the center of the protein. This central RAD50 region contains a CXXC motif that reverses directionality of the coiled coil, coordinating Zinc (Zn^{2+}) to mediate RAD50 hook-hook assembly (Borde and Cobb 2009).

The CXXC motif consists of 14 non-helical residues (aa 440-453) with two main-chain hydrogen bonds, and is important for MRN complex assembly as well as recombinational repair (Hopfner, Craig *et al.* 2002). The heptad-repeat regions fold into an extended intramolecular anti-parallel coiled-coil structure that brings N-terminal Walker A and C-terminal Walker B ATPase motifs in close proximity, stably associating to form a bipartite ATP-binding cassette (ABC)-ATPase domain (Alani, Subbiah *et al.* 1989; Hopfner, Craig *et al.* 2002; Mimitou and Symington 2009). It appears that ATPase motifs in RAD50 are essential for all known activities of MRN including ATM activation by DSBs *in vitro* (Lee and Paull 2005). Adenylate kinase (AK) and ATPase activities act competitively, and regulate the conformational

(allosteric) changes of RAD50. Both activities are important for various functions of MRN *in vivo*, e.g. DNA binding, unwinding and/or DNA tethering (Bhaskara, Dupre *et al.* 2007). However, the proposed main task of RAD50 is to bind damaged DNA ends and to hold them in close proximity.

1.5.1.3 NBS1

NBS1 consists of 754 aa (~90kDa) including two important ATM phosphorylation sites on Ser-278 and Ser-343, as well as three functional regions. Fig. 13 shows the main domains of the protein, which include (1) the amino-terminal forkhead-associated (FHA)-domain, (2) the central BRCT-domain and (3) the C-terminal MRE11-binding and phosphoinositide-3-kinase-related protein kinase (PIKK)-interacting domains (Kobayashi, Tauchi *et al.* 2002; Williams, Williams *et al.* 2007).

Figure 13: Schematic presentation of NBS1 protein domains. Functional FHA- and two BRCT-domains are in the N-terminal half of the protein, followed by two important central ATM phosphorylation sites, whereas essential regions for MRE11 binding (green) and ATM interaction (purple) are located in the C-terminus of NBS1 (Borde and Cobb 2009).

N-terminal NBS1-FHA-domain mediates phospho-specific protein-protein interactions, thus being important for effective DNA damage signaling (Lloyd, Chapman *et al.* 2009). It recognizes phosphorylated target proteins, e. g. γ-H2AX and interacts with them, leading to recruitment of MRN to damaged DNA sites. The BRCT domain contributes to chromatin association, nuclear foci formation, IR-induced responses, and is implicated in intra S-phase checkpoint control (Tauchi, Kobayashi *et al.* 2002; Lee and Paull 2007). The C-terminal NBS1-MRE11-interacting domain is essential for viability, as truncation in this region interrupts MRE11-binding to NBS1, leading to no offspring in mice (Difilippantonio, Celeste *et al.* 2005). In addition, association of ATM and NBS1 is involved in chromatin remodeling processes in order

to permit access of repair-related factors to DNA organized in highly ordered eukaryotic chromatin (Iijima, Ohara *et al.* 2008).

Cells from NBS1 patients with a N-terminal deletion in NBS1 protein, present abrogated MRE11 phosphorylation, and lack nuclear focal recruitment of MRE11 after irradiation, indicating that both MRE11 phosphorylation as well as MRE11 foci formation are NBS1-dependent events (Dong, Zhong *et al.* 1999). However, other results show that the C-terminal half of NBS1 is sufficient to localize MRE11-RAD50 (MR) complex to the nucleus, although these interactions are not sufficient to stimulate nuclear focus formation and/or ATM interaction (Lee and Paull 2007). The catalytic MR complex functions are likely regulated through NBS1 by forming a complex with them (Paull and Gellert 1999; Lee, Ghirlando *et al.* 2003). All in all, NBS1 is an essential eukaryotic protein, as it regulates several different MRN functions, like nucleotide-dependent DNA binding, ATP-dependent DNA unwinding and ATM activation. However, the primary functions of NBS1 are to localize the MR complex to the nucleus and to activate dimeric ATM.

1.5.1.4 Structural appearance of MRN complex

Scanning atomic force microscopy revealed that the core MR complex exists as a heterohexameric assembly ($M_2R_2N_2$), whose morphology can be divided into different molecular regions – a globular head, coiled-coils and hook domains, as presented in Fig. 14 A (Williams, Lees-Miller *et al.* 2010).

The M_2R_2 complex has a bipolar architecture, in which, at the one end, one MRE11 homodimer associates with two RAD50-ATPase domains, leading to the formation of a globular DNA binding head, and mediating MRN binding to chromatin. While at the other end, coiled-coil regions of RAD50 form an extended intra-molecular flexible arm with a CXXC motif at its end (de Jager, van Noort *et al.* 2001; Hopfner, Karcher *et al.* 2001).

As mentioned above, the CXXC motif of RAD50 is important for MRN complex assembly, as MR complex dimerization requires two RAD50 cysteine hooks. These cysteine hooks create one-half of a composite Zn^{2+}-binding site hence linking two MR molecules (Hopfner, Craig *et al.* 2002).

Interestingly, NBS1 and MRE11 availability affect the type of complex formed. When both MRE11 and NBS1 proteins are present in equal amounts, complex formed consists of M_2R_2N or M_2R_xN, where x is greater than two. However, in abundance of NBS1 compared to MRE11, a complex containing RAD50 multimers is preferably formed (Rupnik, Lowndes *et al.* 2009).

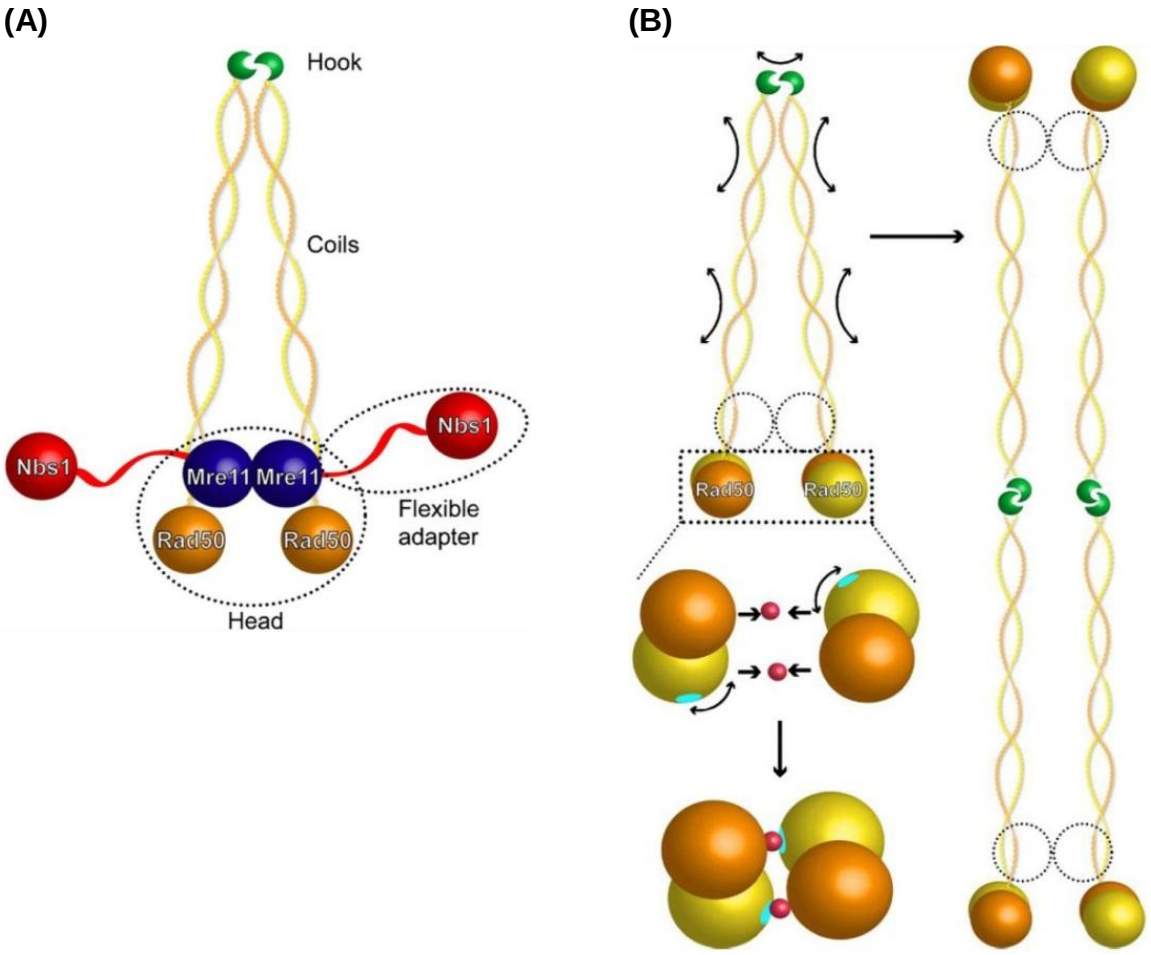

Figure 14: Overall assembly of the MRN complex. (A) MRN can assemble as a hetero-hexamer and consists of 4 key regions: the processing "head", formed by a MRE11 dimer and two RAD50 ATPase domains (indicated by dotted line), the "coils" and "hook" encoded by a region of RAD50 separating the N- and C-terminal ATPase halves, and the NBS1 "flexible adapter" (indicated by dotted line) that provides the key link to signaling function. (B) Illustration showing several possible RAD50 states. The RAD50 Zn-hook can either intramolecularly dimerize RAD50 within a single MRN complex, which connects RAD50 ATPase domains present within an M_2R_2head (top left), or intermolecularly connect two MRN complexes to form a dumbbell-like structure with M_2R_2 heads at either end (right). In these pictures MRE11 is outlined as a dotted circle to show that it can bridge RAD50 molecules in the absence of direct RAD50 dimerization through Zn-hook or ATP-mediated connections. ATP-induced dimerization brings together two RAD50 ATPase domains (bottom left), inducing a ~35° rotation of the C-terminal subdomain (yellow) with respect to the N-terminal subdomain (orange). ATP is indicated in red (Williams, Lees-Miller *et al.* 2010).

Moreover, MRN is able to slide along the DNA, which would allow further MRN molecules to bind to DNA ends (Moreno-Herrero, de Jager *et al.* 2005) – an ability that might also be useful for the initial steps of DNA repair. For instance, Fig. 14 B depicts two microscopically distinct MRN-DNA tethering architectures – a long-range DNA tethering structure and a short range DNA synapsis. Short-range DNA bridging, within a single head of a M_2R_2 complex may promote direct DNA end joining, whereas long-range DNA tethering plays an important role in recombinational DNA repair (Hopfner, Craig *et al.* 2002; Williams, Williams *et al.* 2007; Williams, Lees-Miller *et al.* 2010), as the RAD50 hook structure allows for bridging of dsDNA ends by facilitating the assembly of octameric long-range MRN-DNA-tethering scaffolds (de Jager, van Noort *et al.* 2001), resulting in the formation of heterotetrameric MRE11 complex dimers ($(M_2R_2)^2$). This is in line with the observation that any mutations in the RAD50 hook region disrupt scaffolding abilities of the complex leading to an increased sensitivity to genotoxic stress or radiation sensitivity (Hopfner, Craig *et al.* 2002).

In summary, the MRN complex contains 5 super classes of DNA repair domains: (1) DNA damage recognition, (2) protein-protein interaction and (3) nuclease domains as well as (4) ATP-driven conformational switches and (5) an ATPase motor for opening DNA at DSBs. Hence, it serves in part as a multipurpose DNA tether that acts to directly bridge severed DNA ends and chromatin domains, hence preventing DNA and chromosome separation, respectively.

1.5.2 The function of MRN complex in DDR

In undamaged cells MRE11 is homogenously distributed within the nucleus. Upon DNA damage induction MRN localizes very rapidly to DSBs, showing association with damaged DNA within 10min post-irradiation (D'Amours and Jackson 2002). NBS1 recruits ATM to damage-sites and moreover activates it (Berkovich, Monnat Jr. *et al.* 2007). This process is initiated by autophosphorylation events of inactive ATM dimers on Ser-1981 leading to its monomerization, and hence the activation of ATM kinase activity. For localizing ATM to damage sites, the ATP-dependent DNA unwinding ability of MRE11 is of great importance (Paull and Gellert 1999).

Once ATM is activated and recruited to DNA damage sites, it phosphorylates further ATM substrates such as MRE11 and NBS1, thus activating DNA damage signaling, DNA repair pathways and other cellular responses (Bakkenist and Kastan 2003; Lee and Paull 2007). However, MRN is not only implicated in ATM activation, but is also a target for ATM kinase in amplifying cell-cycle checkpoint signals or in downstream signaling to the DNA-repair machinery (Lavin 2007). Cell-cycle checkpoint signals can be amplified by NBS1-binding to γ-H2AX, resulting in a second wave of MRN recruitment to damage sites (Lee and Paull 2007), which is in line with the results showing that NBS1 mutants (Ser-343A) present no checkpoint response as they fail to stimulate CHK2 phosphorylation by ATM *in vitro* (Difilippantonio, Celeste *et al.* 2005). In addition, phosphorylation of MRN by ATM triggers MRN's inactivation and its disassembly from chromatin, thus down-regulating DNA damage response, following the recovery of checkpoint response (Di Virgilio, Ying *et al.* 2009). This cascade of cellular events in response to DNA damage is illustrated in Fig. 15.

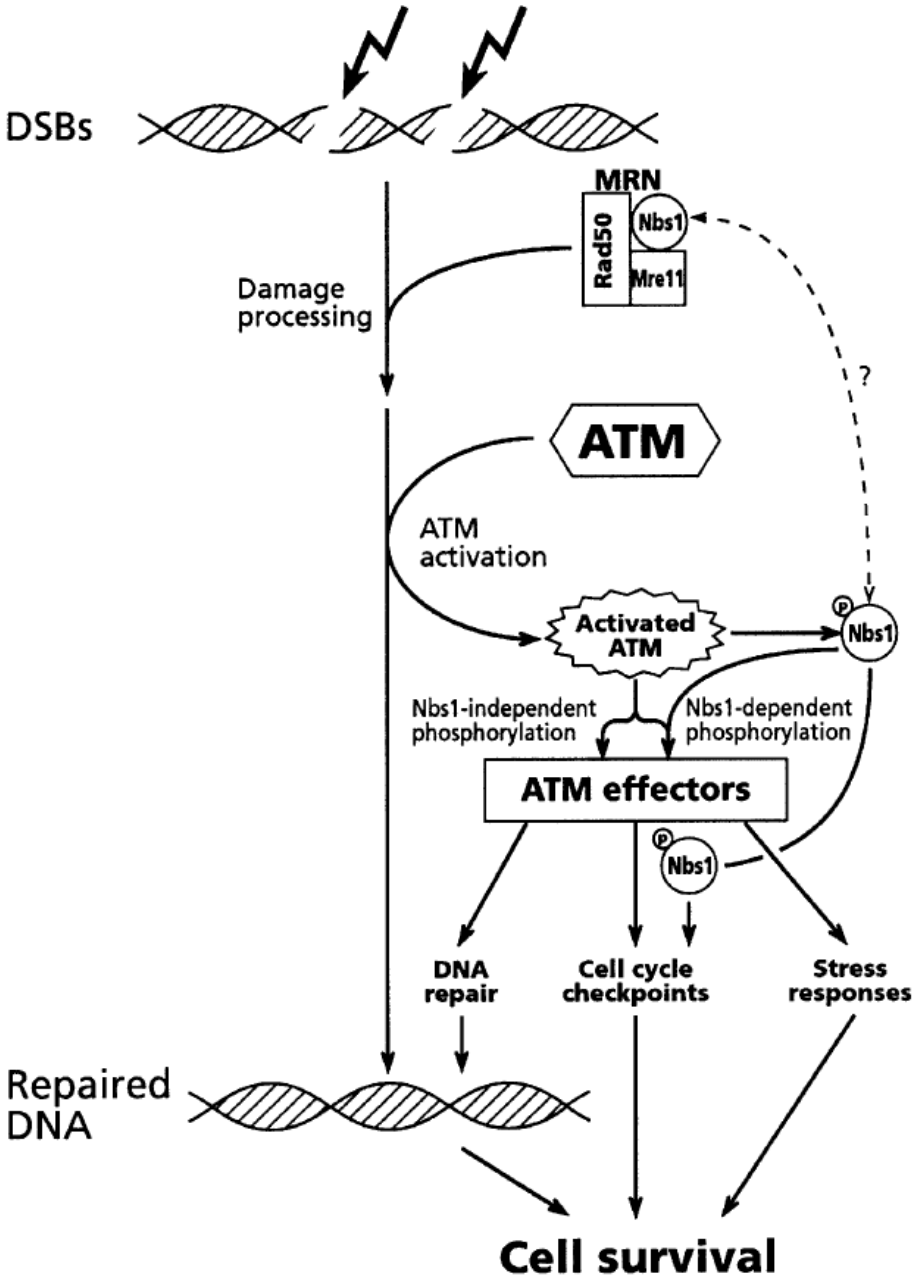

Figure 15: A model for early events in the cellular response to DSBs. MRN is essential for initial damage processing, where processed DNA lesions lead to recruitment of MRN and ATM activation. Active ATM phosphorylates its substrates, like NBS1 and MRE11, whereas phosphorylated NBS1 facilitates phosphorylation of certain ATM substrates, and furthermore plays an important role in activating cell cycle checkpoints (Uziel, Lerenthal *et al.* 2003).

Interestingly, in mammals MRE11 nuclease activity has been implicated in the activation of ATM through several approaches including effects on the stability of replication forks, as well as the initiation of cell-cycle checkpoints and repair processes (Jazayeri, Balestrini *et al.* 2008; Hashimoto, Chaudhuri *et al.* 2010).

Accordingly, there is some evidence for a putative role of MRE11 nuclease activity in a continued ATM activation (Jazayeri, Balestrini *et al.* 2008), suggesting that while nuclease activity of MRE11 is not required for the initiation of ATM activation, it contributes to the maintenance of ATM checkpoint signaling (Uziel, Lerenthal *et al.* 2003; Lee and Paull 2005). Other results show that processing of DSBs into ssDNA ultimately inhibits ATM, and contributes to the switch from ATM to ATR activation (Shiotani and Zou 2009). However, MRN may function to regulate ATM activity during ongoing DSB signaling by controlling the production of suitable DNA substrates at distinct stages of the DSB response, even though nucleolytic processing by MRE11 is an essential function of fundamental importance in DNA repair, distinct from MRN control of ATM signaling (Buis, Wu *et al.* 2008). Taken together, these observations demonstrate that MRN does not only act as a DNA damage sensor and as an upstream regulator of ATM activity but that it also plays an essential role downstream of ATM activation in DNA damage signaling and DSB repair.

1.5.3 The MRN complex in DSB repair

As discussed above, MRN senses DNA breaks, activates cell cycle checkpoints and has a central role in all DSB repair pathways, like HRR, D-NHEJ and B-NHEJ. Depending on the particular function of MRN, there are several distinct models for its role in DNA end tethering and processing during DSB repair.

For instance, HRR of DSBs requires architectural, structural and enzymatic components. Architectural components are needed to tether DSB ends in close proximity to prevent inappropriate recombination, and to pair them with homologous sequences on the sister chromatid, as illustrated in Fig. 16 A. Enzymatic activities are required to process DNA ends and for repair synthesis (de Jager, Trujillo *et al.* 2004; Shin, Chahwan *et al.* 2004). Thus, the structurally implied primary activity of MRN seems to be a linker function for homologous stretches of DNA and/or broken ends (Hopfner, Craig *et al.* 2002), whereas the resecting ability of MRE11 is required for the formation of RAD51 nucleoprotein filament during the presynapsis step of recombination (Hopkins and Paull 2008). In this model, the nuclease activity of MRN is downstream of DNA break binding and the initiation of ATM activation.

The involvement of MRN in HRR is supported by data showing that deletion of MRE11 or NBS1 in chicken DT40 cells results in reduced HR and sister chromatid exchange without affecting end-joining frequencies in plasmid based assays (Tauchi, Kobayashi *et al.* 2002; Yang, Saidi *et al.* 2006). In contrast, other results suggest that MRN deficiency confers a strong defect in CSR, affecting both D-NHEJ and B-NHEJ (Helmink, Bredemeyer *et al.* 2009). Furthermore, other results showed that silencing of MRE11, RAD50 or CTIP decreased NHEJ probably because MRE11 could control end-joining through both, ATM-dependent and ATM-independent pathways. The latter set of results suggests that MRN may play an inhibitory role in NHEJ in mammals (Rass, Grabarz *et al.* 2009).

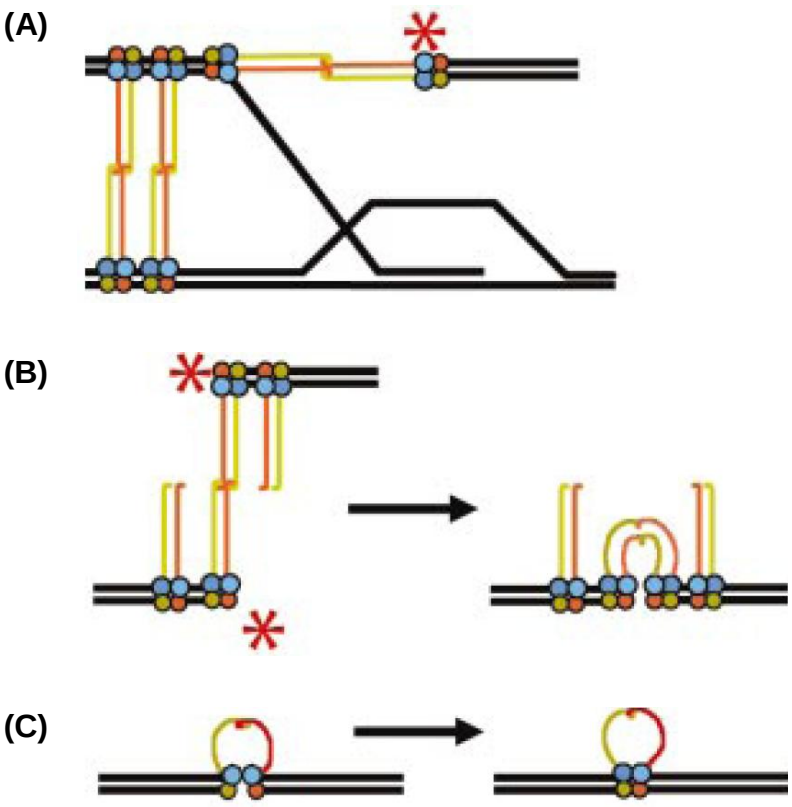

Figure 16: Models for the role of MRN in HRR and NHEJ. (A) The nuclease activity of MRN can process dsDNA ends for the subsequent repair steps. The architecture of tail-to-tail linked MRN complexes suggests a mechanism for bridging sister chromatids, and initiating and stabilizing displacement loop formation – a common intermediate in recombination, break-induced replication and telomere maintenance. (B) In NHEJ, head domains of two M_2R_2 complexes bind separate broken DNA ends, aligning and tethering them after a structural transition. (C) Circularization of a single M_2R_2 complex could potentially contribute to productive repair of broken DNA ends (Hopfner, Craig *et al.* 2002).

However, the DNA end recognition and processing by MRN suggests a role for MRN during the early stage of NHEJ (Daley, Palmbos *et al.* 2005) as MRN can stabilize distant breaks by collapse of a Zn^{2+}-linked $(M_2R_2)^2$ octamer (Fig. 16 B). Alternatively, two broken DNA ends might bind to the head of same MRN complex that has an internal Zn^{2+} linkage, as depicted in Fig. 16 C (Hopfner, Craig *et al.* 2002). There is also evidence that DSB repair by B-NHEJ is facilitated by MRN, particularly as MRE11 processes DNA termini (Deriano, Stracker *et al.* 2009; Lamarche, Orazio *et al.* 2010; Taylor, Cecillon *et al.* 2010), and because rapid accumulation of MRN at DNA damage sites requires PARP-1 (Haince, McDonald *et al.* 2008). Nonetheless, the nuclease activity of MRE11 is not important for accurate D-NHEJ (Moreau, Ferguson *et al.* 1999), so that a specific role of MRN in D-NHEJ is still unclear and hence requires further investigation.

1.6 IR-induced foci formation – protein accumulation at DNA damage sites

As described above, in response to IR-induced DNA damage several proteins involved in DDR signaling or DSB repair are recruited. Many of these proteins have been shown to locally accumulate into large nuclear domains – the so-called ionizing radiation-induced foci (IRIF) (Rogakou, Boon *et al.* 1999; Paull, Rogakou *et al.* 2000; Fernandez-Capetillo, Celeste *et al.* 2003). Indirect immunofluorescence or imaging of live cells expressing fluorescently tagged proteins can be used for the visualization of such protein accumulations. In order to detect discrete protein foci, hundreds to thousands of molecules must be present at DNA damage sites (Paull, Rogakou *et al.* 2000). The examination of IRIF formation and decay of DDR signaling and DSB repair proteins offers a powerful way to analyze effects of DNA damage in signaling and repair.

Nowadays many proteins are known to form IRIF, e.g. γ-H2AX, MRE11, RAD50, NBS1, RAD51, ATM, RPA, 53BP1 etc. (Maser, Monsen *et al.* 1997; Chen, Bhandoola *et al.* 2000; Anderson, Henderson *et al.* 2001; Daboussi, Dumay *et al.* 2002; Balajee and Geard 2004; Young, Jonnalagadda *et al.* 2005; Whalen, Gurai *et al.* 2008).

Human MRE11 and RAD50 form IR-induced discrete and subnuclear foci (Maser, Monsen *et al.* 1997), surrounding the break within a 10kb distance (Di Virgilio, Ying *et al.* 2009), where it exists in two fractions: (1) in a H2AX / MDC1-dependent fraction on chromatin and (2) in a H2AX-independent fraction at DSBs (Bekker-Jensen, Lukas *et al.* 2006; Berkovich, Monnat Jr. *et al.* 2007). However, the best documented foci-forming protein is the chromatin bound histone variant, H2AX, although γ-H2AX foci formation is a special case as no protein movements are involved in the foci forming process. In response to IR, H2AX phosphorylation at Ser-139 occurs at megabase regions surrounding the DSB within seconds after DNA damage induction (Rogakou, Pilch *et al.* 1998; Fernandez-Capetillo, Celeste *et al.* 2003). In the course of DSB repair, the initial γ-H2AX foci number decreases, which makes this protein an indirect marker for studying DSB processing. Thus, scoring of γ-H2AX foci is now generally accepted as a method to evaluate DSB repair kinetics at low radiation doses (up to 4Gy) (Rogakou, Pilch *et al.* 1998; Sedelnikova, Rogakou *et al.* 2002; Sedelnikova, Horikawa *et al.* 2004; Kinner, Wu *et al.* 2008). Although, not every γ-H2AX focus can be linked to a DSB at all times (Tanaka, Huang *et al.* 2007). Moreover, after DNA damage induction γ-H2AX foci colocalize with many other DNA damage signaling and repair protein foci such as ATM, MDC1, 53BP1, BRCA1, RAD51, MRN etc. (Paull, Rogakou *et al.* 2000). Therefore, colocalization analysis of IRIF can be of great importance in analyzing the involvement of different proteins in DSB repair.

However, there are two classes of proteins accumulating to foci after DNA damage induction distinguishable based on their spatial distributions: those present directly at the damage sites, coating ssDNA resulting from DSB resection, and those associated with DSB-flanking chromatin (Bekker-Jensen, Lukas *et al.* 2006).

Furthermore, DDR proteins assemble in a sequential, coordinated manner at DSBs, rather than being recruited as a preformed protein complex. The accumulation kinetics of signaling proteins has been described as a two-stage process in which initial recruitment occurs independently of H2AX phosphorylation, possibly involving MRN, followed by sustained DDR factor retention in a γ-H2AX-dependent manner (Celeste, Fernandez-Capetillo *et al.* 2003; Xie, Kwok *et al.* 2009; Yuan and Chen 2010).

It is widely assumed that foci formation by DDR proteins potentiates interactions between these proteins and damaged DNA, thus mounting rapid and effective responses to DNA breaks. Recruitment of DDR proteins to DNA damage sites is very fast but transient, reaching its accumulation maximum within the first 1-2min (Mortusewicz, Ame *et al.* 2007). Factors involved in DSB repair by NHEJ are recruited within seconds upon break formation, normally dissociating within 2h (Mari, Florea *et al.* 2006), whereas HRR factors show delayed and persistent recruitment to DSBs, reflecting the different repair kinetics between these two pathways (Kim, Krasieva *et al.* 2005).

Importantly, responses to DSBs are markedly influenced by the cell cycle status. Thus, foci from DDR factors like γ-H2AX, MRN, ATM or MDC1 occur regardless of cell cycle stage. In contrast, proteins like CTIP, RPA, ATR, BRCA1 and RAD51, form effective foci only in association with ssDNA formation after DNA resection in S/G2-phase of the cell cycle (Lisby, Barlow *et al.* 2004; Sartori, Lukas *et al.* 2007). Additionally, in most cases the number of focus-positive cells, and of the foci number per cell increase in a dose-dependent manner (van Veelen, Cervelli *et al.* 2005). For some proteins, even the foci size increases over time (van Veelen, Cervelli *et al.* 2005), reflecting the spread of these proteins from the DSB into adjacent chromatin (Rogakou, Boon *et al.* 1999). However, not all DDR or DSB repair factors accumulate at DNA breaks in such a way that foci can be observed, e.g. IRIF of CHK1 or CHK2 (Smits, Reaper *et al.* 2006). No foci are also forming by most of the NHEJ repair proteins. This is probably because NHEJ components do not spread substantially into adjacent chromatin, which would make them visible as foci. As a result accumulation is only observed only when high levels of damage are induced (Bekker-Jensen, Lukas *et al.* 2006).

2 Hypotheses and specific aims

It is evident from the outline above that the cellular mechanisms of DSB repair pathway choice are only incompletely understood, despite their importance in our understanding of the DDR. There are hints that MRN is involved in this function, but the available information of its mechanistic significance is uncertain. Thus, the first aim of this study was to contribute new information on the possible role of MRN in the selection between HRR and D-NHEJ in the repair of IR-induced DSBs. The overarching hypothesis was that MRN has a key function in bridging NHEJ with the initiating steps of HRR.

To this end, we further hypothesized that the analysis of MRN foci formation and decay would provide important insights into its function in DDR, in general, and its contribution to DSB repair pathway choice, in particular. To begin addressing this question, we studied the dynamics of MRN foci formation and decay in different cell types after exposure to IR of different LET. For this purpose, we employed confocal laser scanning microscopy (CLSM) to ensure the highest possible sensitivity and resolution of detection. Furthermore, we attempted an analysis throughout the cell cycle, particularly in G1- and G2-phases, as it is amply documented that the repertoire of DSB repair pathways varies throughout the cell cycle. Analysis of the relative contribution of MRN in DSB repair was carried out with double staining for γ-H2AX and MRE11.

A question we asked beyond a function of MRN in DSB repair pathway choice was its actual contribution to the different DSB repair pathways. This is because there are reports in the literature implicating MRN in all DSB repair pathways. To investigate the contribution of MRN to DSB repair by HRR, we scored RAD51 IRIF in wild-type and MRN-deficient cells. To evaluate DSB repair by D-NHEJ we used PFGE. PFGE was also used to measure DSB repair by B-NHEJ in repair-proficient, MRN-deficient, as well as in repair-proficient and MRN-deficient cells treated with a specific DNA-PKcs inhibitor, NU7441.

Lastly, we made an effort to unveil the putative regulatory role of the DNA-PK protein complex in DSB repair pathway choice. Indeed, there are reports implicating DNA-PK in the regulatory process of DSB repair pathway choice. Therefore, we decided to study to what extent DNA-PK deficiency affects HRR. For this purpose, we examined IR-induced MRE11 and RAD51 foci formation and decay dynamics in different DNA-PK mutants and compared the results to wild-type cells.

3 Materials and methods

3.1 Materials

Table 1: Laboratory apparatuses

Laboratory apparatus	Provider
63x/1.4 oil immersion objective	Leica Microsystems, Mannheim, Germany
Aluminum filter	GE-Healthcare, Piscataway, NJ, USA
Cell counter, Multisizer™ 3	Beckman Coulter, Krefeld, Germany
Centrifugal elutriator centrifuge, J2-21M	Beckman Coulter, Krefeld, Germany
Centrifugal elutriator rotor, JE-6	Beckman Coulter, Krefeld, Germany
Centrifuge, BioFuge (Fresco)	BioFuge Fresco Heraeus, Magdeburg, Germany
Confocal laser scanning microscope	Leica Microsystems, Mannheim, Germany
Cooling unit (external), DC10-K20	Thermo Fischer Scientific, Karlsruhe, Germany
Electrophoresis gel boxes, Horizon 20•25	Life Technologies™, Carlsbad, CA, USA
Flow cytometer, Coulter Epics XL	Beckman Coulter, Krefeld, Germany
FluorImager, Typhoon 9400	Molecular Dynamics, Germany
Inverted phase contrast microscope	Olympus, Hamburg, Germany
Laminar flow hood, HeraSafe	Heraeus, Magdeburg, Germany
Magnetic stirrer	MR Hei-Mix L, Heidolph, Schwaback, Germany
Mai Tai® diode-pumped, mode-locked Tsunami Ti:sapphire laser system with *Model J80* power supply	Spectra-Physics Inc., Mountain View, CA, USA
MCO-18 O_2/CO_2 incubators	Sanyo, Munich, Germany
NanoDrop™ 2000	Thermo Scientific, Schwerte, Germany
Nucleofector® II	Lonza Cologne GmbH, Cologne, Germany
Odyssey® infrared imaging system	LI-COR Biosciences, Bad Homburg, Germany
Peristaltic pump	IDEX Health & Science GmbH, Wertheim-Mondfeld, Germany
pH-Meter	WTW, InoLab, Weinheim, Germany
Pipets	Mettler Toledo GmbH, Giessen, Germany
Pipet-aid	BD Falcon, Heidelberg, Germany
Power supply, PowerPac™ HC	Bio-Rad, Munich, Germany
PTB dosimeter	Physikalisch-Technische Bundesanstalt, Braunschweig, Germany
SDS-PAGE apparatus	Bio-Rad, Munich, Germany

SDS-PAGE mini gels, Mini PROTEAN	Bio-Rad, Munich, Germany
Sonicator, RK225H	Sonorex, Bandelin, Germany
Stereomicroscope SV 8 475057	Carl Zeiss, Jena, Germany
Rocky shaker	Oehmen, Essen, Germany
Tabletop centrifuge, GS-6R	Beckman Coulter, Krefeld, Germany
Temperature control system for microscopes, environmental chamber for live cell imaging experiments, “Cube & Box”	Live Imaging Services, Basel, Switzerland
Thermo-mixer	Eppendorf, Hamburg, Germany
UV spectrophotometer	Shimadzu Deutschland GmbH, Duisburg, Germany
Vortexer, Vortex-Genie 2	Scientific Industries, Bohemia, NY, USA
Water bath	GFL, Hannover, Germany
Weighing balance, BP 110 S	Sartorius, Goettingen, Germany
Western blot imaging system; Odyssey® Infrared Imaging System	LI-COR Biotechnology GmbH, Bad Homburg, Germany
Western blot transfer systems; “iBlot® Dry Blotting System”	Invitrogen, Karlsruhe, Germany
X-ray machine, “Isovolt 320HS”	Seifert/Pantak, General Electric-Pantak, USA

Table 2: Disposable items and commercially available kits

Disposable elements and commercial kits	**Provider**
0.22µm filter	Greiner, Frickenhausen, Germany
3mm diameter glass tubes	CM Scientific Ltd., Shipley, UK
0.5, 1.5ml and 2ml tubes	Greiner, Frickenhausen, Germany
12ml non-cap tubes	Greiner, Frickenhausen, Germany
15 and 50ml tubes	Greiner, Frickenhausen, Germany
2, 5, 10, 25ml pipets	Greiner, Frickenhausen, Germany
20mm glass cover slips	Invitrogen, Karlsruhe, Germany
35mm glass coverslip bottom dishes	MatTek Corporation, Ashland, MA, USA
Cell culture dishes/flasks	Greiner, Frickenhausen, Germany
First strand cDNA synthesis kit	Fermentas, Thermo Scientific, Schwerte, Germany
Flasks, beakers, cylinders	Schott Duran, Wertheim, Germany
Gloves	Peha-soft® Satine, Hartmann, Heidenheim, Germany
High pure RNA isolation kit	Roche Diagnostics Deutschland GmbH, Germany
Hostaphan foil, 1.5µm thick	Dr. Mueller GmbH, Ahlhorn, Germany
Microscope slides	Roth, Karlsruhe, Germany

Para film	Lab Depot, Dawsonville, GA, USA
Pasteur pipettes	BD Falcon, Heidelberg, Germany
Pipettes	Greiner, Frickenhausen, Germany
Pipet tips	Greiner, Frickenhausen, Germany
Real time PCR LightCycler® capillaries	Roche Diagnostics Deutschland GmbH, Germany
Western blot blotting stacks; iBlot® blotting stacks	Invitrogen, Karlsruhe, Germany
UV cuvettes	Hellma, Muellheim, Germany

Table 3: Chemicals

Chemical	Provider
2-Mercaptoethanol	Sigma-Aldrich, Steinheim, Germany
4-(2-hydroxyethyl)-1-piperazineethanesulfonic acid	Roth, Karlsruhe, Germany
4',6-diamidino-2-phenylindole	Sigma-Aldrich, Steinheim, Germany
6-(4-hydroxyphenyl)-2-thioxo-2,3-dihydro-4(1H)-pyrimidinone	Santa Cruz Biotechnology, Inc., Heidelberg, Germany
Agarose	Bio-Rad, Munich, Germany
Aluminum sulphate	Roth, Karlsruhe, Germany
Ammonium persulfate	Sigma-Aldrich, Steinheim, Germany
Boric acid	Roth, Karlsruhe, Germany
Bovine serum albumin fraction IV	Roth, Karlsruhe, Germany
Bromophenol blue	Sigma-Aldrich, Steinheim, Germany
Chicken serum	Gibco™, Invitrogen, Karlsruhe, Germany
Coomassie brilliant blue R 250	SERVA Electrophoresis GmbH, Heidelberg, Germany
Crystal violet	Merck, Darmstadt, Germany
Dimethyl sulfoxide	Sigma-Aldrich, Steinheim, Germany
Dithiothreitol	Roth, Karlsruhe, Germany
Doxycycline hydrochloride	Sigma-Aldrich, Steinheim, Germany
Dulbecco's Modified Eagle Medium	Gibco™, Invitrogen, Karlsruhe, Germany
Ethanol	Sigma-Aldrich, Steinheim, Germany
Ethidium bromide	Roth, Karlsruhe, Germany
Ethylenediaminetetraacetic acid	Roth, Karlsruhe, Germany
Ethyleneglycoltetraacetic acid	Sigma-Aldrich, Steinheim, Germany
Fetal bovine serum	Biochrom, Berlin, Germany; PAA, Coelbe, Germany; Gibco™, Invitrogen, Karlsruhe, Germany
Gelatin	Calbiochem, Invitrogen, Karlsruhe, Germany
Glycerol	Roth, Karlsruhe, Germany
Glycine	Roth, Karlsruhe, Germany

Isopropanol	Sigma-Aldrich, Steinheim, Germany
KCl	Roth, Karlsruhe, Germany
KH_2PO_4	Roth, Karlsruhe, Germany
KOH	Roth, Karlsruhe, Germany
L-15 Leibovitz medium	Sigma-Aldrich, Steinheim, Germany
Low melting agarose	Roth, Karlsruhe, Germany
Mc Coy's 5A medium	Sigma-Aldrich, Steinheim, Germany
Methanol	Sigma-Aldrich, Steinheim, Germany
$MgCl_2$	Merck, Darmstadt, Germany
Minimum Essential Medium	Gibco™, Invitrogen, Karlsruhe, Germany
Mirin	Santa Cruz Biotechnology, Heidelberg, Germany
NaCl	Roth, Karlsruhe, Germany
$NaHCO_3$	Roth, Karlsruhe, Germany
Na_2HPO_4	Roth, Karlsruhe, Germany
N-lauryl sarcosine	Merck, Heidelberg, Germany
Nocodazole	Sigma-Aldrich, Steinheim, Germany
Non-fat dry milk	Roth, Karlsruhe, Germany
NU7441	Tocris Bioscience, Ellisville, MO, USA
Paraformaldehyde	Honeywell Specialty Chemicals GmbH, Seelze, Germany
Penicillin	Sigma-Aldrich, Steinheim, Germany
Phenylmethanesulfonylfluoride	Roth, Karlsruhe, Germany
Phosphoric acid	Roth, Karlsruhe, Germany
Poly-L-lysine	Biochrom AG, Berlin, Germany
ProLong® Gold antifade reagent	Invitrogen, Karlsruhe, Germany
Propidium iodide	Sigma-Aldrich, Steinheim, Germany
Protease inhibitor cocktail	Sigma-Aldrich, Steinheim, Germany
Puromycin	Sigma-Aldrich, Steinheim, Germany
RIPA buffer	Thermo Scientific, Schwerte, Germany
RNase A	Sigma-Aldrich, Steinheim, Germany
Rotiphorese® Gel 30 (37.5:1)	Roth, Karlsruhe, Germany
RPMI medium	Sigma-Aldrich, Steinheim, Germany
SeeBlue plus2 pre-stained protein ladder	Invitrogen, Karlsruhe, Germany
Sodium dodecyl sulfate	Roth, Karlsruhe, Germany
Streptomycin	Calbiochem, Invitrogen, Karlsruhe, Germany
Sucrose	Sigma-Aldrich, Steinheim, Germany
Tetramethylethylenediamine	Sigma-Aldrich, Steinheim, Germany
Tris(hydroxymethyl)aminomethane	Roth, Karlsruhe, Germany
Tris base	Roth, Karlsruhe, Germany
Tris-HCl	Roth, Karlsruhe, Germany

Triton X-100	Sigma-Aldrich, Steinheim, Germany
Trypsin	Biochrom AG, Berlin, Germany
Tween 20	Roth, Karlsruhe, Germany

Table 4: Antibodies

Antibody	Provider
MRE11 (NB 100-142) (rPAb)*	Novus Biologicals, Littleton, CO, USA
MRE11 (12D7) (mMAb)	Novus Biologicals, Littleton, CO, USA
MRE11 (12D7) (mMAb)	GeneTex, Irvine, CA, USA
RAD50 (13B3) (mMAb)	GeneTex, Irvine, CA, USA
NBS1 (NB100-143) (rPAb)	Novus Biologicals, Littleton, CO, USA
RAD51 (14B4) (mMAb)	GeneTex, Irvine, CA, USA
pS1981-ATM (rPAb)	Abcam, Cambridge, UK
γ-H2AX (3F2) (mMAb)	Abcam, Cambridge, UK
Cyclin B1 (H433) (rPAb)	Santa Cruz Biotechnology, Heidelberg, Germany
GAPDH (mMAb)	Millipore, Darmstadt, Germany
LAMIN A/C (636) (mMAb)	Santa Cruz Biotechnology, Heidelberg, Germany
α-TUBULIN (AA13) (mMAb)	Sigma-Aldrich, Steinheim, Germany
Alexa Fluor 488 (mPAb, rPAb)	Invitrogen, Karlsruhe, Germany
Alexa Fluor 568 (mPAb, rPAb)	Invitrogen, Karlsruhe, Germany
Alexa Fluor 633 (mPAb, rPAb)	Invitrogen, Karlsruhe, Germany
IRDye 680 (mPAb, rPAb)	LI-COR Biosciences, Bad Homburg, Germany
IRDye 800 (mPAb, rPAb)	LI-COR Biosciences, Bad Homburg, Germany

*In immunofluorescence applications, the antibody MRE11 (NB 100-142) was used in all experiments, as this antibody was the only functional one, among all other tested MRE11 antibodies, in detecting human MRE11 IRIF. None of the antibodies tested worked in other species.

Table 5: Plasmid

Plasmid	Description	Provider
pLEGFP-MRE11	Wild-type MRE11 cDNA cloned into a pLEGFP vector	Huichen Wang, Department of Radiation Oncology, Emory University School of Medicine, Atlanta, GA, USA

Table 6: Softwares

Software	Provider
Adobe® Creative Suite® 5.5	Adobe Systems Inc., USA
ImageQuant™ 5.0	GE Healthcare Life Sciences, USA
ImarisXT® 6.0	Bitplane Scientific Software, Switzerland
Microsoft Office 2010®	Microsoft, USA
Quantity One®	Bio-Rad Laboratories, Inc., USA
SigmaPlot® 11.0	Systat Software, USA
Wincycle™	Phoenix Flow Systems, USA

Table 7: Alphabetical list of cell lines used in experiments

Cell line	Description [Reference]	Culture medium
A549	Human lung carcinoma, repair-proficient cell line with wild-type p53 expression level but decreased repair of mismatched DNA bases.	Mc Coy's 5A + 10% FBS
AT5-BIVA	Human AT fibroblasts (Luo, Tang *et al.* 1996)	MEM + 10% FBS
CHO-10B4	Chinese hamster ovarian fibroblasts, standard repair-proficient cell line (Jeggo and Kemp 1983)	Mc Coy's 5A + 10% FBS
DT40-*DNA-PKcs*$^{-/-}$ DT40-MRE11 DT40-*MRE11*$^{-/-}$MRE11^{+}	Chicken B cell lymphocytes, KO for DNA-PKcs (Fukushima, Takata *et al.* 2001) Wild-type cell line for MRE11 and conditional KO for MRE11 (Yamaguchi-Iwai, Sonoda *et al.* 1999)	RPMI + 10% FBS + 1% chicken serum + 10µM 2-ME
HT1080 HT1080-YFP-MRE11 HT1080-MRE11-YFP	Human osteosarcoma tumor fibroblasts Cell clones stably express YFP-tagged MRE11 proteins with high and low expression rates, respectively (Giesen, Langner *et al.* 2011).	DMEM + 10% FBS + 0.4µg/ml Puromycin
Human lymphocytes	Human lymphocytes from a healthy donor	
M059K M059J	Human glioma control cell line for M059J cells Mutant in DNA-PKcs; counterpart of M059K	DMEM + 10% FBS
MEF PK34N (*DNA-PKcs*$^{+/+}$) PK33N (*DNA-PKcs*$^{-/-}$) KU70$^{-/-}$ KU80$^{-/-}$ PK80-193A (*DNA-PKcs*$^{-/-}$*KU80*$^{-/-}$)	Mouse embryonic fibroblasts Wt cell line for DNA-PKcs KO KO for DNA-PKcs (Kurimasa, Ouyang *et al.* 1999) KO for KU70 KO for KU80 (Nussenzweig, Chen *et al.* 1996) Double KO for DNA-PKcs and KU80	MEM + 10% FBS DMEM + 10% FBS MEM + 10% FBS
MRC5-SV1	Human repair-proficient fibroblasts	MEM + 10% FBS
NBS1-LB	Human fibroblasts from NBS patients with defective NBS1 function	MEM + 10% MEM

3.2 Methods

3.2.1 Tissue culture and growth conditions

Tissue culture was performed in SANYO MCO-18 O_2/CO_2 incubators at 37°C (in case of DT40 cells at 39.5°C) in a humidified atmosphere with 5% CO_2 and 95% air. Adherent cells were grown in 100mm cell culture dishes with 15ml of the appropriate growth medium, supplemented with fetal bovine serum (FBS). Suspension cells were maintained in 100mm bacteria dishes with 10ml growth medium supplemented with chicken serum and 10µM 2-ME (Table 7). All the media included 100µg/ml penicillin as well as 100µg/ml streptomycin.

Adherent cells were grown as a monolayer and were passaged every 3 days while avoiding confluency levels above 80%. For passage, media was removed and cells were briefly washed with 10ml cold 1x phosphate-buffered saline (PBS; 137mM NaCl, 2.7mM KCl, 10mM Na_2HPO_4, 1.76mM KH_2PO_4, pH 7.4). Cells were then covered with 2ml trypsin solution (0.05% trypsin in EDTA) and incubated for 5min at 37°C. Detached cells were resuspended in 10ml cold media. Single cell suspensions were counted (Multisizer™ 3, Beckman Coulter), and appropriate numbers of cells were further incubated for experiments or for subculture. HT1080-MRE11-YFP, as well as HT1080-YFP-MRE11 cells were maintained in selection marker-containing medium (0.4µg/ml puromycin) in order to ensure stable transgenic cells expressing MRE11 tagged with YFP protein. Suspension cells were subcultured every 3 days without exceeding a cell number of 2 million cells per ml of medium. For splitting, the cell suspension was gently pipetted to break clumps and the cell density was determined. Calculated cell volume with desired cell number was re-seeded into a new dish and incubated for growth.

When frozen cells were taken to subculture, they were passaged at least two times before being used in experiments and were discarded after about 40 passages. In all experiments exponentially growing cells were used unless otherwise indicated. The distribution of cells throughout the cell cycle was measured by flow cytometry.

3.2.2 Drug treatments

All inhibitors were dissolved in dimethyl sulfoxide (DMSO), and were applied to culture medium 1h before irradiation unless otherwise indicated. Table 8 presents all used inhibitors/drugs with their mechanism of action and the concentrations used.

Table 8: Used inhibitors with mechanism of action and final concentrations

Drug	Drug description/mechanism of action	Final concentration
Doxycycline hydrochloride	Synthetic tetracycline derivative	1µg/ml
Nocodazole	Interferes with the polymerization of microtubules; cells are prevented to progress through M-phase	0.04µg/ml
Mirin	Inhibits the nuclease activity of MRE11	200µmol/l
NU7441	Specific DNA-PKcs inhibitor	2-5µmol/l

Sterile doxycycline hydrochloride stock solution (2mg/ml) was prepared by dissolving an appropriate amount of doxycycline hydrochloride in ddH_2O and passing it through a 0.22µm filter.

3.2.3 Cell transfection by electroporation

For nucleofection, exponentially growing cells were transfected with pLEGFP-MRE11 plasmid using Nucleofector® II device according to the instructions of the manufacturer.

Typically, $2.5*10^6$ cells were transfected in an Amaxa cuvette with 1.2µg of the pLEGFP-MRE11 plasmid in 100µl of prewarmed (RT) Nucleofector™ solution using T20 program. After transfection cells were grown in special coverslip-bottom imaging chambers for 48-72h prior to live-cell imaging.

3.2.4 Cell synchronization

Cell populations enriched in G1- or G2-phases of the cell cycle were obtained by centrifugal elutriation – a method for isolating cellular subpopulations on the basis of their sedimentation coefficient. For the elutriation process exponentially growing single cell suspension of 140-200 millions cells were placed into a specially designed centrifuge rotor chamber (Beckman JE-6 Elutriation Rotor, Beckman Coulter). They were subjected to a centrifugal field that was balanced by a counter-flow (25ml/min) of medium (culture medium with 1% FBS) that was selected to ensure that cells remained in the chamber and aligned themselves according to size. Cells were then sequentially elutriated out of the rotor based on their size, with small cells coming out first. For an exponentially growing culture, cell size approximates the phase of the cell cycle, with G1-phase cells being small and G2-phase cells being large.

Rotor speeds for cell cycle fractionations of eukaryotic cell populations were usually in the 1,200-3,000rpm range with 100-200rpm steps.

Cell fractions of 250ml were collected by gradually reducing the rotor speed. Cell cycle analysis was carried out by flow cytometry. Typically, cell populations with at least 90% G1-phase cells were obtained in G1-fraction, and 65-75% G2-phase cells in G2-fraction, respectively.

3.2.5 Fluorescence activated cell sorting

Flow cytometry allows measurement of several different cellular parameters as well as cell sorting on the basis of different properties by assessing fluorescence intensity. This technique is also termed as fluorescence activated cell sorting (FACS). For instance, cell cycle distribution can be evaluated by measuring fluorescence intensity of propidium iodide (PI) bound to DNA, as PI binds to DNA proportionally to its mass. Hence, the fluorescence intensity of PI is proportional to the DNA amount present in a cell. Because after replication the DNA amount is doubled, there are twice as many signals generated from G2-phase cells as compared to G1-phase cells. In this way, cells in different cell cycle phases are distinguishable from each other by the DNA amount detected.

For measurements, single cell suspensions of about one million cells were fixed overnight in 70% ethanol at -20°C. Supernatant was removed by centrifugation at 100 x g for 5min, and the pellet was incubated in 500µl of PI stain (40µg/ml PI, 62µg/ml RNaseA; PI stain buffer: 0.1M Tris, 0.1M NaCl, 5mM $MgCl_2$, 0.05% Triton X-100, RNaseA buffer: 10mM Tris, 100mM EDTA, 50mM NaCl, pH 7.6) for 15min at 37°C. Samples were measured in a flow cytometer (Coulter Epics XL, Beckman Coulter) according to pre-established protocols (Table 9); 15,000 events were counted, and gated to obtain standard histograms for each sample. Histogram files (*.HST) were generated by counting the frequency of cells with the same PI signal intensity. The fraction/percentage of cells in different cell cycle phases was automatically calculated using Wincycle™ software. For that, HST files were loaded into Wincycle™, and the parameter “S-phase growing order” was carefully chosen between 0-2 until the prediction model fitted the histogram shape.

Table 9: Settings for flow cytometer, Coulter Epics XL

Parameter	Setting/value
Flow cytometry	Coulter Epics XL
Sheath speed	middle
Total cells sampled	15,000
Maximal running duration	900s
Working mode	carousel
Excitation	488nm
Filter spectrum	655-735nm
FS-PMT	55V
FS-Gain	2
SS-PMT	400V
SS-Gain	1
AUX-PMT	300V
AUX-Gain	2
PI-PMT	520-650V
PI-Gain	2
Discriminator	PI>5
Gate	single

3.2.6 Irradiation

For irradiation experiments exponentially growing cells were plated at the appropriate cell density as required by the experimental protocol, and were grown for two days. In experiments analyzing IRIF, cells were seeded at 125,000 cells onto sterilized 20mm glass cover slips in 35mm dishes with 2ml growth medium, two days prior to IR exposure. In case of using synchronized cells, 500,000 cells were seeded onto poly-L-lysine coated cover slips, and given 1h time to attach before irradiation. To coat cover slips with poly-L-lysine, sterilized cover slips were incubated in 2ml poly-L-lysine solution (1mg/ml) for 15min, followed by a washing step with ddH_2O.

3.2.6.1 X-ray irradiation

X-rays were generated by an x-ray machine (“Isovolt 320HS”, Seifert/Pantak, General Electric-Pantak) with an effective photon energy of approximately 90keV. The machine was operated at 320kV and 10mA using a 1.65mm aluminum filter (GE-Healthcare) to absorb soft x-rays. Dosimetry was performed with a PTB dosimeter (Physikalisch-Technische Bundesanstalt, Braunschweig, Germany) that was used to calibrate an in-field ionization monitor. Radiation dose was confirmed with Fricke’s chemical dosimetry. Even irradiation was ensured by rotating the radiation table. Cells were irradiated with different x-ray doses at a dose rate of 1.3Gy/min. Immediately after IR exposure cells were returned to the incubator, and collected at different times according to the experimental procedure. Unirradiated control cells were treated similarly (sham-irradiated).

3.2.6.2 Neutron irradiation

Neutrons cannot be accelerated like charged particles as they are uncharged. Therefore, neutrons have to be produced in nuclear reactions by accelerating light ions and letting them collide with selected target nuclei, e.g. beryllium nuclei. The ion accelerator used was a rotatable, variable energy “TCC CV-28 cyclotron” operated by the Departments of Nuclear Medicine and Radiotherapy, University Hospital Essen, Germany. This cyclotron provides beams of protons (19MeV), deuterons (13.5MeV) and α-particles (28MeV). Cells were irradiated with different neutron doses (mean energy: 5.8MeV) at a dose rate of 0.3Gy/min in a rectangular 25 x 25cm^2 irradiation field with a photon contamination of ~10%.

3.2.6.3 Heavy ion irradiation

Heavy ion irradiation experiments were performed at the irradiation facility of the Helmholtz Centre for Heavy Ion Research, Darmstadt, Germany (GSI), where ion beams of all elements up to the heaviest, uranium, can be generated in any state of electric charge, and accelerated to nearly the speed of light. The GSI has two different accelerators: (1) UNILAC, a linear 120m long accelerator that accelerates ions up to 20% of light speed, and (2) the heavy-ion SIS synchrotron, shown in Fig. 17, which is able to accelerate ion beams up to 90% of the speed of light in the course of several hundred thousand revolutions.

Figure 17: Outer view of the heavy-ion synchrotron facility (SIS) at the Helmholtz Centre for Heavy Ion Research, Darmstadt, Germany (GSI). Electromagnets, which direct and focus the ion beam, are shown in red and yellow. Copyright: Helmholtz Centre for Heavy Ion Research, Darmstadt, Germany (GSI).

We performed two different experiments at the GSI. Fe and Ni heavy ions, respectively with an ion fluence of $1.12*10^6$ ions/cm^2 per scan were generated by the SIS synchrotron. These heavy ions had a kinetic energy of 1GeV/nucleon, and a corresponding LET of 150keV/µm.

3.2.6.4 Multiphoton irradiation

Multiphoton (MP) absorption processes resulting in light-induced subcellular alterations have been detected in living cells (Calmettes and Berns 1983). The study of MP absorption can yield new information about the basic interactions within and between molecules. Due to the fact that spatial resolution of two-photon (2-P) absorption can produce subcellular destructive events (Berns, Wang *et al.* 2000), MP (2-P) laser irradiation of individual live cells can be used for localized intracellular DNA damage induction. This kind of approach has been already used extensively for cell division, and gene expression analyses in cells with organelles altered by micro-irradiation.

The obvious advantage of near-infrared (NIR) MP laser micro-irradiation consists in its three-dimensional confinement of the lesions as the laser can specifically target single cells and subnuclear structures, such as nucleoli, mitochondria, nuclear membranes, and any other structures that can be labeled and visualized by a fluorescent tag. However, the specificity with respect to damage type is limited. Thus, this technique is a powerful tool to study intracellular protein localization processes as a function of space and time (Meldrum, Botchway *et al.* 2003), enabling investigation of DNA repair dynamics, intracellular signaling, and cell-cell communication processes with a spatio-temporal resolution.

To generate strictly localized and clearly tractable sub-nuclear DNA damage, cells were brought into focus and positioned in such a way that the pulsed 2-P femtosecond laser (Mai Tai® Tsunami Ti:sapphire laser, Spectra-Physics) would center on a cell nucleus. The region to be damaged was always of the same size and shape (bleaching points). Laser treatment was done at constant maximum laser output power of 80mW to exclude variations in dose. Time of cell exposure to the focused laser beam was 850ms (pulse width <100fs, pulse repetition rate ~80MHz, MP gain 40%, MP offset 65%, Attenuation min). This process was controlled by a software-connected internal electromechanical shutter.

3.2.7 Immunofluorescence staining

For immunofluorescence staining, cells were briefly washed with cold 1x PBS, fixed in 2ml 2% paraformaldehyde (PFA) for 15min at room temperature (RT), washed with 1x PBS, permeabilized in 2ml P-solution (100mM Tris, pH 7.4, 50mM EDTA, 0.5% Triton X-100) for 10min at RT, again washed with 1x PBS and finally blocked in 2ml PBG blocking solution (0.2% gelatin, 0.5% BSA fraction V in 1x PBS, pH 7.4) overnight at 4°C or for 1h at RT.

Primary and conjugated secondary antibodies (Table 4) were diluted 1:200 and 1:400 in PBG, respectively; 70µl of the antibody solution were dispensed on parafilm, cover slips were mounted on top of the antibody solution and incubated at RT for 1.5h with primary antibodies and for 1h with secondary antibodies.

After each antibody incubation, cover slips were returned into the dishes and washed three times with 1x PBS for 5min each. Subsequently, cell nuclei were counterstained in 2ml 4',6-diamidino-2-phenylindole (DAPI) solution (2µg/ml DAPI, 0.1M Tris, 0.1M NaCl, 5mM $MgCl_2$, 0.05% Triton X-100), with a final DAPI concentration of 50ng/ml, for 15min at RT, three times washed with 1x PBS and mounted in 13µl ProLong® Gold antifade reagent on microscope slides. For the polymerization of ProLong® Gold antifade, slides were kept in the dark for at least 24h at RT and then stored at 4°C before analysis.

However, immunofluorescence staining with anti-MRE11 antiserum, after fixing the cells with PFA, exhibited very high background signals, thus making MRE11 foci analysis impossible (data not shown). High background signals can be a consequence of remaining non-bound protein; probably because of high cross-linking ability of PFA, and the high nuclear abundance of the MRN complex. To reduce background signal of non-bound MRE11 in the nucleoplasm, cell fixation was performed using a methanol-acetone fixation protocol. For this purpose, cells were fixed in 2ml 100% methanol for 20min at -20°C, permeabilized in acetone for 10s at RT, washed with 1x PBS and blocked in 2ml 10% FBS in PBS solution overnight at 4°C, or alternatively 1h at RT.

3.2.8 Confocal laser scanning microscopy

In contrast to conventional two-dimensional light microscopy, CLSM comprises three process steps: (1) line-by-line scanning of the specimen with a focused laser beam (monochromatic light of a discrete wavelength) deflected in X-Y directions by means of two mirrors mounted on two so-called – galvanometric scanners, (2) pixel-by-pixel detection of the fluorescence emitted by the scanned specimen details, by means of a photomultiplier tube (PMT), and (3) digitalization of the optical object information contained in the electrical signal provided by the PMT (Wilhelm, Gröbler *et al.* 2009).

The decisive design feature of a CLSM compared to a conventional microscope is the confocal aperture – the pinhole, a small diaphragm in front of the detector, arranged in a plane conjugate to the intermediate image plane and thus to the object plane of the microscope. As a result, the detector (PMT) can only detect light that has

passed the pinhole. The significant amount of fluorescence emission that occurs at points above and below the objective focal plane is not confocal with the pinhole, and is termed as “out-of-focus light rays”; this extraneous light is not detected by the PMT, and does not contribute to the resulting high-resolution optical image. By varying the pinhole diameter, the degree of confocality can be adapted to practical requirements (Claxton, Fellers *et al.*).

In a CLSM system a laser beam passes through a light source aperture, and is then focused to a diffraction-limited spot, using a diffraction mirror, which illuminates only a small focal volume at a time within or on the surface of a specimen. After illuminating this defined focal plane, secondary fluorescence emitted from illuminated points on the specimen in the same focal plane, passes back through the dichroic mirror, and is focused as a confocal point at the detector pinhole aperture. Thus, specimens are irradiated in a pointwise fashion, where the point illuminated and the point observed are situated in conjugate planes, i.e. they are focused onto each other. The result is what is called a confocal beam path. In order to obtain information about the entire specimen, it is necessary to guide the laser beam in X and Y directions across the specimens. A schematic diagram of CLSM key components is shown in Fig. 18.

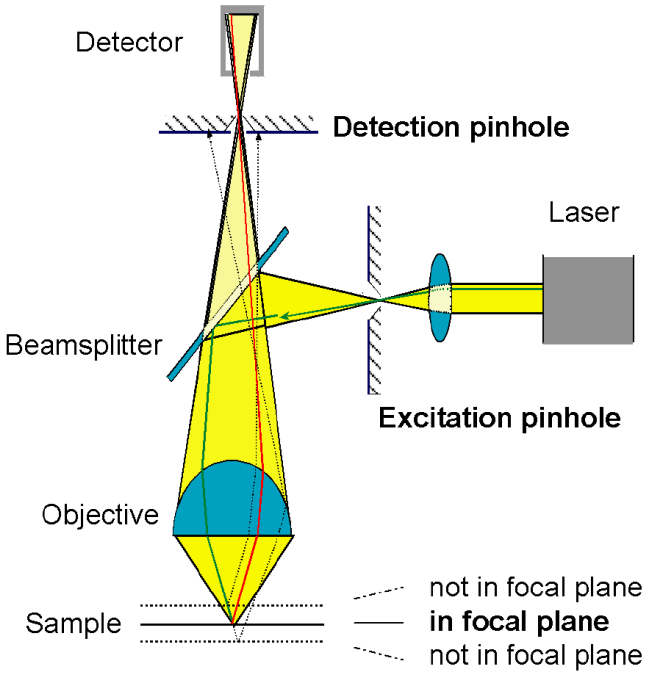

Figure 18: Schematic diagram of principal components and optical pathway in a CLSM system. Illustration from: Leica Microsystems, Mannheim, Germany.

In addition, to observe a single plane (or slice) of a thick specimen in good contrast, optical sectioning allows a great number of slices to be cut and recorded at different planes of the specimen, with specimens being moved along the optical axis (Z) by controlled increments. The result is a 3-dimensional data set – a "z-stack", which provides information about the spatial structure of the object (Wilhelm, Gröbler *et al.* 2009). Moreover, by using more than one fluorescent dye with different spectral properties, several target molecules can be identified simultaneously (Wilhelm, Gröbler *et al.* 2009). Taken together, the CLSM system is used to acquire high-resolution optical images with depth selectivity, in both, fixed specimens and living cells.

3.2.8.1 Live cell imaging by CLSM imaging systems

Live cell imaging is the observation of living cells over time using images acquired by imaging systems such as confocal scanning microscopes. CLSM systems can record images like a camera, and can therefore be used to record a series of time-resolved confocal images, known as a time series. Such time-lapse experiments provide an important tool in studies of cell physiology, cellular developmental and cancer biology, whenever interest is focused on the visualization and quantification of cellular dynamic changes. Thus, live-cell imaging provides critical insights into the fundamental nature of cellular and tissue functions.

A major challenge of live cell imaging is keeping cells alive and functioning as naturally as possible for the duration of the experiment since fluorescence illumination, especially in the UV range, is harmful for cells, and causes photobleaching and phototoxicity. The use of high power lasers as an excitation source adds to this challenge. Successful experiments must be designed to minimize such specimen illumination whilst maintaining an appropriate environment for the cells. Fig. 19 represents a general setup of a live cell imaging apparatus with heating capabilities, consisting of a microscope inside an environmental chamber. Within this temperature-controlled system for microscopes, cells can be maintained at an appropriate temperature.

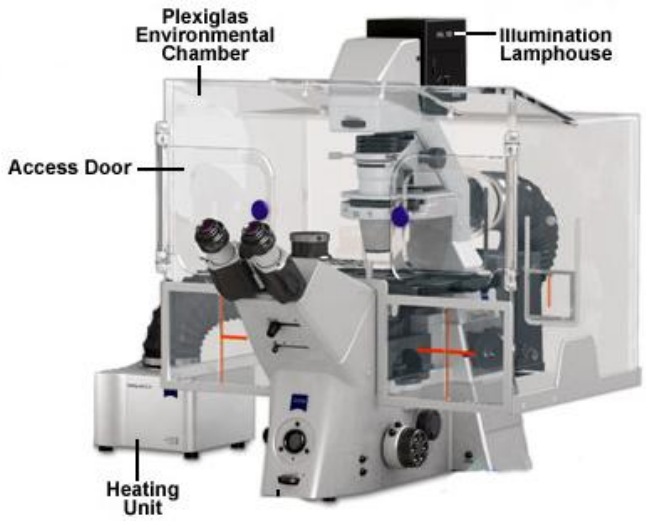

Figure 19: Schematic illustration of a live cell imaging microscope inside an environmental chamber. Illustration from: Carl Zeiss Microscopy, Jena, Germany.

For live cell imaging experiments, human fibroblasts (HT1080-MRE11-YFP and HT1080-YFP-MRE11 cells; detailed described in Table 7) that stably express yellow fluorescent protein (YFP) tagged to MRE11, were grown in 35mm coverslip bottom dishes with 2ml growth medium at an initial cell number of 300,000 cells for 24h. In experiments using cells that transiently express MRE11 tagged to a green fluorochrome (GFP), CHO-10B4 and MEF-PK34N cells were grown in coverslip bottom live cell imaging chambers for 48-72h post transfection (transfection conditions in 3.2.3).

The requirement of keeping cells at 5% CO_2 during the investigation span can be minimized by using 4-(2-hydroxyethyl)-1-piperazineethanesulfonic acid (HEPES) buffered medium, e.g. L-15 Leibovitz medium, which was formulated for the use in CO_2-free systems requiring sodium bicarbonate. Hence, before starting live cell imaging experiments, growth medium was exchanged with 1ml of L-15 Leibovitz medium to ensure proper and stable pH for the duration of experiment. The software was programmed to start image sequence acquisition just before irradiation for an initial control image, and immediately after damage induction to take z-stack images for 1-8h in 5min intervals. Further details concerning image acquisition and image analysis are described below. Normally, the scanned field included also some unirradiated cells, to ensure a proper control for protein accumulation at damage sites.

3.2.9 Image acquisition and digital image analysis

For image acquisition, fixed, immunofluorescently stained cells were imaged at a resolution of 1024 x 1024 and a zoom factor of 1.2, resulting in a pixel size of 240.74nm, whereas live cells were imaged in a 512 × 512 pixel format and a zoom factor of 3. Fluorescence protein signals were visualized by exciting fluorochromes with an appropriate laser line, and by detecting the spectral range of the fluorescence emitted with proper PMT gain and offset settings. To minimize photobleaching of fluorescence protein-signal during data collection, laser power was kept at about 10-15% of maximum. Scanning parameters, like laser intensity, PMT gain and offset settings (Table 10, 11) were individually adjusted for different fluorochromes, and kept constant within an experiment to ensure comparability of data. When using multiple fluorescent proteins, bidirectional scans were applied in a sequential scan modus with predefined scanning parameters in order to avoid cross talk between different channels.

Table 10: Image acquisition settings of the confocal microscope, Leica TCS SP5

Parameter	Mode/setting/value
Instrument parameter setting	Confocal LMD
Argon laser intensity	30%
Objective	HCX PL APO lambda blue 63.0x1.4 OIL UV
Sequential scan	Between stacks
Speed	400Hz
Refraction index	1.52
Scan direction	Bidirectional
Pinhole	1
Frame average	2
Frame accumulation	2
Line average	2
Line accumulation	2
Zoom	1.2-3
Resolution	512 x 512 or 1024 x 1024, 8bits
Z-step size	0.5µm

Typically, at least 5 fields were scanned by taking z-stack images with 0.5µm steps. After each scan, three-dimensional data sets (LIF files), and maximum intensity projection TIFF images of the field scanned were generated and processed for further analysis.

Table 11: Scanning parameters for the detection of fluorescent proteins by CLSM

Fluorochrome / parameter	DAPI	Alexa-488; GFP	YFP	Alexa-568	Alexa-633
Excitation	405nm	488nm	514nm	568nm	633nm
Laser intensity	15%	10-15%	10%	15%	15%
Detected spectral range	410-480nm	495-560nm	520-580nm	570-635nm	640-760nm
PMT gain	500-750V	550-850V	650-1200	650-850V	750-950V
PMT offset	-0.3V	-0.3V	-0,3	-0.3V	-0.3V

The recorded (time-resolved) z-stack images were analyzed for foci numbers, foci colocalization, fluorescence total signal intensity, and protein accumulation dynamics at damaged sites, using the quantitative image processing software – ImarisXT® 6.0 (Bitplane).

LIF files of imaged live cells were processed with the “Easy 3-D” mode, and subsequently converted into video clip files to visualize protein accumulation, and dissociation dynamics in a spatio-temporal resolution. In contrast, foci number and foci colocalization analyses were achieved by using “spots”, “split spots” and “colocalize spots” functions, respectively. During foci analysis, a gray value threshold was set to separate signal from background. This threshold value varied from 12 to 20, and was kept constant throughout one experiment in order to be able to compare the data. Only objects with a minimum diameter of 0.5µm and intensity above the threshold were counted as foci. For each dose and repair time point, about 200 cells were analyzed. Finally, mean foci number per nucleus, standard deviation as well as standard error were calculated using Microsoft Excel 2007® and graphs generated with SigmaPlot® 11.0.

3.2.10 Biochemical protein fractionation

For sub-cellular biochemical protein fractionation, 2-3x10^6 cells were collected with a cell scraper and washed twice in 1x PBS. Pellets were resuspended and incubated for 10min on ice in 200µl cytoskeleton buffer (10mM Hepes-KOH (pH 6.8), 100mM NaCl, 300mM sucrose, 1mM EGTA (pH 8.0), 3mM $MgCl_2$, 0.5% Triton X-100, 0.2mM PMSF, 1mM DTT), containing 1x protease inhibitor cocktail (complete inhibitors). Skeletal frameworks were pelleted by centrifugation at low speed (700 x g, 5min, 4°C) and 2/3 of the supernatant was collected. The insoluble pellet was incubated in 200µl buffer A (10mM Tris-HCl (pH 8.0), 10mM NaCl, 250mM sucrose, 1mM EGTA (pH 8.0), 5mM $MgCl_2$), containing 1x protease inhibitors and 0.2M ammonium sulphate, in order to extract proteins that are loosely attached to chromatin. After 10min incubation on ice, insoluble chromatin-bound proteins were collected by centrifugation at 2,000 x g for 5min at 4°C; eluted proteins were added to the previous supernatant. Total supernatant was clarified by high speed centrifugation (10,000 x g, 10min, 4°C) and termed as soluble protein fraction. Final insoluble chromatin-enriched nuclear fraction, containing chromatin-bound proteins was resuspended in 50µl of 2x Laemmli sample buffer (126mM Tris-HCl (pH 6.8), 0.01M EDTA, 10% glycerol, 3% SDS, 0.02% bromophenol blue, 1/20 2-mercaptoethanol), and subjected to five pulses of sonication.

3.2.11 Electrophoresis and immunoblotting

3.2.11.1 Cell lysate preparation and electrophoresis

For cell lysate preparation, 2-3x10^6 cells were once washed with cold 1x PBS by centrifugation and subsequently lysed in 200µl cold RIPA buffer (ready-to-use cell lysis reagent), containing 1x protease inhibitor cocktail. After 30min incubation on ice, cell lysate was spun down (14,000 x g, 15min, 4°C) to pellet cell debris, and the supernatant, with mostly all membrane, cytoplasmic, soluble and nucleoplasmic proteins, was transferred into a new tube. Protein concentration in solution was determined by colorimetric Bradford assay. RIPA buffer cell lysates or biochemically fractionated soluble protein reactions were mixed with 50µl 2x Laemmli sample

buffer, denaturated at 95°C for 5min and spun down for 1min at 13,000 x g before electrophoresis. Protein separation was performed by electrophoresis on SDS-polyacrylamide mini gels (“Mini PROTEAN”, Bio-Rad), consisting of a 5% stacking gel and a resolving gel of varying polyacrylamide concentrations. RIPA buffer cell lysates and biochemically fractionated soluble protein reactions were loaded with a total protein amount of 20µg on SDS-10% polyacrylamide gels, whereas only 3-5µl of chromatin-bound protein reactions were electrophoresed on SDS-12.5% polyacrylamide gels at a constant voltage of 130V for 1.5h at RT. SDS-PAGE gels were cast following instructions of the manufacturer.

3.2.11.2 Immunoblotting and western blot detection

For western blot analysis, electrophoretically resolved proteins were transferred onto a nitrocellulose membrane using the “iBlot® Dry Blotting System” (Invitrogen) following the manufacturer’s instructions. The self-contained iBlot® device uses disposable blotting stacks with integrated nitrocellulose membranes that efficiently and reliably blots proteins from polyacrylamide gels on membranes in less than 10min without the need for additional buffers or an external power supply. Equal loading and transfer was monitored by immunodetection with antibodies against appropriate protein fraction loading controls. After transfer, gels were removed from the blotting stacks and stained in Coomassie Brilliant Blue R 250 solution (0.02% Coomassie Brilliant Blue R 250, 2% (w/v) phosphoric acid, 5% aluminum sulphate in 10% ethanol) overnight with gentle agitation, whereas membranes were incubated in blocking buffer (5% non-fat dry milk in PBS-T (0.05% Tween-20 in 1x PBS)) for 1h at RT or overnight at 4°C. Subsequently, membranes were incubated with the primary antibody overnight at 4°C, gently washed 3 times for 10min with PBS-T and probed with the secondary antibody for 1h at RT. Primary antibodies were diluted 1:5000 in PBS-T containing 2.5% non-fat dry milk, whereas secondary antibodies were diluted 1:10,000 (Table 4 includes all used antibodies). Subsequently, membranes were gently washed 3 times for 10min with PBS-T and processed for western blot detection using “Odyssey® Infrared Imaging System” (LI-COR Biosciences) following instructions of the manufacturer.

3.2.12 Pulsed field gel electrophoresis – PFGE

Pulsed field gel electrophoresis (PFGE) was introduced by Stamato and Denko in 1990 (Stamato and Denko 1990) and is a specific technique to measure IR-induced DSBs. This technique takes advantage of the fact that fragmentation of chromosomal DNA with radiation leads to a linear dose-dependent increase in the fraction of DNA that enters the gel, whereas intact mammalian chromosomes are unable to enter the gel. PFGE resolves DNA fragments ranging in size from 0.2-6Mbp, and detects damage induced by as little as 2Gy of x-rays, whereas gel electrophoresis with a constant electric field cannot resolve DNA fragments much above 50kbp.

To evaluate induction of DSBs at different radiation doses (i.e. dose response experiment) asynchronous cells were used. Cells were resuspended in cold HEPES-buffered (20mM HEPES, 5mM $NaHCO_3$) serum-free media, and mixed with an equal volume of pre-warmed (50°C) HEPES-buffered serum-free media containing 1% low melting agarose to reach a concentration of $3x10^6$ cells/ml. The cell-agarose suspension was then pipetted into 3mm diameter glass tubes and placed into ice to allow for solidification. Solidified cell-agarose suspension was extruded from glass tubes and cut into 5mm long cylindrical plugs containing approximately $2x10^5$ cells/plug. Subsequently, agarose plugs were placed in a 60mm dish containing 5ml cold serum-free medium and exposed to different x-ray doses (3.2.6.1). Plugs were immediately placed in lysis buffer (10mM Tris-HCl, 50mM NaCl, 100mM EDTA, 2% N-lauryl sarcosine (NLS), pH 7.6 and freshly added 0.2mg/ml protease), and incubated first at 4°C for 1h and then at 50°C for 16-18h.

For repair kinetics of IR-induced DSBs, irradiated cells were returned to the incubator for the indicated repair times. After completion of the repair time interval, cells were collected by centrifugation at 100 x g for 5min at 4°C and embedded into agarose. This was followed by an immediate lysis step as described above. For each dose and repair time point at least four plugs were prepared. Due to technical difficulties in determining the 0h repair time point, the initial value of repair kinetics was obtained from dose response curves. After lysis, agarose plugs were washed with washing buffer (10mM Tris-HCl, 50mM NaCl, 100mM EDTA, pH 7.6) for 1h at 37°C while gently shaking, and were then treated for 1h at 37°C in the same buffer with 0.1mg/ml freshly added RNase A.

To determine the signals generated by non-irradiated cells as background, cells from identically treated non-irradiated cultures were processed at pre-defined times, e.g. 15min and 4h.

Asymmetric field inversion gel electrophoresis was used for quantification of IR-induced DSBs. This was carried out in 0.5% agarose gels containing 0.5µg/ml·ethidium bromide (stock solution 10mg/ml in ddH_2O). Agarose plugs were loaded into the gel-wells and sealed with 1% agarose. Gel electrophoresis was run in 0.5x TBE buffer (45mM Tris, 4.5mM boric acid, 0.1mM EDTA, pH 8.8) using conventional gel boxes (Horizon 20•25, Life Technologies™) connected to a switching apparatus that regulated both, forward and reverse pulse times as well as voltages, from a standard power supply (PowerPac™ HC, Bio-Rad). PFGE was performed with 40 alternating cycles – a 900s pulse of 1.25V/cm in (forward) direction of DNA migration, followed by a 75s pulse of 5V/cm in reverse direction. Before starting electrophoresis, 0.5x TBE buffer was pre-cooled through an external cooling unit (DC10-K20, Thermo Fischer Scientific) to 8°C and circulated at constant temperature throughout the run. After electrophoresis, the gel was scanned with a FluorImager (Typhoon™ 9410, Molecular Dynamics) using appropriate settings (see Table 12).

Table 12: Scanning Parameters for FluorImager, Typhoon™ 9410

Mode	Setting
Acquisition mode	Fluorescence
Laser	Green (532)
PMT gain	470V
Sensitivity	Normal
Emission filter	610 BP SPYRO RyPy EtBr
Pixel size	200 microns
Focal plane	+3mm

To estimate DSBs, the fraction of DNA released (FDR) was calculated using ImageQuant™ 5.0. The FDR parameter is defined as the fraction of DNA found in the lane and is calculated by dividing the signal in the lane with the total signal of the sample; it is equivalent to the fraction of unrepaired DSBs in the sample.

Measured FDR in non-irradiated cells (background) was subtracted from the FDR of irradiated cells. When induction of DSBs was measured at different radiation doses, FDR was plotted against radiation dose to obtain dose response curves. In order to facilitate the inter comparison of results obtained, and to account for differences in the dose response curves between different cell lines and experiments, repair kinetics are not presented as FDR versus time but rather as dose equivalent (DEQ) versus time. We used dose response curves to estimate DEQ values from each FDR value. This way of analysis has an advantage as it corrects for non-linear dose response curves. Repair kinetics curves were fitted using non-linear regression analysis to calculate repair half times. In general, two components were assumed to exist in the repair curves and fitting algorithms were selected accordingly. For all graphs and curve fitting analyses SigmaPlot® 11.0 was used.

4 Results

4.1 Analysis of nuclear MRN relocalization dynamics in response to IR

As discussed above, the precise functions of the MRN complex, although clearly critical for the cellular DDR, are only incompletely understood, and are therefore presently under intensive investigation. We reasoned that analysis of the dynamics of foci formation and decay for proteins implicated in DDR will yield relevant insights into their function. Therefore, as a first step, we studied the IRIF dynamics of MRN in different cell types after exposure to IR of different LET. Experiments were carried out either by monitoring time-resolved MRE11-GFP/YFP protein accumulation to DNA damage sites in live cells, or by quantitatively analyzing, using LSCM, IR-induced MRN foci in cells fixed after irradiation and repair.

4.1.1 MRE11 forms foci after IR

We used indirect immunofluorescence to examine the response of MRE11 to radiation-induced DNA damage. We wished to examine whether MRE11 foci form in cells exposed to low LET radiation. For this purpose, several repair-proficient, human cell lines were used in the exponential phase of growth. These included: A549, MRC5-SV1, M059K and HT1080 cells (see Table 7 for more information regarding cell origin and other cell line characteristics). Cells were irradiated with 1Gy x-rays, and immediately returned to pre-irradiation conditions. Cells were subsequently fixed and stained with an anti-MRE11 antibody, while DNA was counterstained with DAPI. LSCM was used to image randomly selected cell nuclei. Representative micrographs of captured images from unirradiated as well as irradiated cells are presented in Fig. 20.

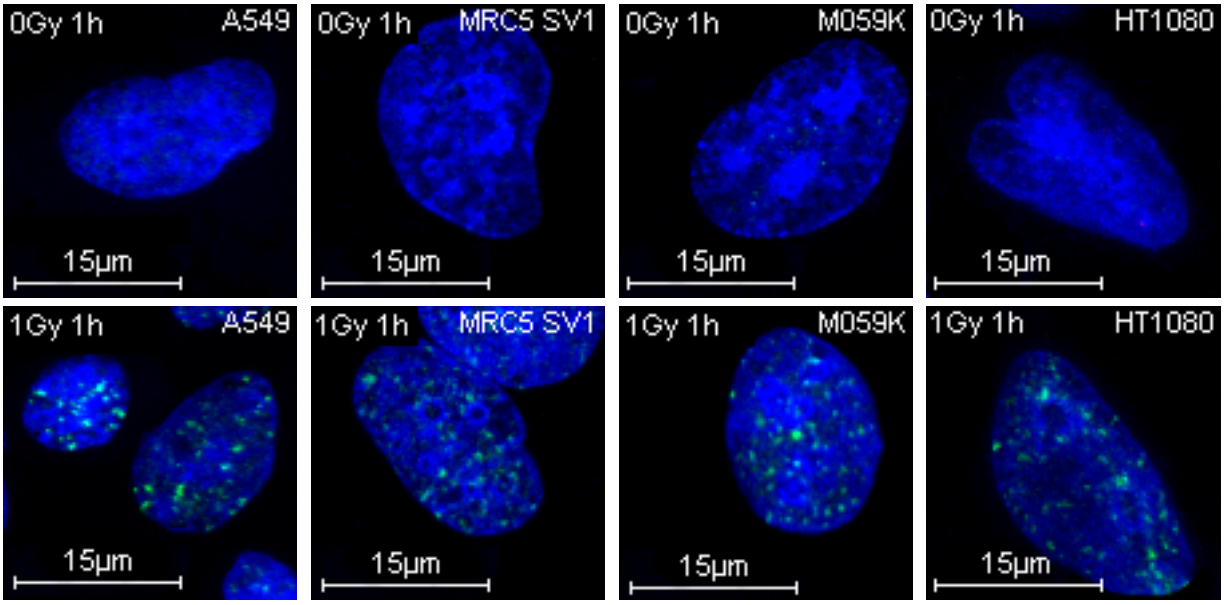

Figure 20: MRE11 forms nuclear foci in response to IR. Cells shown were either mock irradiated (upper panel) or irradiated with 1Gy x-rays (lower panel), and fixed 1h post-irradiation. Cells were then processed for immunofluorescence staining with an anti-MRE11 antiserum (green) while the DNA was counterstained with DAPI (blue). Merged maximum intensity projection (MIP) images represent an overlay of the green and blue channels.

Evidently, after IR all tested cell lines showed detectable MRE11 protein accumulation to discrete nuclear foci, visible in the majority of irradiated cells (up to 95%). In contrast, almost no MRE11 foci could be detected in unirradiated cells. Non-specific binding of the fluorochrome-labeled secondary antibody (Alexa Fluor 488), or auto-fluorescence was not observed in cells only stained with the secondary antibody or with DAPI. Moreover, DAPI counterstaining of irradiated cells indicated that IRIF-containing nuclei were not grossly aberrant, and did not show signs of apoptosis. In line with this, flow cytometry analysis of irradiated cells did not detect a significant population of apoptotic cells (data not shown).

4.1.2 MRE11, RAD50 and NBS1 IRIF colocalize within the cell nucleus

Due to the fact that MRE11, RAD50 and NBS1 proteins act as a complex, we wondered whether IRIF of each of these proteins colocalize within the cell nucleus. Hence, exponentially growing A549 cells were irradiated with 1Gy x-rays and fixed 1h post-irradiation. Indirect immunofluorescence and LSCM were applied to visualize nuclear IR-induced foci forming from MRN proteins. Fig. 21 shows characteristic images of unirradiated control and irradiated A549 cells.

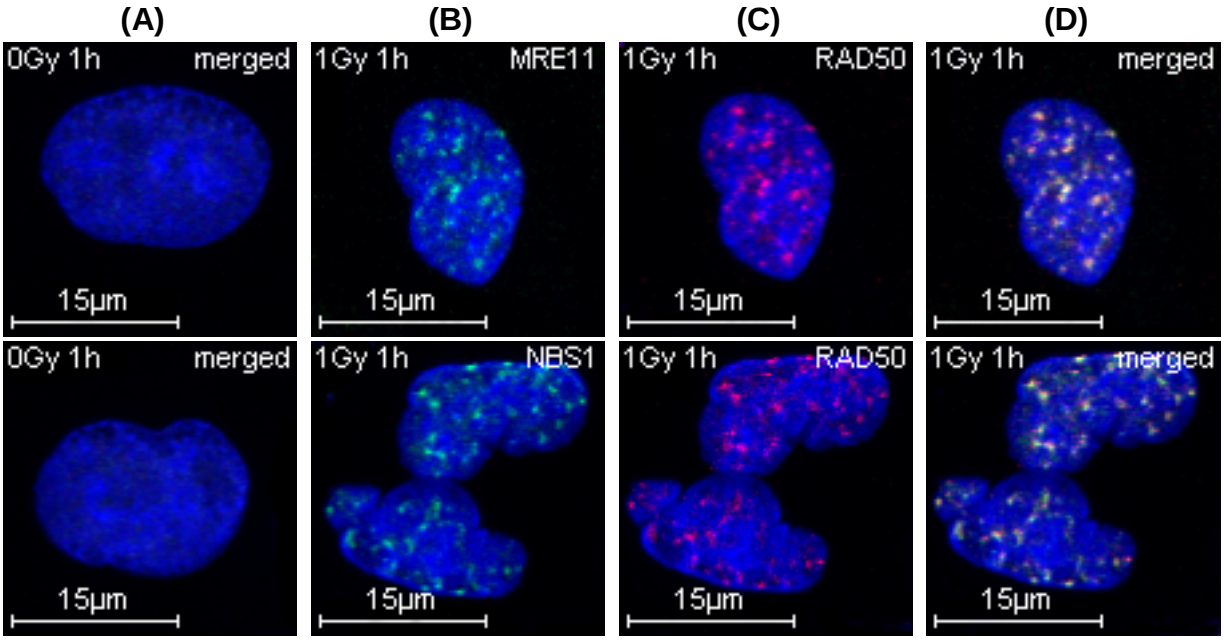

Figure 21: Nuclear MRE11, RAD50 and NBS1 foci colocalize after treatment with IR. Human lung carcinoma A549 cells were either left untreated (A), or irradiated with 1Gy x-rays (B-D). Image acquisition of cell nuclei following immunofluorescence staining of the MRN proteins with anti-MRE11 and anti-RAD50 (upper panel), and with anti-NBS1 and anti-RAD50 antibodies (lower panel), respectively were performed. MIP overlay images of all three recorded channels are presented in (D). Color allocation: DAPI (blue), MRE11 or NBS1 (green), RAD50 (red).

It is evident, that MRE11, RAD50 and NBS1 proteins formed nuclear foci in response to radiation (Fig. 21 B-C), whereas unirradiated control cells (Fig. 21 A) displayed no such foci.

In addition, simultaneous immunofluorescence analysis of nuclear IR-induced MRE11, RAD50 and NBS1 foci revealed a strong colocalization (>80%) between the MRN proteins (Fig. 21 D), in agreement with their function as a complex. In summary, this data clearly showed that MRN foci formation was highly radiation-dependent. This observation implicated the formation and the function of MRN in the cellular responses to DNA damage.

4.1.3 MRE11 interacts with damaged DNA *in vivo*

The interpretation that nuclear MRN foci formation after IR is DNA damage dependent, and that it reflects the interaction of the MRN complex with damaged DNA could be further tested by partial-volume irradiation using high power lasers. The methodology permits induction of highly localized DNA damage in discrete sub-nuclear volumes of individual cells. For this purpose, repair-proficient human HT1080 fibroblasts (HT1080-YFP-MRE11 and HT1080-MRE11-YFP fibroblasts), were generated that stably express YFP-tagged MRE11 protein (either N- or C-tagged), and tested in the exponential phase of growth (detailed cell line characteristics in Table 7). In addition, rodent CHO-10B4 and MEF-PK34N cells, transiently expressing MRE11-GFP protein, by transfection with the pLEGFP-MRE11 plasmid (3.2.3), were used for experiments. Indicated cells were exposed to a pulsed 2-P, or an UV laser to induce localized DNA damage. After this treatment, cells were analyzed to record time-resolved MRE11 protein accumulation to the DNA damage sites.

Before laser irradiation, an initial control image was taken as reference. Moreover, fields containing micro-irradiated as well as unirradiated cells, were scanned to provide an internal control for specific IR-induced MRE11 protein accumulation to damaged DNA. Fig. 22 shows the intracellular relocalization of MRE11 to the sites of DNA damage induced by this approach. Similar results were also obtained in cells exposed to UV laser (data not shown).

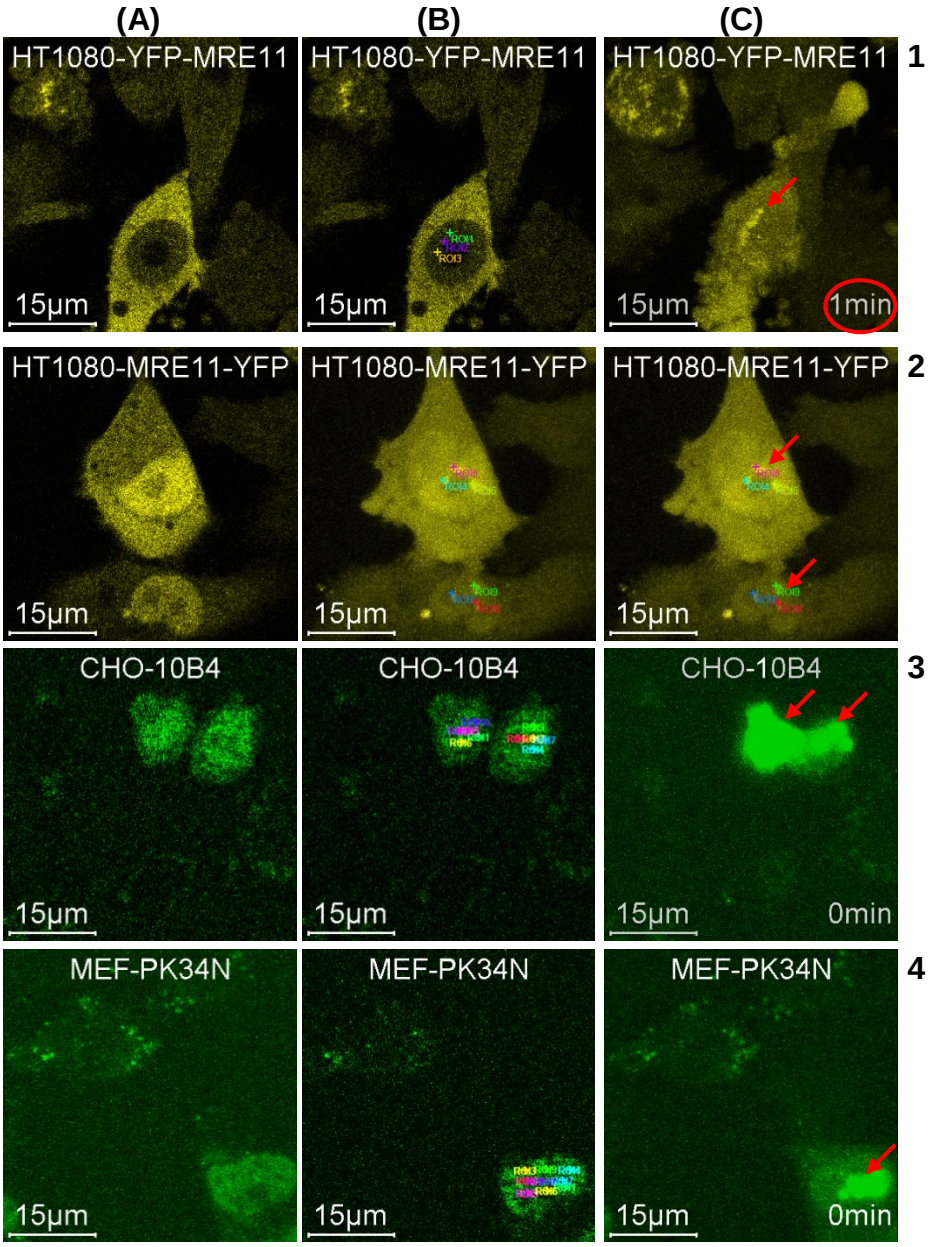

Figure 22: MRE11 rapidly accumulates to sites of localized DNA damage. Control images of unirradiated cells are shown in column (A). Subnuclear areas (B) were exposed to a pulsed 2-P laser, each for 850ms. Z-stack images, taken at the indicated times after laser irradiation, show a prompt MRE11 protein accumulation to the DNA damage sites (red arrows in column C). All pictures shown are MIPs.

It is evident, that upon localized DNA damage all examined cell lines showed a fast redistribution of intracellular MRE11 to the sites of DNA damage (Fig. 22 C).

However, nuclear MRE11 protein accumulation in irradiated HT1080-YFP-MRE11 cells (Fig. 22 C-1) was slower in comparison to other examined cell lines (Fig. 22 C-2-4). The HT1080-YFP-MRE11 cell clone expresses N-terminally tagged MRE11-YFP protein. It is likely that this protein somehow hinders the function of MRE11 and delays its localization to the sites of DNA damage.

In aggregate, these results demonstrated a prompt association and interaction of MRE11 with damaged DNA. We concluded that MRN foci formation was DNA damage-dependent.

4.1.4 IR-induced MRE11 foci have qualitatively distinguishable features

The analysis of MRN IRIF in different repair-proficient cell lines (described below, in 4.1.5) revealed distinct qualitative features regarding localization patterns as a function of radiation dose and post-irradiation time. Images in Fig. 23 illustrate IR-induced MRE11 foci in A549 cells in a typical experiment. Data of RAD50 and NBS1 IRIF, showed similar responses in all cell lines tested, and are therefore not shown here separately.

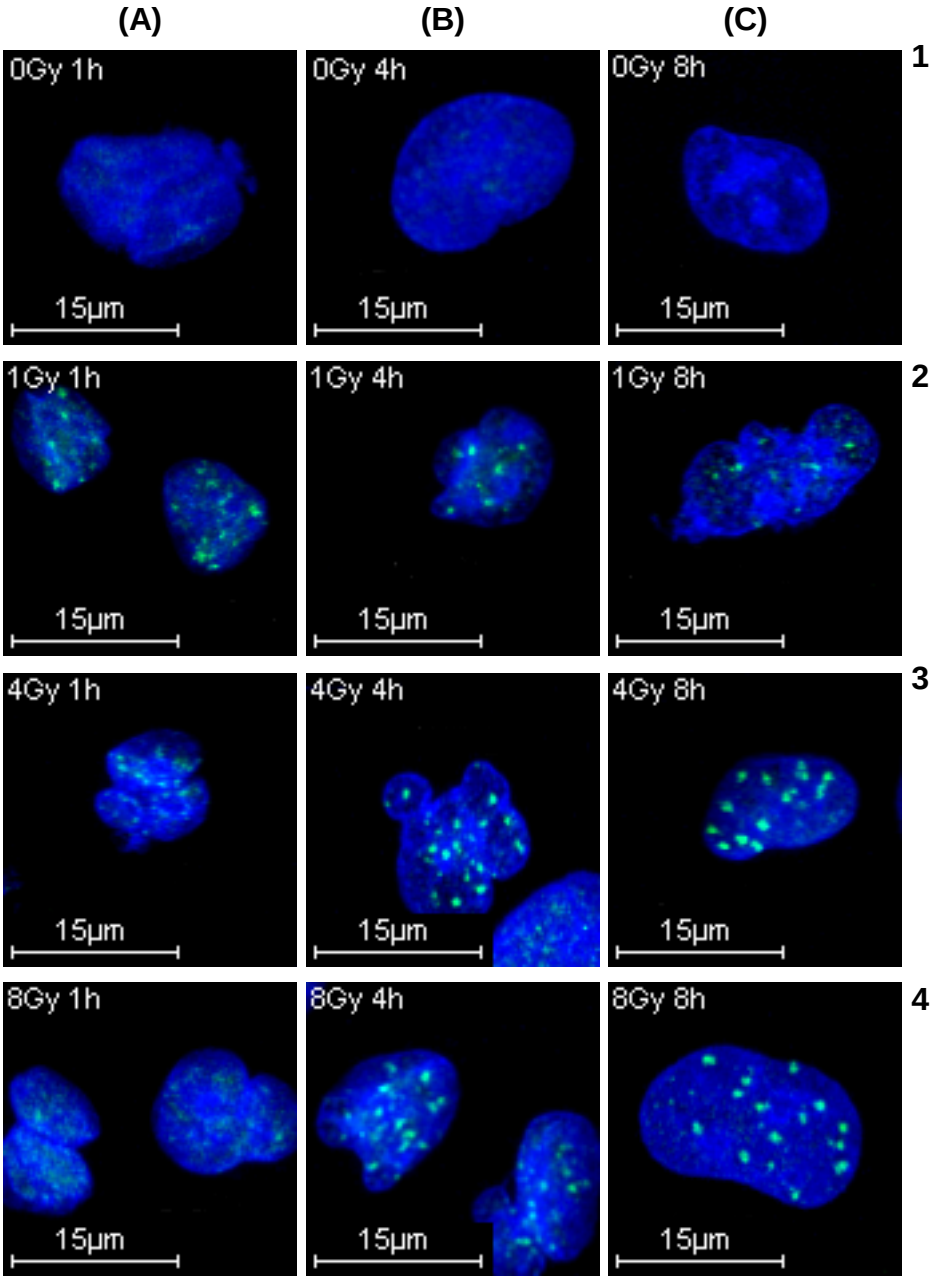

Figure 23: MRE11 IRIF show different patterns depending on the observation time. Exponentially growing A549 cells were either mock irradiated (panel 1), or exposed to different x-ray doses; 1Gy = panel 2, 4Gy = panel 3, 8Gy = panel 4. Cells were fixed at various times after IR (1h = (A), 4h = (B) 8h = (C)), and MRE11 was visualized. Overlays of green and blue channels are displayed as MIP images.

It is evident that in response to radiation different MRE11 foci localization patterns were observed, depending on applied radiation dose and post-irradiation time. One hour after IR exposure, a punctuate pattern of evenly distributed small MRE11 IRIF was detected (Fig. 23 A 2-4).

These small MRE11 foci begun to change at about 4h after irradiation to large, irregularly shaped and more sparsely distributed foci (Fig. 23 B/C 2-4). Interestingly, this was only observed after irradiation with a low x-ray dose of 1Gy. After high radiation doses (4-8Gy) the early response diminished leaving the late and large MRE11 foci to dominate. Thus, two distinct MRE11 localization patterns could be distinguished: small MRE11 IRIF mainly detected at early time points; and late developing larger MRE11 foci that persisted for up to 8h after exposure to IR.

4.1.5 The bimodal response of MRN IRIF is cell cycle-independent

As discussed above, among proteins involved in DDR, MRN takes a unique place through its apparent intimate involvement in the cellular response to DNA damage and DSB repair (1.5.2, 1.5.3). IRIF of many DDR factors form, more or less, in all phases of the cell cycle. An exception to this rule, presents proteins that effectively form foci only in association with ssDNA formation generated by DNA resection – a process that appears to reach a maximum in S/G2-phase of the cell cycle. We were thus wondering whether MRN IRIF formation is cell cycle-dependent. This is because, MRN is involved, on the one hand in DNA damage sensing, which occurs irrespective of the cell cycle phase and, on the other hand in DSB repair by HRR, which operates in the S/G2-phase of the cell cycle.

For this purpose, we examined several repair-proficient cell lines in G1- and G2-phase of the cell cycle IR-induced MRN foci formation. We started with the human lung carcinoma A549 cell line, which is deficient in mismatch repair, but express a wild-type p53. The presence of a functional p53 in A549 cells is advantageous to our studies, as it leaves intact important DNA damage signaling cascades (Tanaka, Huang *et al.* 2007). Thus, enriched G1- and G2-phase A549 cells were irradiated with 0, 1, 4 or 8Gy, and MRE11, RAD50 and NBS1 protein localization was measured by immunofluorescence on fixed samples using CLSM. For a quantitative analysis we measured over 200 cell nuclei for MRE11, RAD50 or NBS1 foci at different times after exposure to different doses of radiation.

The cell cycle specific time course of IR-induced MRN foci dynamics in G1- and G2-phase A549 cells after different radiation doses are summarized in Fig. 24 A-D. Comparable results were obtained for RAD50 and NBS1 and were therefore omitted for clarity.

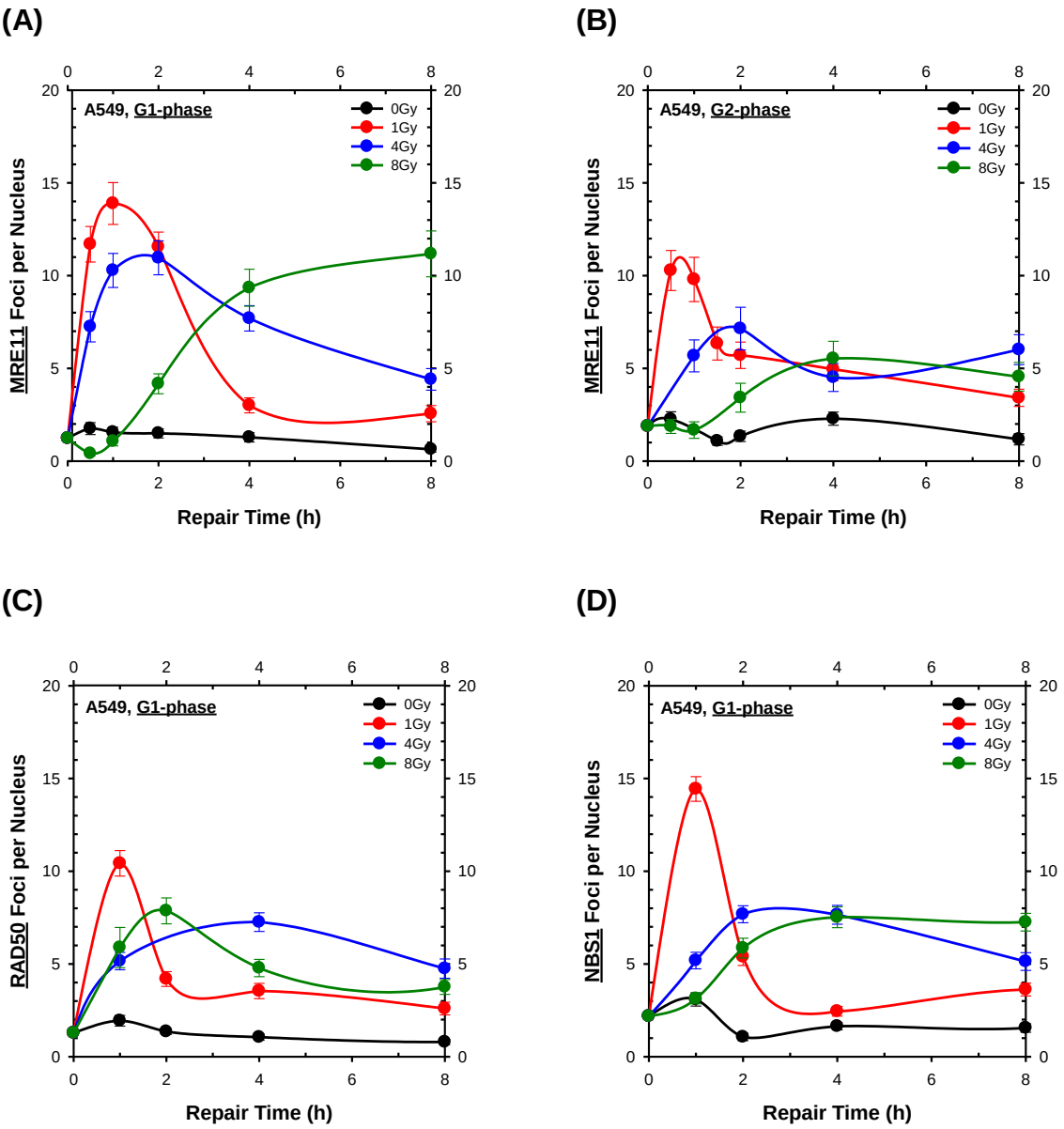

Figure 24: The bimodal response of IR-induced MRN foci is cell cycle-independent. Centrifugal elutriation was applied for the enrichment of A549 cells in different cell cycle phases, as described in 3.2.4. Enriched G1- and G2-phase A549 cells were irradiated with 0, 1, 4 or 8Gy x-rays, fixed after the indicated recovery times, and MRN foci numbers quantitatively analyzed, as described above. Mean MRE11 foci numbers per cell nucleus (A, B) were enumerated from four independent experiments, whereas average RAD50 and NBS1 (C, D) foci numbers per nucleus were determined from two different experiments. Error bars represent +/- standard errors.

Quantitative analysis of MRE11, RAD50 and NBS1 IRIF in enriched G1- and G2-phase A549 cells revealed that irrespectively of the cell cycle phase, comparable MRN foci formation and decay dynamics with similar MRN foci patterns (4.1.4) were obtained. The dose response of MRN IRIF was cell cycle-independent and sub-linear in the range of doses tested (1 to 8Gy). Remarkably, the MRN foci formation kinetics depended on radiation dose, with a maximum been reached at later times as the dose of radiation increased. After low radiation doses (1Gy), fast developing MRN foci maxima were detected at 0.5-1h post-irradiation. However, these fast developing MRN foci promptly decayed to almost background values within a repair time interval of ~3h. In contrast to that, high doses of radiation (4-8Gy), led to a slower formation of MRN IRIF.

After observing this bimodal response of MRN IRIF in A549 cells, we wished to examine the generality of this phenotype. Therefore, we measured MRE11 IRIF formation and decay in MRC5-SV1 and M059K cells. Here again, cells were enriched in different cell cycle phases by centrifugal elutriation, treated and analyzed as described above. Fig. 25 A-B shows MRE11 foci formation and decay dynamics only in G1-phase MRS5-SV1 and M059K cells, respectively.

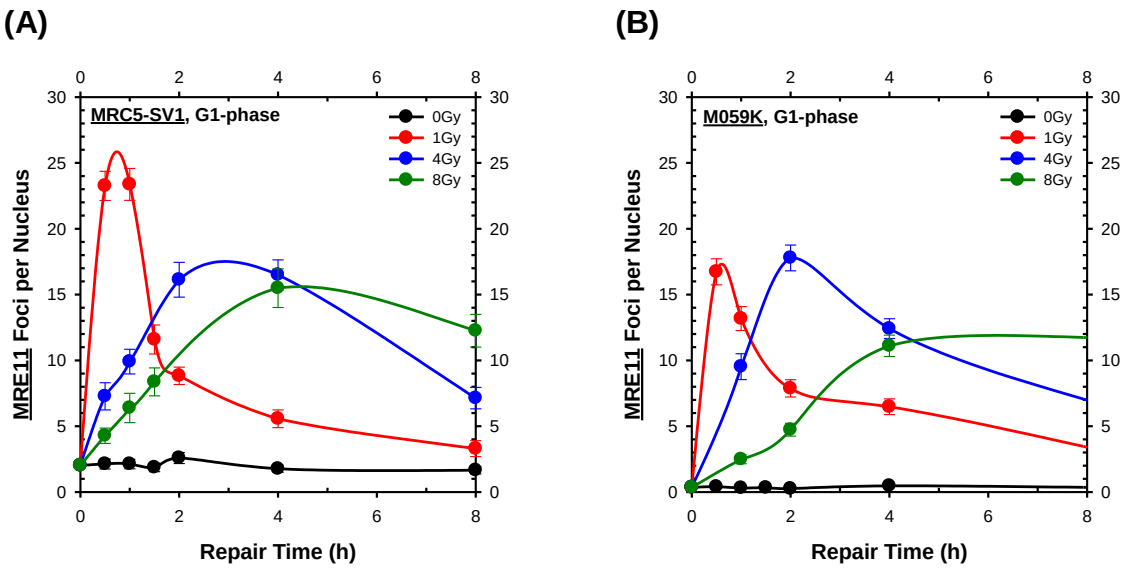

Figure 25: All examined human repair-proficient cell types show a comparable bimodal cell cycle-independent response of MRE11 IRIF. Cells were enriched by centrifugal elutriation in different phases of the cell cycle, irradiated with different x-ray doses (0, 1, 4, 8Gy), fixed at specified times after irradiation, and the mean MRE11 IRIF numbers per cell nucleus were evaluated, as described above. Three and two independent experiments were quantitatively analyzed for average MRE11 foci numbers in MRC5-SV1 cells (A) and M059K cells (B), respectively. Error bars represent +/-standard errors.

Obviously, all examined repair-proficient cell lines showed nearly the same phenotype – a fast response, with MRE11 foci number maxima developing at 30-60min after exposure to low radiation doses, and a slower MRE11 foci formation after exposure high doses of radiation (4-8Gy).

In all experiments and with all cell lines tested, the response of MRE11 IRIF showed a sub-linear dose dependency in the range of doses tested (1 to 8Gy). For a better visualization of this bimodal but quite general response of MRE11 foci formation as a function of radiation dose, quantitative data of all investigated cell lines is summarized in Fig. 26 A-D.

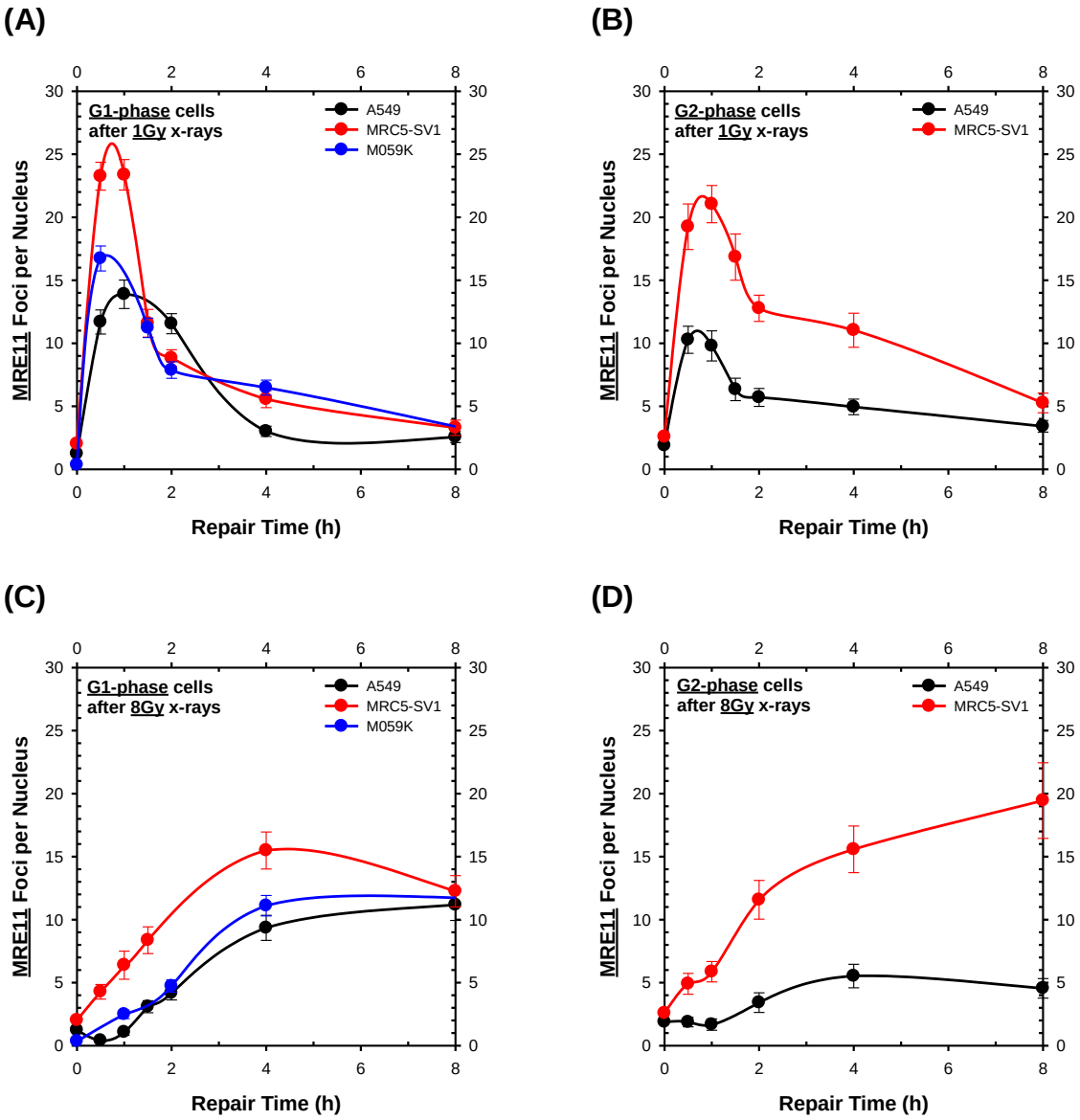

Figure 26: The bimodal response of IR-induced MRE11 foci is cell cycle-independent and similar in different cell lines. MRE11 foci formation and decay dynamics are depicted for the indicated cell lines in G1- and G2-phases, after exposure to 1 (A-B) and 8Gy x-rays (C-D), respectively. Error bars on data points represent +/-standard errors of the mean.

Evidently, all examined repair-proficient cell lines showed fast and slow MRE11 IRIF formation and decay dynamics depending on the applied radiation dose. Notably, MRE11 foci numbers per cell nucleus were higher in irradiated MRC5-SV1 cells as compared to A549 or M059K cells. However, all cell lines showed a cell cycle-independent bimodal response for the IR-induced MRE11 foci formation with a sub-linear dose response.

4.1.6 High LET irradiation alters the response of MRE11 IRIF

As discussed in 1.2, one distinguishes between sparsely and densely ionizing radiation, i.e. low and high LET radiation. X-rays is low LET radiation modality, whereas neutrons or charged particles are high LET radiation modalities. In general, the biological effects of high LET radiations are larger compared to those of low LET radiations, when compared at the same absorbed dose (Kadhim, Hill *et al.* 2006). It is thought that this is because high LET radiation deposits relatively large amounts of energy within a small volume producing thus highly complex or clustered DNA damage (Goodhead and Nikjoo 1989; Holley and Chatterjee 1996; Hada and Georgakilas 2008).

We wondered whether high LET radiation alters the response of MRE11 IRIF. To examine this, we exposed A549 and M059K cells to radiations of different LET and recorded the dynamics of MRE11 foci formation and decay. As radiation modality of intermediate LET, we used 5.8MeV neutrons, while 1GeV heavy ions were employed as high LET radiation modality. To account for the higher relative biological effectiveness (RBE) of high LET radiations, we reduced the doses of radiation applied.

Here again, enriched G1- and G2-phase A549 and log-phase M059K cells were exposed to neutrons or heavy ions (Fe or Ni heavy ions), respectively. MRE11 IRIF were measured by immunofluorescence on fixed samples using confocal microscopy, as described above. The development and decay of MRE11 foci at different times and different radiation doses, are summarized in Fig. 27 A-B. Fig. 27 C-D shows characteristic images of MRE11 foci in the same cells.

To allow comparison of MRE11 IRIF dynamics after exposure to radiations of different LET, results of MRE11 foci dynamics obtained after exposure to x-rays were also included in the figure (dashed line). For neutrons, results obtained with enriched G1-phase cells are shown, but comparable results were also obtained with G2-phase cells (data not shown). Notably, for heavy ion irradiation experiments, centrifugal elutriation for cell enrichment in different cell cycle phases could not be performed, due to missing laboratory equipment at the irradiation site.

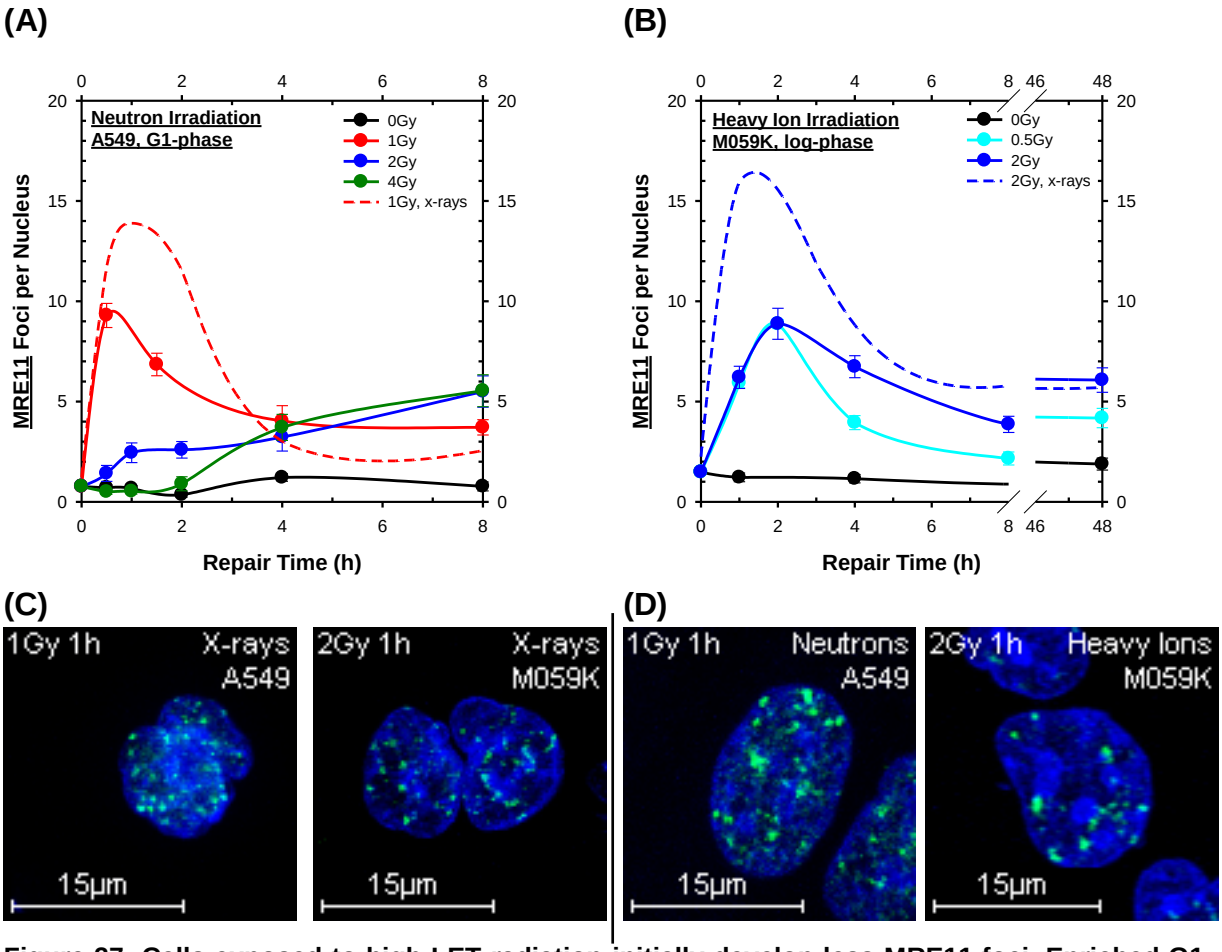

Figure 27: Cells exposed to high LET radiation initially develop less MRE11 foci. Enriched G1-phase A549 (A) and cycling M059K (B) cells were exposed to neutrons and heavy ions, respectively. Cells were fixed at the indicated times and processed for immunofluorescence staining. About 200 cell nuclei were scored for the presence of MRE11 foci at each time point, and the mean MRE11 foci number per cell nucleus calculated, as described under "Materials and Methods". The time course of MRE11 IRIF was plotted at different radiation doses. Experiments were repeated two times. Error bars on data points represent +/- standard errors. Representative images of IR-induced MRE11 foci in the indicated cell lines after low (C) and high LET (D) irradiation, presented as MIP overlay images. Color allocation: DAPI (blue) and MRE11 (green).

Quantitative analysis of MRE11 IRIF exposed to high LET radiation revealed that repair-proficient A549 and M059K cells developed less MRE11 foci initially, but retained more foci at later times. Moreover, there were remarkable differences in MRE11 foci formation and decay dynamics between cells irradiated with neutrons and heavy ions. At low neutron doses (1Gy), MRE11 foci developed fast, reached a maximum at 0.5h post-irradiation and decayed relatively fast in the time course of the experiment. However, this fast MRE11 IRIF response was not observed in cells exposed to higher neutrons doses (2-4Gy) (Fig. 27 A).

On the other hand, in response to heavy ions, M059K cells showed, independently of the radiation dose applied, similar MRE11 foci formation dynamics. Hence, a MRE11 foci peak appeared at 2h post-irradiation; however cells exposed to 2Gy heavy ions showed slower MRE11 foci decay kinetics over time than cells irradiated with heavy ions at doses of 0.5Gy (Fig. 27 B). In aggregate, these results confirmed the sub-linear dose-dependency of MRE11 foci formation for radiations of high LET.

Notably, after high LET irradiation the initial MRE11 IRIF response included mostly large MRE11 foci (Fig. 27 D), which decreased in size over time (data not shown), suggesting a progress in the repair of the underlying complex lesions. In contrast, low doses of low LET radiation quickly induced the formation of small MRE11 foci (Fig. 27 C), which developed to larger foci at later times. However, these small MRE11 foci were only observed after low doses (1Gy); after high doses (4-8Gy) the small MRE11 foci diminished leaving the late, slower developing and larger foci to dominate the response (see also the discussion in 4.1.4). These observations indicated that the dynamic assembly of large MRE11 foci may be required for the repair of particularly complex and difficult to repair lesions associated with high LET irradiation, and when high doses of low LET radiation are applied.

We concluded that high LET radiation changed the response of MRE11 to DNA damage, since in general comparatively low numbers of large and longer persisting foci were observed as compared to low LET irradiation. The significance of this observation remains to be elucidated.

4.1.7 The yields of MRE11 IRIF are cell line specific

The fact that irradiated MRC5-SV1 cells showed higher MRE11 foci numbers compared to other cell lines, such as A549 and M059K, led us inquire on the possible causes of this phenomenon. One likely explanation is differences in the DNA content among the cell lines tested; higher DNA content is expected to result in a larger number of foci for the same radiation dose.

To test this hypothesis, quantitative measurements of the nuclear DNA content for the cell lines employed, were carried out using flow cytometry. Generally, DNA content measurements are expressed as DNA index (DI) values, representing the ratio of sample DNA G1 peak channel to reference DNA G1 peak channel. Thus, a DI of 1.0 is equal to normal diploid DNA content, while DI values greater than 1.0 implicate DNA aneuploidy. We evaluated the nuclear DNA content of exponentially growing A549, MRC5-SV1 and M059K cells by FACS (detailed information in 3.2.5), using human lymphocytes as reference. The results of these measurements are presented as FACS histograms in Fig. 28 A-C.

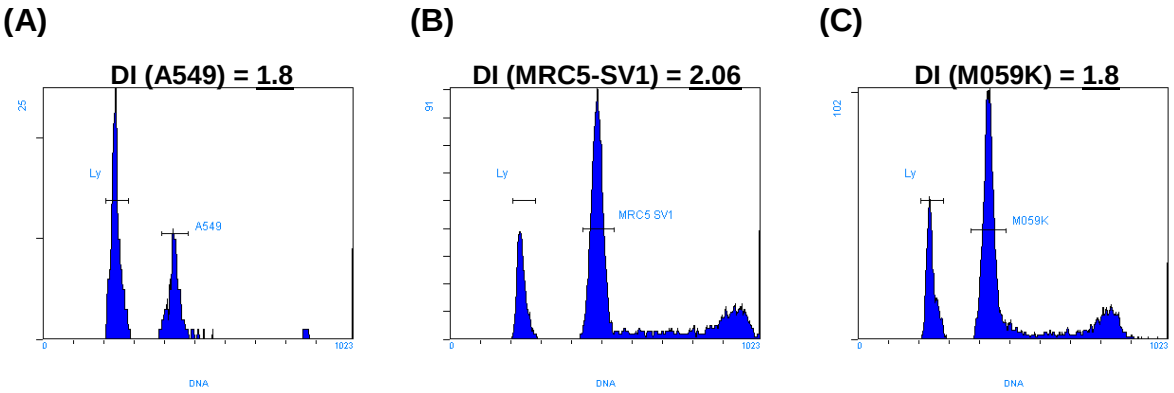

Figure 28: Exponentially growing MRC5-SV1 cells have the highest nuclear DNA content among the investigated cell lines. The nuclear DNA content was measured in exponentially growing A549 (A), MRC5-SV1 (B) and M059K (C) cells, using human lymphocytes as reference (i.e. DI of 1.0). To obtain the histograms, about 15,000 events were counted for each sample, and files were generated as described above. DI values were determined as G1 cell DNA content of the test cell line relative to G1 cell DNA content of the lymphocytes used as standard.

Evidently, cycling MRC5-SV1 cells had the highest cellular DNA content with a DI of 2.06, compared to exponentially growing A549 and M059K cells, which had a DI of 1.8. This result suggests that MRE11 IRIF numbers depend on cellular DNA content. Indeed, higher IR-induced MRE11 foci numbers were detected in cells with higher nuclear DNA content, e.g. for A549, MRC5-SV1 and M059K cells.

4.1.8 Dose-dependent accretion of MRE11 in the cell nucleus after IR

It is estimated that each Gy of low LET radiation, e.g. x-rays, will induce ~20-40 DSBs. Higher radiation doses will therefore induce hundreds of DSBs. Our observation that after exposure to high x-ray doses (4-8Gy) only very small MRE11 foci formed at early post-irradiation times, led us consider whether the bimodal response (4.1.5) derived from detection limitations. Possibly, in response to high radiation doses only few MRN molecules bind to damage sites, limiting thus their detectability. This possibility is supported by the fact that the detection of cytologically discrete foci by indirect immunofluorescence depends on the number of protein molecules that accumulate at the site, and is estimated to be of the order of one thousand (Paull, Rogakou *et al.* 2000). Sites with fewer protein molecules might thus escape detection.

To test this possibility, we performed an evaluation of total nuclear MRE11 fluorescence in cells irradiated with different x-rays doses as a function of time. This kind of analysis provides quantitative information on local protein accretion in imaged cells, and allows examination whether the degree of local protein accretion is dose-dependent. Nuclear MRE11 and DAPI fluorescence total signal intensities were measured in specific regions of interest (ROI), in A549 cell nuclei. Subsequently, normalized MRE11 fluorescence total signal intensity values of analyzed ROIs were calculated by the formula below and plotted as a function of time for the different radiation doses in Fig. 29.

$$Normalized\ MRE11\ Fluorescence\ Total\ Signal\ Intensity\ (\%) = \frac{Mean\ MRE11\ Fluorescence\ Total\ Signal\ Intensity\ of\ ROI(x)}{Mean\ DAPI\ Fluorescence\ Total\ Signal\ Intensity\ of\ ROI(x)} * 100$$

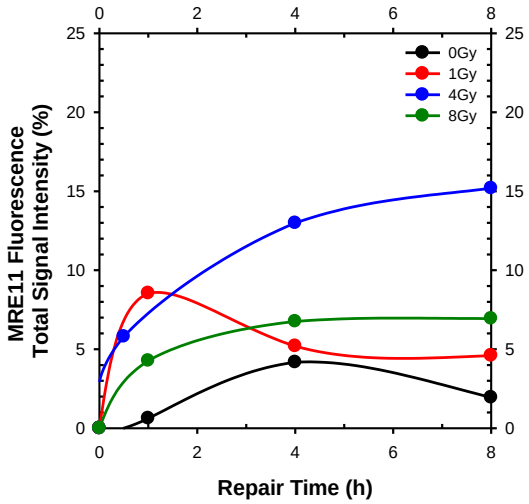

Figure 29: Accretion of nuclear MRE11 is dose-dependent. Exponentially growing A549 cells were irradiated with various x-ray doses (1-8Gy), fixed at the indicated times, and stained for MRE11 IF analysis as previously described. About 20 nuclei were analyzed for MRE11 and DAPI fluorescence total signal intensities for each dose and repair time. Normalized MRE11 fluorescence intensities were calculated and graphically presented as a function of time.

The results showed that nuclear MRE11 total signal intensities fluctuated with the applied radiation dose and the time measured. After low radiation doses (1Gy), a fast developing MRE11 fluorescence signal maximum was observed at 1h post-irradiation, reaching a higher fluorescence intensity than that measured after exposure to high radiation doses. However, this signal promptly decreased to almost background fluorescence values within 4h. On the other hand, no fluorescence intensity maxima formed in response to higher radiation doses (4-8Gy) within the observed time intervals. Remarkably, after irradiation with 4Gy higher fluorescence intensities were detected than after 8Gy.

This data showed that nuclear MRE11 fluorescence signal intensities followed non-linear dose-yields in the range of doses tested (1-8Gy). Moreover, MRE11 protein accretion was dependent on dose and showed distinct time dependencies. We concluded that the observed slow MRN IRIF response after high dose irradiation treatment was not due to technical limitations; if this were the case, we would have expected a higher MRE11 protein accretion at high x-ray doses.

4.1.9 MRE11 chromatin association does not limit its availability

The detection of nuclear IR-induced MRN foci suggests that MRE11 interacts with damaged DNA, which should be associated with active retention on chromatin. However, after exposure to low x-ray doses (1Gy), only a subset of the total intracellular MRE11 protein should be associated with damaged DNA, and this association should increase with dose. We considered that at high radiation doses, limitations in MRE11 protein availability lead to the accretion characteristics described above.

To address this question, an analysis of MRE11 protein availability was carried out in cells exposed to different radiation doses. A549 cells were irradiated with 0, 1, 4 and 8Gy x-rays, harvested at different post-irradiation times, and subsequently subjected to sub-cellular biochemical protein fractionation (3.2.10). This analysis allows estimates of the intracellular chromatin-bound and soluble protein levels. Immunoblots of showing the results of this fractionation are shown in Fig. 30 A-B.

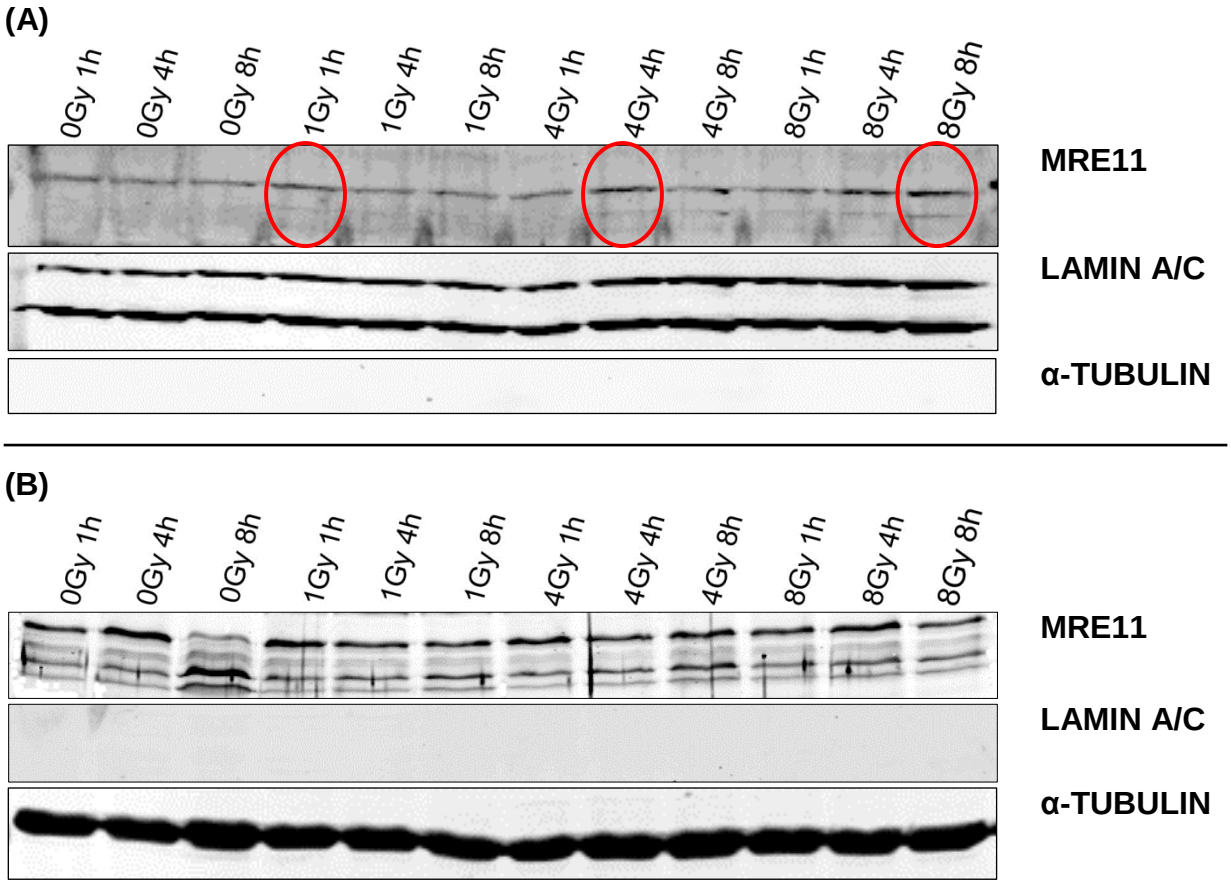

Figure 30: IR-induced MRE11 chromatin association is not limited by its availability. Log-phase A549 cells were either mock irradiated or irradiated as indicated, collected at 1, 4 and 8h post-irradiation and biochemically fractionated into chromatin-bound (A) and soluble protein (B) fractions. Protein fractions were loaded on gels and analyzed by Western blotting, as described under "Materials and Methods". LAMIN A/C served as control for the chromatin-bound protein fraction, whereas the cytoskeletal microtubule protein, α-TUBULIN, was used as control for the soluble protein fraction. The absence of α-TUBULIN and LAMIN A/C in chromatin-bound and soluble protein fractions, respectively, confirmed the quality of the biochemical protein fractionation.

Western blot analysis of the resulting fractions demonstrated that both the chromatin-bound and the soluble protein fractions contained MRE11. Surprisingly, IR treatment induced only a slight increase of MRE11 chromatin association. In addition, chromatin-bound MRE11 protein maxima were observed at different times after irradiation. After exposure to higher radiation doses, the maximum in MRE11 chromatin association developed at later times (red circles in Fig. 30 A). However, the detection of chromatin-bound MRE11 protein in unirradiated cells reflects also a radiation-independent MRE11 chromatin association. On the other hand, no notable reduction in MRE11 protein level could be detected in the soluble protein fraction in response to radiation exposure (Fig. 30 B).

The biochemical fractionation shown here indicated that although there was a dose-dependent increase in MRE11 chromatin association, enough protein remained soluble at the highest dose to exclude availability as the cause for the accretion kinetics observed above.

4.1.10 The formation of MRE11 and ATM foci is inter-dependent

As discussed in 1.5, MRN is considered to be the major sensor of DSBs, initiating signaling and regulating effector responses to DSBs. A key signaling function of MRN is the recruitment and activation of ATM, which then initiates a cascade of phosphorylation events that leads to signal amplification, cell cycle arrest and DNA repair. It has been reported that MRN and ATM are inter-dependent in the recognition and signaling of DSBs (Lavin 2007), as MRN mutations abolish ATM activation (Difilippantonio, Celeste *et al.* 2005).

We showed above a rapid DNA damage-dependent relocalization of MRE11 to sites of DNA damage. To examine the dependence of MRE11 IRIF formation on the ATM-controlled response to DNA damage, we measured the time course of MRE11 foci formation in SV40 immortalized human A-T fibroblasts, AT5-BIVA cells and compared the results to those obtained with A549 cells (Luo, Tang *et al.* 1996). Furthermore, to investigate the possible interdependence between ATM and MRE11 in response to DNA damage, we also examined the formation of phospho-Ser-1981 (pS1981) ATM IRIF in NBS1-deficient, NBS1-LB cells and used A549 cells as a control. Exponentially growing cells were exposed to 1Gy x-rays and fixed at different times post-irradiation. The results obtained are summarized in Fig. 31 A-B.

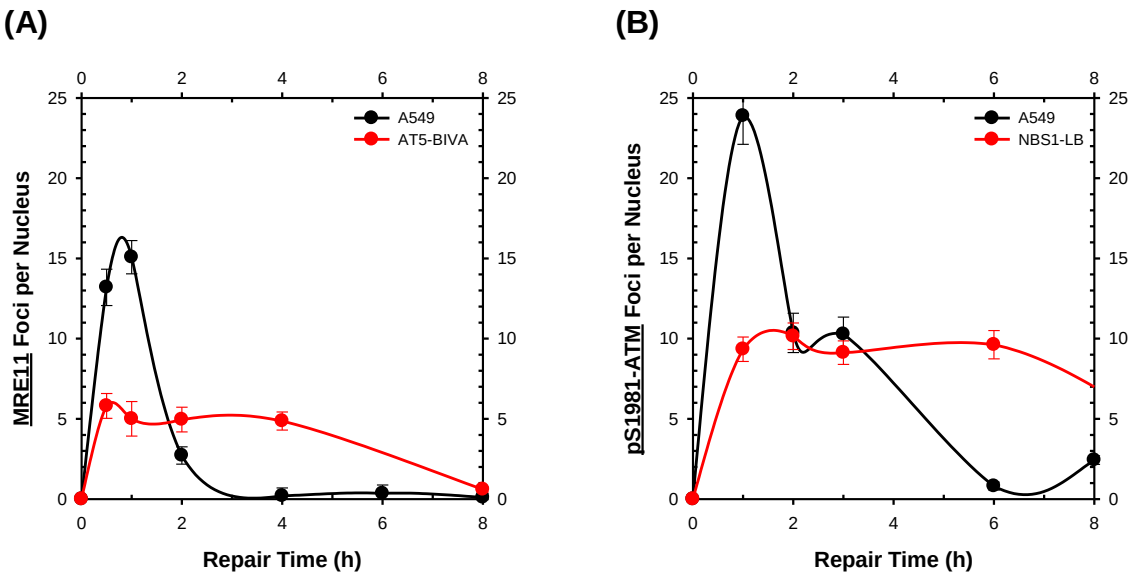

Figure 31: The formation of MRE11 and pS1981-ATM IRIF is inter-dependent. Cycling A549, AT5-BIVA and NBS1-LB cells were either irradiated with 0 or 1Gy x-rays, and returned to 37ºC for different periods of time. At each time point, cells were collected, fixed, permeabilized, and immunostained with anti-MRE11 (A) and anti-pS1981-ATM (B) antibodies, respectively. Foci numbers were scored, the mean foci number per nucleus calculated and plotted as a function of time. Results are from two independent experiments with error bars representing +/- standard errors.

In repair-proficient A549 cells, MRE11 and pS1981-ATM foci rapidly increased and reached a maximum at 1h after 1Gy x-rays. After this maximum, foci decayed and their numbers reached background levels within 3-6h post-irradiation. In contrast, we found that MRE11 IRIF formation was severely reduced in ATM-deficient cells that developed only about 1/3 of the MRE11 foci scored in ATM proficient cells (Fig. 31 A). Similarly, NBS1-deficient cells presented less pS1981-ATM IRIF as compared to NBS1-proficient cells (Fig. 31 B). In addition, IR-induced foci in deficient cells persisted longer than in wild-type controls. Interestingly, the curve shapes of MRE11 and pS1981-ATM IRIF in ATM- and MRN-deficient cells, respectively, were similar. Notably, in the absence of ATM or NBS1 protein, MRE11 and activated ATM respectively, were not present as distinct foci but rather in a diffuse pattern in the nucleus as observed in unirradiated control cells (data not shown).

Thus, ATM did influence the MRN's ability to localize to nuclear foci and *vice versa*, as also MRN did influence the formation of pS1981-ATM foci, suggesting interdependence in the functions of MRE11 and ATM – as suggested by the signaling cascade shown in Fig. 15.

4.1.11 MRE11 has distinct functions in DDR

As described above, in response to DNA damage, MRN recruits and activates ATM. Activated ATM molecules phosphorylate various downstream ATM substrates such as H2AX (Burma, Chen *et al.* 2001), thus initiating DNA damage signaling. Phosphorylation of H2AX occurs on megabase regions surrounding DSBs within seconds after DNA damage induction, indicating that H2AX phosphorylation (γ-H2AX) is a critical component in early DNA damage signal transduction (Rogakou, Pilch *et al.* 1998). Moreover, γ-H2AX foci form at or near the sites of DSBs and colocalize with ATM, MDC1, 53BP1, BRCA1, MRN, and many other proteins implicated in DNA damage response (Paull, Rogakou *et al.* 2000; Kim, Minter-Dykhouse *et al.* 2006). It is generally thought, that γ-H2AX foci are markers for DSBs, as the number of γ-H2AX foci scored approximates the number of DSBs induced, and increases linearly with the amount of induced DNA damage (Rothkamm and Löbrich 2003).

Given the very rapid and specific modification of H2AX after induction of DSBs, we wished to investigate functional relationships between DSBs, as visualized by γ-H2AX foci and IR-induced MRE11 foci. Thus, we performed double staining analysis for γ-H2AX and MRE11. Such colocalization experiments provide insights into the participation of MRE11 in the response to DSBs because they compare the accretion of MRE11 at the sites of DSBs. Cycling A549 cells were mock irradiated or exposed to 1 and 8Gy x-rays, respectively, and allowed to recover for 1h, 4h or 8h prior to fixation and antibody staining. Fig. 32 shows representative images of irradiated A549 cells following DNA counterstaining with DAPI and immunofluorescent staining with anti-γ-H2AX and anti-MRE11 antibodies. Data of unirradiated control cells is not shown as only very few γ-H2AX and MRE11 foci were detected.

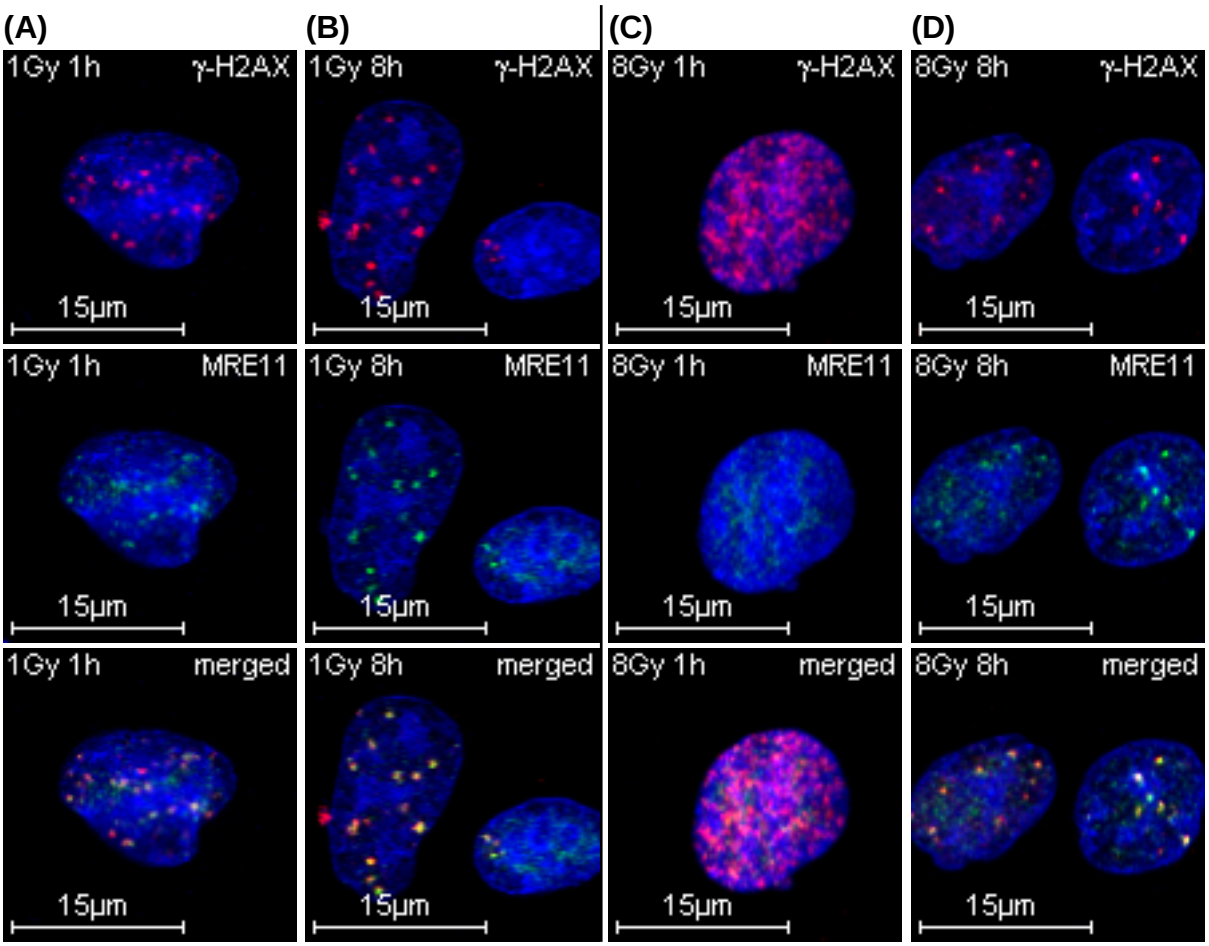

Figure 32: γ-H2AX and MRE11 foci colocalize at sites of DSBs. Exponentially growing A549 cells were irradiated with 1Gy (A-B) or 8Gy (C-D), and fixed at the indicated times. Subsequently, cells were stained with anti-γ-H2AX (red; panel 1) and anti-MRE11 antibodies (green; panel 2); cell nuclei were counterstained with DAPI (blue). Image acquisition was performed as described above. MIP overlay images of all three recorded channels are presented in panel 3.

Immunostaining with antibodies directed against γ-H2AX and MRE11 revealed that after damage induction both molecules formed nuclear foci. After exposure to IR, γ-H2AX appeared in 100% of the cell population and formed distinct foci that developed to larger foci over time. The number of γ-H2AX foci increased with higher radiation doses (Fig. 32, panel 1). In contrast, two major MRE11 IRIF patterns were detected: At early post-irradiation times mainly small MRE11 foci developed, which subsequently formed a larger MRE11 focus (Fig. 32, panel 2). However, this was only observed after low dose radiation (1Gy); after high dose radiation (8Gy) the early response diminished leaving the late and large MRE11 foci to dominate (4.1.4).

For example, at one hour, γ-H2AX foci were clearly present. On the other hand, after high x-ray doses MRE11 foci formed at later times (8h) (Fig. 32 C), and a fraction of them co-localized with γ-H2AX foci (Fig. 32 D). After irradiation with low doses (1Gy) colocalization of γ-H2AX with MRE11 foci was also observed even shortly after irradiation (Fig. 32 A). However, the percentage of γ-H2AX colocalizing with MRE11 seemed to increase to later post-irradiation times irrespective of radiation dose.

To examine this γ-H2AX-MRE11 colocalization quantitatively we used ImarisXT® 6.0 software. Colocalizing foci were counted in 100 nuclei using a threshold reading only colocalized foci. Subsequently, we set the highest foci number to 100%, and plotted the normalized mean of γ-H2AX, MRE11 and of colocalizing foci as a function of time after different radiation doses. The results obtained are summarized in Fig. 33 A-B.

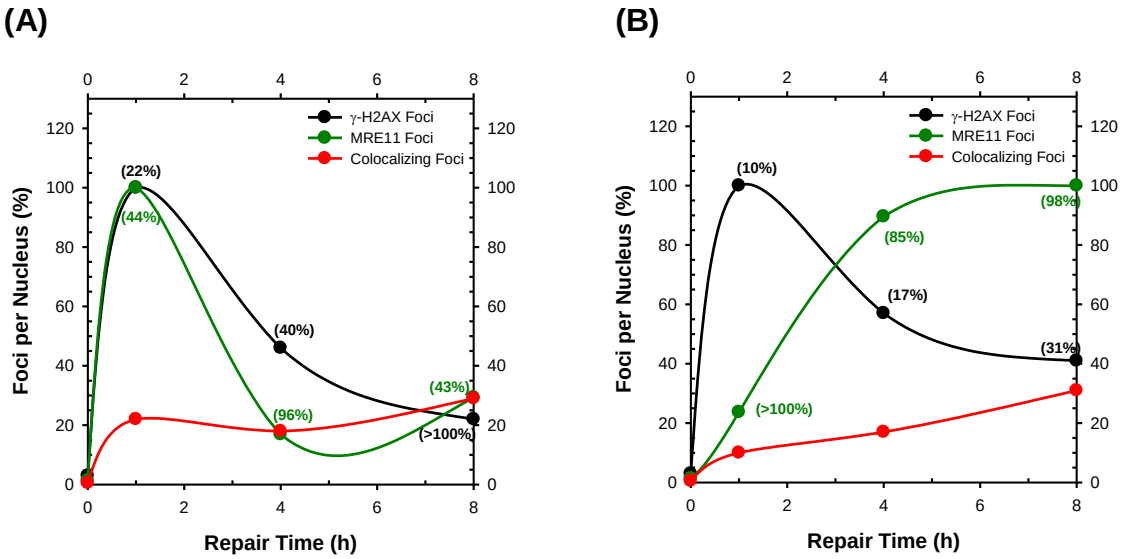

Figure 33: Colocalization of IR-Induced MRE11 and γ-H2AX foci is dose- and time-dependent. Exponentially A549 cells were exposed to 1Gy (A) or 8Gy (B) x-rays. Mean MRE11, γ-H2AX and colocalized foci numbers per cell nucleus for each time point were evaluated as described above. Numbers in parentheses indicate the percentage of MRE11 foci colocalizing with γ-H2AX foci (green), and the percentage of γ-H2AX foci colocalizing with MRE11 foci (black), respectively, at the indicated time points post-irradiation.

As shown in Fig. 33 A-B, in response to IR, γ-H2AX foci formed promptly, reaching a maximum at one hour post-irradiation and decreased by 8h to 20-40% of the maximum, depending on radiation dose. In contrast, MRE11 IRIF were strongly dependent on applied radiation dose and time, as discussed in 4.1.5.

Evidently, there was no one-to-one colocalization between γ-H2AX and MRE11 IRIF. In cells exposed to 1Gy x-rays, the amount of colocalized foci per nucleus was relatively constant, varying between 18-29%, whereas after irradiation with 8Gy, colocalization gradually increased from 10-31%. However, the percentage of γ-H2AX IRIF colocalizing with MRE11 foci (black numbers in parentheses, Fig. 33) increased over time and was highest at later time points, when DSB repair had progressed, as indicated by the decay of γ-H2AX foci. On the other hand, the presence of MRE11 to γ-H2AX sites (green numbers in parentheses, Fig. 33) was strongly dose- and time-dependent. In general, DSBs at early recovery times were typically not associated with MRE11, whereas DSBs, detectable as γ-H2AX foci at later times, showed with higher probability the presence of MRE11. One might speculate that these structures represent MRE11 accumulation at irreparable or slowly repairing DSBs.

Overall, the colocalization analysis presented above revealed that MRE11 clearly localized to sites of γ-H2AX, which are considered sites of DSBs. However the kinetics of localization appears complex and pertains only for a subset of the DSBs. These results in aggregate suggest functionally distinct modes of MRE11 activity in DDR that manifest in the complex kinetics and dose response relationships measured.

4.2 Investigation of complex functions of MRN in DSB repair

The above results implicate different functions of MRN in DDR. Moreover, one could hypothesize that MRN acts as a repair factor in DSB repair, as MRE11 was associated with γ-H2AX sites, particularly at later times post-irradiation. This is in line with published reports which indicate that MRN is involved in all DSB repair pathways: HRR, D-NHEJ and B-NHEJ (Hopkins and Paull 2008; Helmink, Bredemeyer *et al.* 2009; Rass, Grabarz *et al.* 2009). However, from our investigations, information on the contribution of MRN to HRR versus NHEJ could not be extracted. Thus, its precise role and exact contribution to different DSB repair pathways is still unknown. This is partly because studies on MRN functions are complicated by the fact that null mutations in any of its constituent proteins are embryonically lethal in mice and are lethal as well in cells.

To begin addressing the complex functions of MRN in DSB repair, we investigated the contribution of MRN to different DSB repair pathways using wild-type cell lines or cell lines with different MRN deficiencies. DSB repair efficiency by HRR was evaluated by documenting decay of RAD51 foci formation and decay in fixed cells after IR exposure, whereas PFGE was used to quantitate radiation-induced DSBs and thus to evaluate DSB repair by NHEJ.

4.2.1 HRR is incomplete in cells without a functional MRN and ATM

There is ample evidence that MRN is involved in DSB repair by HRR. This repair pathway requires architectural, structural and enzymatic components, which can be partly provided by MRN. The DNA-tethering architectures of MRN implicate it in a linker function for homologous stretches of DNA to tether the ends of the DSB in close proximity, and to pair the damaged molecule with the homologous section of the sister chromatid. Furthermore, the end-resecting activity of MRE11 is implicated in DNA end processing that is essential for the formation of RAD51 nucleoprotein filament during the presynapsis step of recombination (see 1.4.1). It also needs to be pointed out that mutation in key proteins that recognize and signal DSBs, such as MRN or ATM, results in genetic disorders, which generate hyper sensitivity to IR, genome instability, cancer and/or neurodegeneration. However, frequently, these mutation do not dramatically reduce the capacity of cells to repair DSBs overall (Girard, Foray *et al.* 2000; Riballo, Kühne *et al.* 2004).

To examine the contribution of MRN to DSB repair by HRR, and moreover to investigate the inter-dependent function of MRN and ATM in HRR, we carried out experiments, in which RAD51 foci formation and decay were quantitatively analyzed in wild-type cells, NBS1-deficient and ATM-deficient cells. The formation of a RAD51 focus is generally taken as evidence that a DSB is engaged by HRR (van Veelen, Cervelli *et al.* 2005). Thus, it is thought that the number of RAD51 foci detected reflects the number of DSBs that are repaired by HRR at a given radiation dose and repair time point. Exponentially growing cells were irradiated, and RAD51 foci were detected and scored in G2-phase cyclin B1 positive cells at different times after exposure to a range of radiation doses. The development and decay of RAD51 foci in repair-proficient, NBS1- and ATM-deficient cells could be established at three representative doses, as summarized in Fig. 34 A-C. Control experiments with HRR-deficient cells revealed no RAD51 foci formation after irradiation (data not shown).

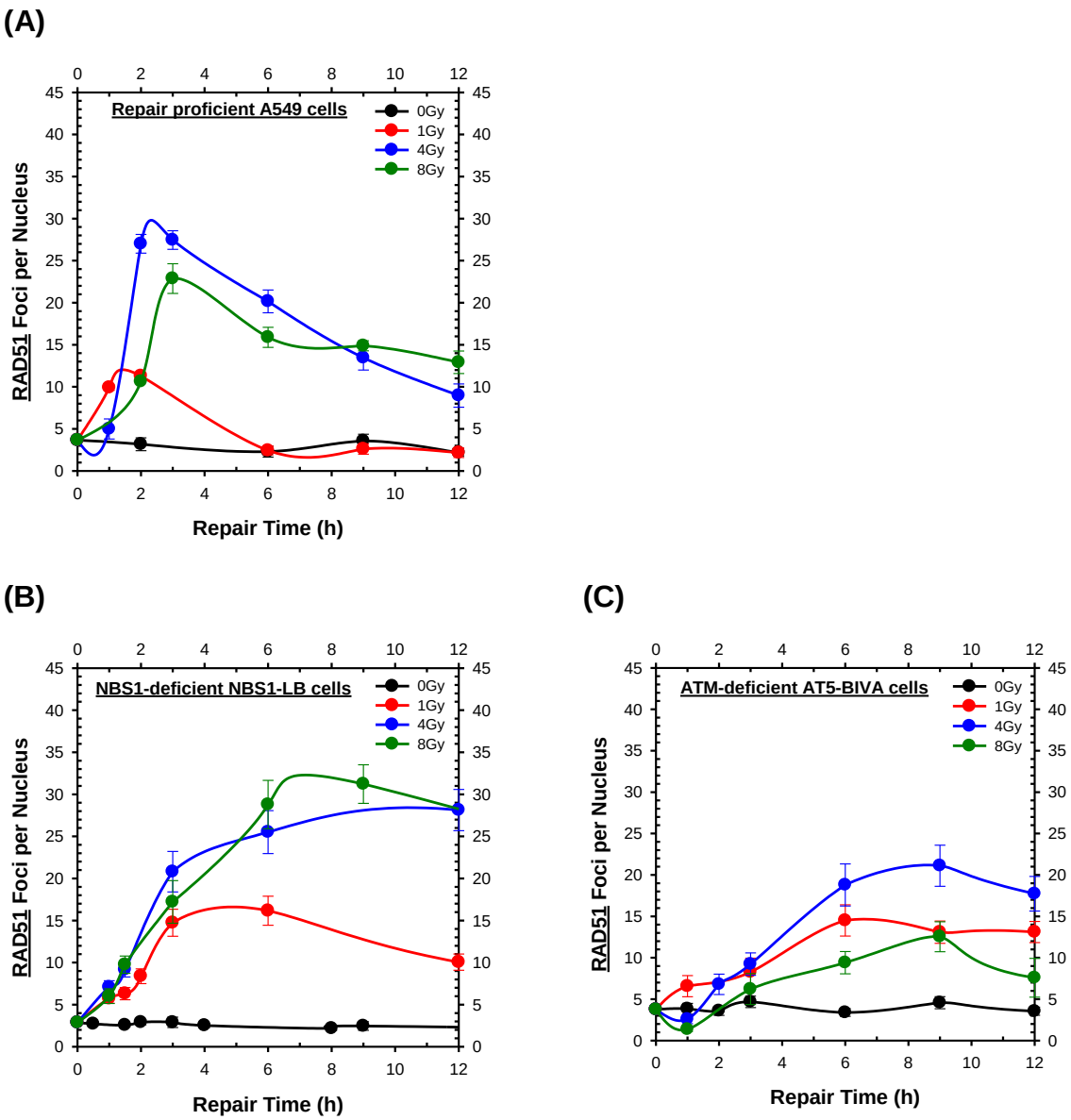

Figure 34: HRR is incomplete in cells without a functional MRN or ATM. Log-phase A549 cells (A), NBS1-deficient (B), and ATM-deficient (C) cells were either left untreated, or were irradiated with different doses, fixed at the indicated repair times, and co-stained with anti-RAD51 and anti-cyclin B1 antibodies, as described under "Materials and Methods". Late S- and G2-phase cells were identified for analysis by cyclin B1 staining, scored for the presence of RAD51 foci, and the average foci number per nucleus calculated. About 200 nuclei from each cell line were examined at each time point. The time course of RAD51 IRIF is plotted after different x-ray doses. Experiments were performed three times. Error bars on data points represent +/- standard errors of the mean RAD51 IRIF numbers.

Quantitative analysis of RAD51 foci in repair-proficient A549 cells uncovered a notable RAD51 IRIF response, showing a fast and slower formation of RAD51 foci, depending on the radiation dose applied.

At low doses (1Gy), RAD51 foci development reached a maximum at 2h, while at intermediate (4Gy) and high (8Gy) doses, RAD51 foci developed slower and the maximum was reached 2-3h after irradiation. In addition, the dose response for RAD51 foci formation was not linear in the range of doses tested (1 to 8Gy). In contrast to that, RAD51 foci formation was delayed but not completely blocked, and no pronounced foci maxima were developed in cells with defects in NBS1 and ATM, respectively. Accordingly, the dose response for RAD51 foci formation was sub-linear for the tested x-ray doses of 1 to 8Gy. However, in NBS1- and ATM-deficient cells RAD51 foci persisted for much longer than in wild-type controls.

Taken together, these results demonstrated a dose-dependent RAD51 foci formation – with fast and slow developing RAD51 foci maxima in repair-proficient cells, while in MRN- or ATM-deficient cells, RAD51 foci formation dynamics were slower and showed a much slower decay. This indicated that in cells without a functional MRN complex or a functional ATM, DNA end resection was initiated, as visualized by RAD51 foci, but the DSB repair could not be efficiently completed. This observation demonstrated that HRR was indeed severely impaired in NBS1- and ATM-deficient cells. We could thus conclude that MRN and ATM had a strong impact on HRR.

4.2.2 MRN complex is not required for DSB repair by D-NHEJ

There are reports suggesting that MRN contributes to DSB repair by D-NHEJ. However, the evidence is contradictory with some reports showing that MRN deficiency confers a strong defect in DSB repair by D-NHEJ (Rass, Grabarz *et al.* 2009), while others conclude that MRE11 is not important for accurate D-NHEJ (Moreau, Ferguson *et al.* 1999) (1.5.3). To investigate the functional significance of MRN in DSB repair by D-NHEJ, we measured DSB repair capability by PFGE in cells with different known MRN deficiencies, and compared the results to those of repair-proficient cells.

Since depletion of MRE11 is lethal, we used conditional MRE11-null mutants (DT40-*MRE11*$^{-/-}$MRE11^{+} cells). This mutant was generated in the lab of Prof. Shunichi Takeda through targeted integration of MRE11 deletion constructs, which disrupt the reading frame of *MRE11* sequence from aa 98 to 385. For viability, *MRE11*$^{-/-}$ clones carry a chicken *MRE11*-transgene (complementary DNA (cDNA) of a complete open reading frame of *GdMRE11*) that is under the control of a tet-repressible promoter. Notably, this transgene has a 10- to 20-fold higher MRE11 expression level than that of endogenous MRE11. Upon addition of tetracycline, which suppresses the expression of *MRE11*-transgene, the level of MRE11 expression is reduced by 10-fold 12h later, and is undetectable at 24h after the addition of tetracycline. Reverse transcription-polymerase chain reaction (RT-PCR) revealed that the transcript level of *GdMRE11* is reduced by two orders of magnitude three days later (Yamaguchi-Iwai, Sonoda *et al.* 1999). In our experiments we used doxycycline hydrochloride, a synthetic tetracycline derivative, which is more stable than tetracycline, and thus does not need to be replaced in the culture medium during the time course of the experiment.

At the beginning we tested the proliferative properties of wild-type DT40-MRE11 and DT40-*MRE11*$^{-/-}$MRE11^{+} cells in the absence of doxycycline by monitoring cell number and carrying out cell-cycle analysis. The growth curve of DT40-*MRE11*$^{-/-}$ MRE11^{+} cells was indistinguishable from that of the wild-type DT40-MRE11 cells, which divided approximately every 8h. FACS analysis revealed that the cell-cycle distribution was essentially the same in both cell lines (data not shown). To suppress the expression of chicken *MRE11*-transgene, exponentially growing DT40-*MRE11*$^{-/-}$ MRE11^{+} cells were cultivated in media containing doxycycline (1µg/ml). As a function of time thereafter, we examined cell growth and viability. DT40-*MRE11*$^{-/-}$MRE11^{-} cells were capable of proliferating for several rounds and started to die at day 5. During the time course of this measurement MRE11 protein level was followed. We observed that MRE11 significantly decreased at 24h, and was undetectable at 48h after addition of doxycycline hydrochloride (Fig. 35).

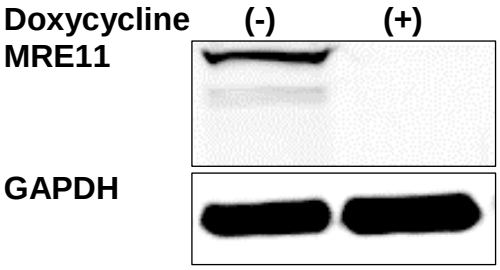

Figure 35: MRE11 is undetectable in DT40-*MRE11*$^{-/-}$MRE11^{-} cells. Whole cell lysates were prepared 2.5d after the addition of doxycycline hydrochloride from cycling conditional MRE11-null mutants. Untreated DT40-*MRE11*$^{-/-}$MRE11^{+}cells were used as control for MRE11 expression. Following SDS-PAGE, western blots were simultaneously probed with anti-MRE11 and anti-GAPDH antibodies, which served as loading control.

Western blot analysis revealed that at 2.5d after the addition of doxycycline hydrochloride no MRE11 could be detected in DT40-*MRE11*$^{-/-}$MRE11^{-} cells, whereas untreated cells expressed robust levels of MRE11. On the basis of this result, subsequent experiments with DT40-*MRE11*$^{-/-}$MRE11^{-} cells were performed at 2.5d after addition of doxycycline.

To begin addressing the contribution of MRN to DSB repair by D-NHEJ, we measured DSB repair capacity by PFGE in repair-proficient DT40-*MRE11*$^{-/-}$MRE11^{+} and A549 cells as well as in two MRN mutants, the MRE11-deficient DT40-*MRE11*$^{-/-}$ MRE11^{-} cells and human NBS-defective, NBS1-LB cells. Fig. 36 A-B shows the results obtained, with typical gels and cell cycle distribution, from wild-type cells that were compared to those of MRN-deficient cells.

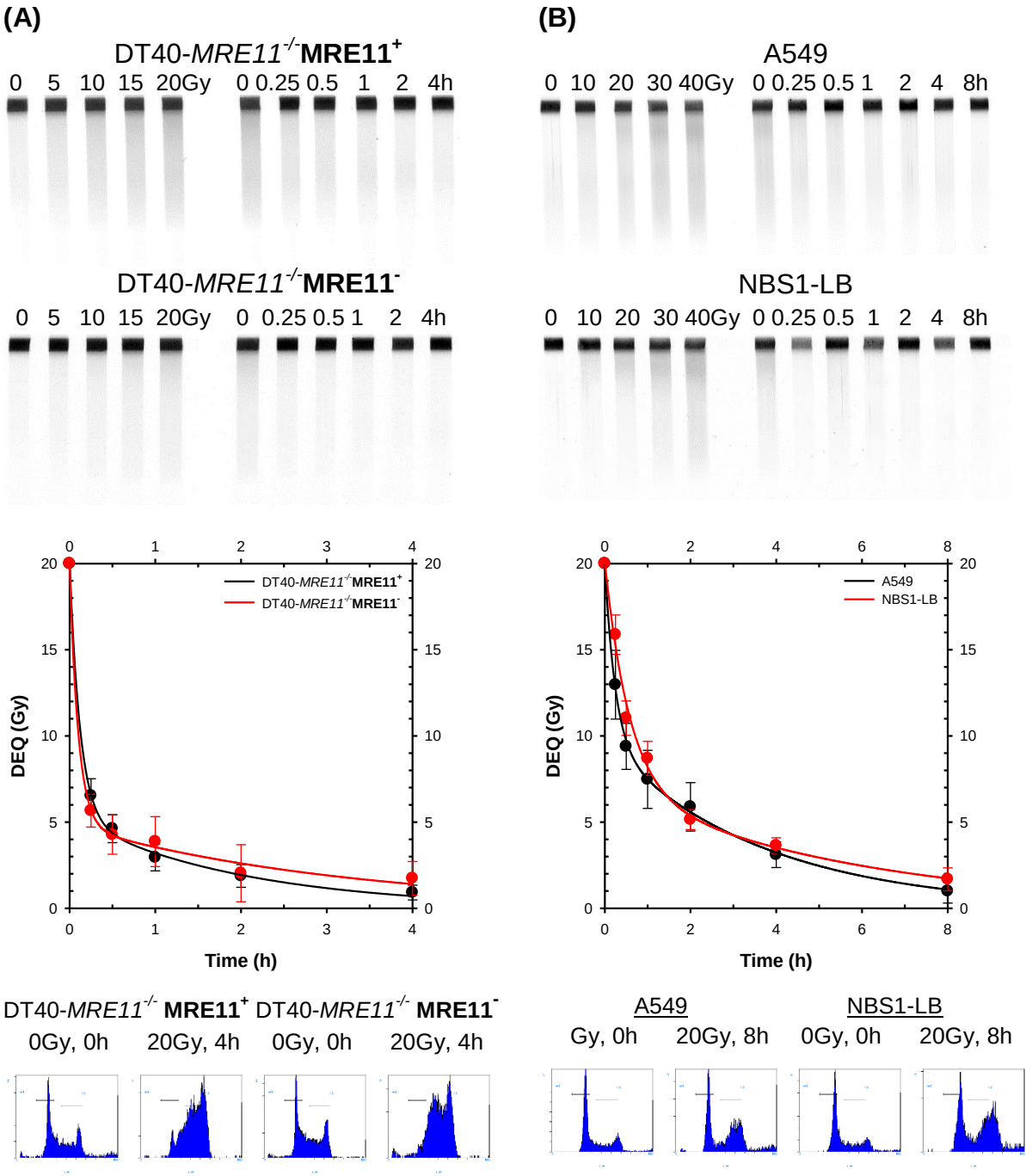

Figure 36: MRN has no effect on DSB repair by D-NHEJ. Upper two panels show typical gels obtained with repair-proficient and MRN-deficient cells exposed to x-rays. To measure the dose response, cells were irradiated with different IR doses, whereas repair kinetics of the same cells was followed after exposure to 20Gy x-rays. The amount of DSBs present in the cells is reflected by the value of FDR. In the calculation, the value of FDR measured in non-irradiated cells was subtracted from all data points with irradiated samples. To account for non-linear dose-response curves as well as for differences among cell lines and experiments, the DEQ was calculated and plotted as a function of time. Plotted are the mean and standard errors calculated from four determinations in three independent experiments. Results obtained were fitted to the sum of two exponentials. Bottom panel shows DNA histograms for the different cells before and after exposure to IR. Evidently, radiation exposure led to the activation of cell cycle-dependent checkpoints that caused an increase in the fraction of cells in G2-phase of the cell cycle several hours after irradiation.

The top panel shows characteristic gels of dose response and repair kinetics experiments obtained with repair-proficient, DT40-*MRE11*$^{-/-}$MRE11^{+} and A549 cells. The lower gel panel shows typical gels of MRN-deficient cells, such as DT40-*MRE11*$^{-/-}$MRE11^{-} and NBS1-LB cells. The released DNA from the well into the lane, as a function of dose, demonstrates the increase in the induction of DSBs, whereas the gradual reduction in the amount of DNA released into the lane, as a function of time after exposure to IR, is a measure of the ability of cells to repair DSBs. Non-irradiated control cells were used to determine the background FDR at 0Gy (data not shown) that was subsequently subtracted from the FDR values of irradiated cells.

The determination of the dose response is very important as it allows the recalculation of the repair kinetics from the initially measured FDR versus time plots to DEQ versus time plots. The plotting of DEQ, instead of FDR as a function of time, has the advantage that it eliminates differences deriving from fluctuations in the migrating characteristics of the DNA. An additional advantage is that it corrects for non-linear dose response curves that can significantly skew the repair kinetics data. Accordingly, we plotted calculated DEQ values as a function of time, where the initial values for DEQ at t=0h were derived from the dose response curves, since these measurements are carried out under conditions that ensure nearly complete absence of DSB repair.

DSB repair efficiency by D-NHEJ was followed in indicated cells after exposure to x-rays. The analysis of the repair kinetics obtained with repair-proficient and MRN-deficient cells clearly showed efficient rejoining of DSBs in all used cell lines, with most of the DSBs rejoined at 0.25h in DT40 cells (Fig. 36 A) and at 2h in A549/NBS1-LB cells (Fig. 36 B), respectively. This is indicated by the observed rapid reduction in DEQ as a function of the repair time. Moreover, the overall rates of DSB-rejoining in repair-proficient DT40-*MRE11*$^{-/-}$MRE11^{+} and A549 cells were found to be very similar to those of MRN-deficient DT40-*MRE11*$^{-/-}$MRE11^{-} and NBS1-LB cells.

Taken together, the above results demonstrated that MRN did not contribute detectably to DSB repair by D-NHEJ, at least as measured by PFGE.

4.2.3 DSB repair by B-NHEJ requires MRN

As outlined in the introduction (1.5.3), there is evidence that MRN is involved in DSB repair by B-NHEJ – possibly because MRE11 processes DNA termini that facilitates B-NHEJ. It was also reported that MRN deficiency is associated with strong defects in the repair of RAG-mediated DSBs generated during V(D)J recombination, when repaired either by D-NHEJ and B-NHEJ (Helmink, Bredemeyer *et al.* 2009). However, there are no results showing clear contribution of MRN to DSB repair by B-NHEJ. This void prompted us to investigate the possible role of MRN in B-NHEJ.

Here again, we used PFGE to measure DSB repair by B-NHEJ in repair-proficient and MRN-deficient cells, treated with a specific DNA-PKcs inhibitor (NU7441) as a tool for inhibiting D-NHEJ. One hour after addition of NU7441, cells were irradiated and DSB repair kinetics were obtained with wild-type A549 cells as well as with the conditional MRE11-null DT40 and the NBS1-LB mutants. Control experiments with DT40-*DNA-PKcs*$^{-/-}$ cells revealed best results, using NU7441 at a concentration of 5µM; at higher inhibitor concentrations repair was inhibited suggesting off-target effects (data not shown). Therefore, subsequent experiments with NU7441 were carried out at a concentration of 5µM, given 1h prior to irradiation.

A summary of the results obtained with repair-proficient cells and MRN mutants regarding rejoining of DSBs by B-NHEJ is given in Fig. 37 A-B. To allow direct comparison of the repair capability by D-NHEJ and B-NHEJ, results of untreated cells were also included (dashed line). Finally, the figure includes flow cytometry data of the cell-cycle distribution of the initial cell populations, and those exposed to radiation at 4 and 8h post-irradiation.

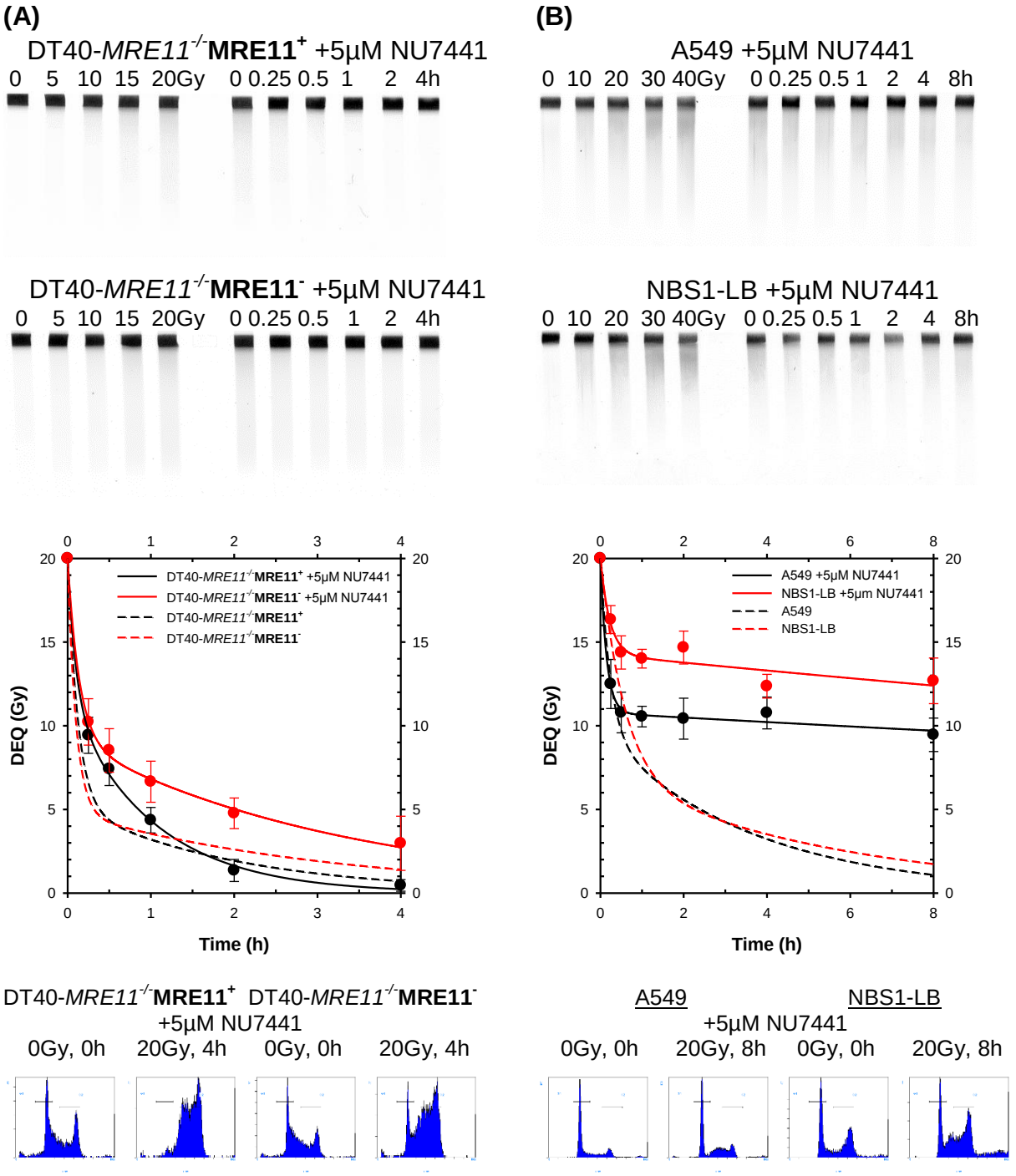

Figure 37: MRN contributes to DSB repair by B-NHEJ. For B-NHEJ repair experiments, the indicated cell types were incubated for 1h with 5µM NU7441 to inhibit D-NHEJ, were subsequently exposed to 20Gy x-rays and returned to 37°C for repair. The upper two panels show typical gels for dose response and repair kinetics experiments, obtained with repair-proficient cells and the MRN mutants. To measure DSBs present in cells, PFGE was performed as described above. Repair kinetics for the same cells is plotted as DEQ versus time. The reduction of DEQ as a function of the repair time signifies rejoining of DSBs. Results shown are the average of four determinations in three independent experiments, along with standard errors. Results were fitted to the sum of two exponentials. The bottom panel shows DNA histograms of mock-irradiated as well as irradiated cells at the indicated times post-irradiation. IR treatment led to the activation of cell cycle-dependent checkpoints and increased the fraction of cells in the G2-phase of the cell cycle at 4 and 8h post-irradiation.

Repair was evident in all cell types tested. However, when D-NHEJ was inhibited, to allow B-NHEJ to dominate, the DSB rejoining kinetics were slowed down in all cells as compared to their untreated counterparts (dashed line). This decrease in DSB rejoining efficiency is especially visible in human A549 and NBS1-LB cells (Fig. 37 B), where nearly 50% and 65% of the initial IR-induced DSBs were still present 8h after irradiation. In contrast, a significant rejoining of DSBs was observed in treated A549 cells at early times. Interestingly, chicken DT40 cells showed superior ability to repair DSBs, even when D-NHEJ was inhibited. In these cells, the observed DSB rejoining kinetics was very efficient although slightly slower than those obtained with untreated cells. Remarkably, no significant difference in the rejoining of DSBs was detectable between untreated and D-NHEJ-inhibited DT40-*MRE11*$^{-/-}$MRE11^{+} cells at later post-irradiation times. These results demonstrated the strong potential of DT40-*MRE11*$^{-/-}$MRE11^{+} cells to remove DSBs from their genome despite inhibited DNA-PKcs, as nearly 95% of the initial DSB load was rejoined by 2h after IR exposure. Repair of DSBs in the presence of NU7441 that inhibits DNA-PKcs is thought to be carried out by alternative pathways of end joining.

Following NU7441 treatment, MRN mutants showed a significant reduction in DSB rejoining as compared to MRN proficient cells. Interestingly, the kinetics of both MRN-deficient mutants indicated faster rejoining at early times, which later slowed down. In addition, D-NHEJ-inhibited DT40-*MRE11*$^{-/-}$MRE11^{-} cells were more efficient in rejoining IR-induced DSBs, than NBS1-deficient cells; they removed the majority of DSBs (>85%) by 4h, whereas nearly 65% of the initial DSBs remained unrepaired 8h post-irradiation in NBS1-LB cells. Overall, these results unveiled a substantial role of MRN in DSB repair by B-NHEJ.

4.3 Examination of DNA-PK impact in DDR and DSB repair

As discussed above (1.4), DSBs can be repaired by various pathways including NHEJ and HRR. It is widely assumed that in higher eukaryotes NHEJ is the main DSB repair pathway and that HRR has only a small contributing function to DSB repair, restricted to the G2-phase of the cell cycle (Jeggo and Löbrich 2005; Beucher, Birraux *et al.* 2009). However, the cellular mechanisms that regulate DSB repair pathway choice are not well understood. Some studies suggest that these two mechanistically distinct repair pathways compete for DNA ends, whereas others report that DDR signaling and DSB repair pathways are actively controlled, and thus act in a well-coordinated manner to detect and process IR induced DNA damage (Allen, Kurimasa *et al.* 2002; Cui, Yu *et al.* 2005). In apparent agreement with the competition model, cells with defects in D-NHEJ showed increased HRR (Allen, Kurimasa *et al.* 2002). In particular, inactivation of D-NHEJ by eliminating DNA-PKcs resulted in elevated HRR (Delacote, Han *et al.* 2002; Shrivastav, Miller *et al.* 2009).

To determine the impact of DNA-PK in DDR and DSB repair by HRR, we examined IR-induced MRE11 and RAD51 foci in different DNA-PK mutants after different radiation doses and at different repair times.

4.3.1 DNA-PKcs influences the MRE11 IRIF response

To begin addressing the significance of DNA-PKcs in DDR, we examined MRE11 foci formation and decay dynamics in M059J cells. These cells are known to be completely lack DNA-PKcs (Lees-Miller, Godbout *et al.* 1995), and to also have low levels of ATM (Gately, Hittle *et al.* 1998) as a result of a frame-shift mutation. Thus, the expression level of DNA-PKcs in M059J cells is about 200 times lower than in M059K cells and DSBs cannot be repaired using the D-NHEJ repair pathway with fast half-time kinetics as an essential protein for D-NHEJ is missing. We therefore speculated that M059J cells would present an altered DNA damage response as measured by MRE11 IRIF.

To test this, enriched G1- and G2-phase, as well as log-phase M059J cells were irradiated with different radiation doses using radiation modalities of different LET. The time course of MRE11 IRIF response in M059J cells was examined and compared to that of M059K cells. To allow better comparison of MRE11 foci formation and decay dynamics in M059J and M059K cells, results of MRE11 IRIF response with M059K cells (dashed line), were also included in the graphs. Comparable results were obtained for both cell cycle phases after x-ray and neutron irradiation, respectively. For heavy ion irradiation experiments, centrifugal elutriation could not be performed, due to missing laboratory equipment at the irradiation facility. The results summarized in Fig. 38 A-C show MRE11 foci formation and decay dynamics in enriched G2-phase M059J cells after x-rays or neutrons and in log-phase cells after heavy ion irradiation.

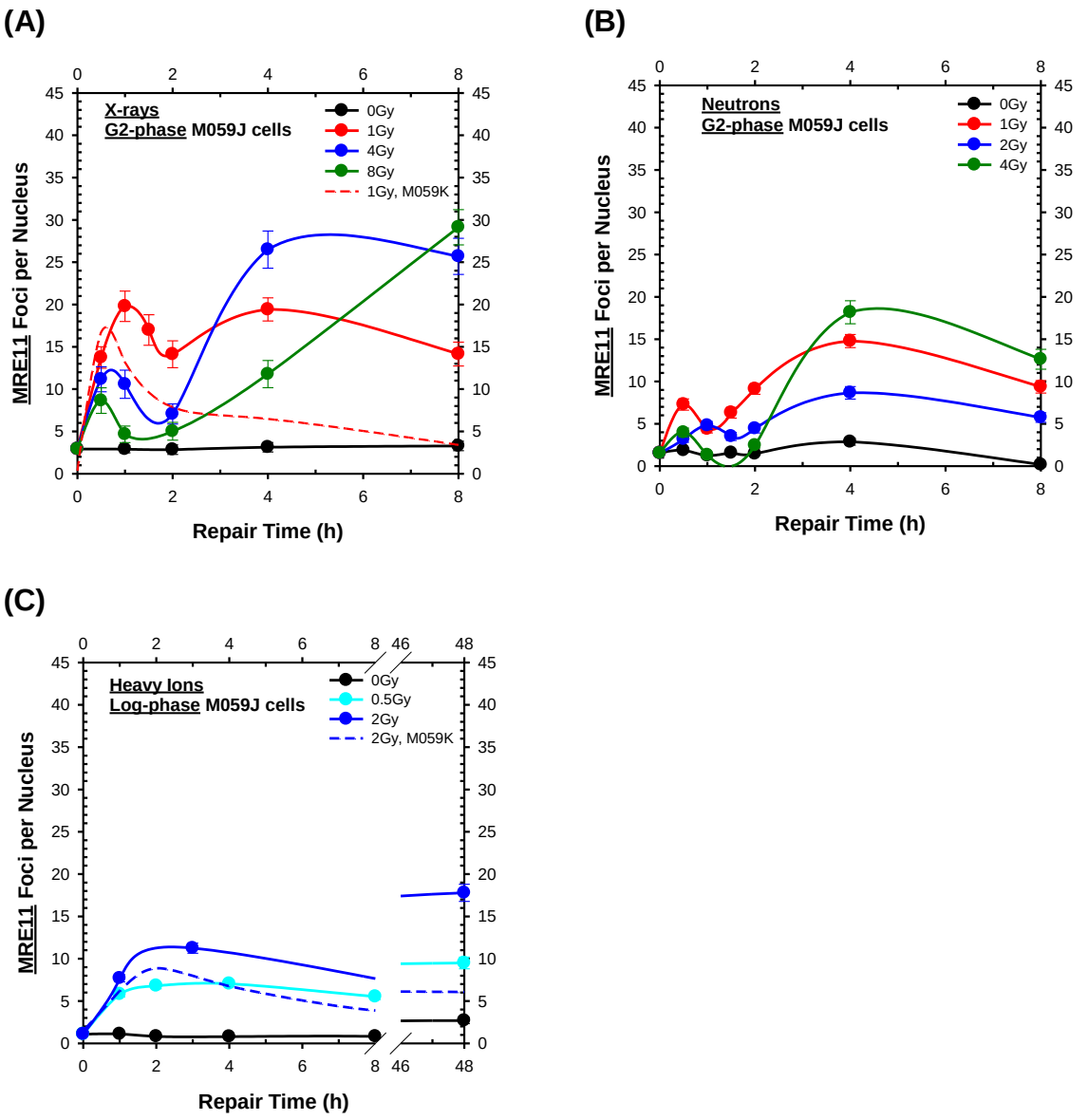

Figure 38: MRE11 IRIF response is altered in DNA-PKcs-deficient cells. Enriched G2-phase and log-phase M059J cells, respectively, were either mock treated or irradiated with the indicated radiation doses using radiation modalities of different LET. Cells were fixed after different recovery times and processed for immunofluorescent staining using anti-MRE11 antiserum, as described above. The mean MRE11 foci numbers were calculated and plotted as a function of time. Experiments were performed two times after x-ray (A), neutron (B) and heavy ion (C) irradiation, respectively. Error bars represent +/- standard errors.

Quantitative analysis of MRE11 foci revealed an enhanced MRE11 IRIF response in the DNA-PKcs-deficient M059J cells as compared to repair-proficient cells, M059K or A549 cells (4.1.5, 4.1.6). After exposure to high LET radiation, M059J cells presented higher MRE11 foci numbers, and clearly distinct MRE11 foci formation and decay dynamics.

After x-ray and neutron irradiation (Fig. 38 A-B), respectively, a fast MRE11 foci formation was observed with an additional MRE11 foci formation induction after 2h, whereas the MRE11 IRIF response was different in heavy ions irradiated M059J cells (Fig. 38 C). After heavy ion irradiation MRE11 foci formed as rapidly as after x-ray or neutron irradiation but their number slowly increased in the time course of the experiment with signs of recovery. Here again, the MRE11 IRIF response was sub-linear with increasing radiation dose.

In summary, a higher MRE11 foci number could be detected in DNA-PKcs-deficient M059J cells, which retained more MRE11 foci longer than repair-proficient cells, suggesting a slower completion of the overall repair process.

4.3.2 DNA-PK has a regulatory function in DSB repair by HRR

With the above results we show that DNA-PKcs-deficient cells have an altered response to DNA damage with more IR-induced MRE11 foci forming, which then decay very slowly over time, irrespective of the applied radiation dose or LET. This observation suggests a slower DSB repair process, as in D-NHEJ mutants, like M059J, a larger number of DSBs will be handled by HRR or B-NHEJ, both showing slower repair half-times.

Therefore we investigated next whether DNA-PK deficiency enhances HRR, as measured by RAD51 foci formation. For this purpose, we quantitatively analyzed RAD51 IRIF in enriched G2-phase *DNA-PKcs*$^{-/-}$ (PK33N), *KU70*$^{-/-}$, *KU80*$^{-/-}$ and *DNA-PKcs*$^{-/-}$*KU80*$^{-/-}$ (PK80-193A) mouse embryonic fibroblasts, and compared the results to wild-type cells (PK34N). Fig. 39 A-D shows the results of RAD51 foci formation and decay dynamics in the indicated cell lines after different x-ray doses and repair times. Comparable results were obtained in *KU70*$^{-/-}$ MEFs and are thus excluded for clarity from the figure below.

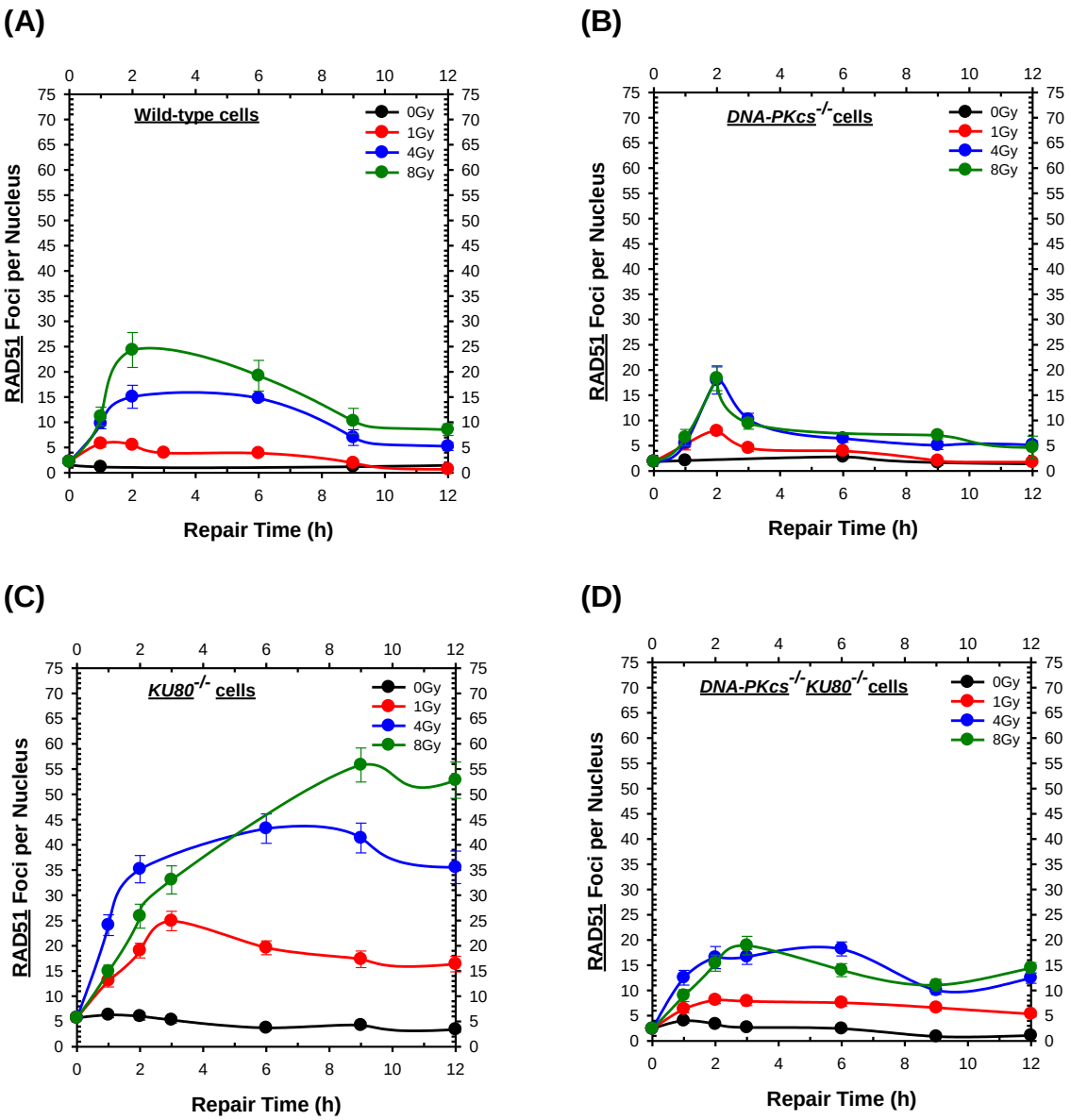

Figure 39: KU heterodimer strongly affects the initiation of HRR. The indicated cell lines were enriched in G2-phase of the cell cycle by centrifugal elutriation, and were irradiated with 0, 1, 4 and 8Gy x-rays. After different repair times cells were fixed, and stained with anti-RAD51 antibody. RAD51 foci were scored as described under "Materials and Methods". The time course of mean RAD51 IRIF per cell nucleus is plotted after different radiation doses in wild-type (A), *DNA-PKcs*$^{-/-}$ (B), *KU80*$^{-/-}$ (C) and *DNA-PKcs*$^{-/-}$*KU80*$^{-/-}$ (D) mouse embryonic fibroblasts. Results are from three independent experiments. Error bars represent +/- standard errors.

Evidently, in response to IR similar RAD51 foci formation and decay dynamics were obtained in wild-type (PK34N) and DNA-PKcs-deficient (PK33N) cells (Fig. 39 A-B). In these cells, IR-induced RAD51 foci reached a maximum within 1-2h post-irradiation, and decayed to almost background levels during the time course of the experiment.

In contrast to that, KU80-deficient cells presented a different RAD51 IRIF response (Fig. 39 C), with three times higher RAD51 foci numbers per cell nucleus as compared to the other used cell lines. Remarkably, IR-induced RAD51 foci in these cells only moderately decayed over time following 1Gy of x-rays. On the other hand, less RAD51 IRIF developed in *DNA-PKcs*$^{-/-}$*KU80*$^{-/-}$ (PK80-193A) cells (Fig. 39 D), which rapidly reached a plateau and did not decay during the time interval of analysis. This plateau was not caused by scoring limitations because it was reached at ~20 foci per cell, which could be readily counted. The dose response for RAD51 foci formation was not linear in the range of doses tested (1 to 8Gy) in any of the cell lines examined.

Thus, following IR treatment significantly higher RAD51 foci numbers were obtained in KU-deficient cells, indicating a higher initiation of HRR in those cells. Moreover, KU and DNA-PK deficiency, resulted in incomplete HRR as almost no decay of RAD51 foci was observed in KU-deficient cells and the double KO for KU and DNA-PKcs. Hence, this observation suggests a regulatory function for DNA-PK in DSB repair by HRR. However, it raises questions regarding its mechanistic basis and warrants further investigations.

5 Discussion

5.1 The formation of MRN foci is IR- and DNA damage-dependent

We were able to show that MRE11 accumulates to discrete nuclear foci following exposure to IR. This was confirmed for several different human cell lines, such as lung carcinoma A549 cells, MRC5-SV1 fibroblasts, osteosarcoma tumor HT1080 fibroblasts and glioma M059K and M059J cells (4.1.1). All examined cell lines presented a detectable MRE11 protein accumulation to discrete nuclear foci only after radiation exposure, since almost no MRE11 foci could be detected in unirradiated cells. Moreover, simultaneous immunofluorescence analysis of nuclear IR-induced MRE11, RAD50 and NBS1 foci revealed a strong colocalization of MRN IRIF (4.1.2). These results allowed two important conclusions – (1) the formation of MRN foci was radiation-dependent, and (2) foci forming generally comprised all three component of the MRN complex, i.e. MRE11-RAD50-NBS1, indicating functional interaction between the MRN components and damaged DNA upon irradiation. In addition, by inducing localized DNA damage using high power lasers in discrete subnuclear volumes in live cells, we could demonstrate that MRE11 rapidly associates with damaged DNA *in vivo* (4.1.3).

These results are in line with several other studies, which showed that in response to treatment with DSB-inducing agents, human MRE11, RAD50 and NBS1 proteins accumulated to discrete small nuclear foci. It has been demonstrated that these proteins colocalized at DNA damage sites, confirming that MRE11-RAD50-NBS1 proteins act as a complex (Maser, Monsen *et al.* 1997; Carney, Maser *et al.* 1998; Mirzoeva and Petrini 2001; Lee, Fernandez-Capetillo *et al.* 2005; Robison, Dixon *et al.* 2007; Dellaire, Kepkay *et al.* 2009; Takahashi, Mori *et al.* 2010). Thus, the Kenshi Komatsu group provided *in vivo* direct evidence that MRE11, RAD50 and NBS1 proteins localized to IR-induced nuclear foci (Tauchi, Kobayashi *et al.* 2001). Furthermore, the Wyman laboratory demonstrated *in vitro* by scanning force microscopy-based volume analysis that MRE11, RAD50 and NBS1 formed stable complexes (van der Linden, Sanchez *et al.* 2009).

We confirmed that the formation of MRN IRIF was dependent on NBS1 as NBS1-deficient cells, which have no functional NBS1 protein as a result of a 5bp deletion within the NBS1 gene, showed no MRE11 foci formation (data not shown). It is known, that upon DNA damage induction, NBS1 recruits the MR complex from the cytoplasm to the nucleus, and then to sites of DSBs (Carney, Maser *et al.* 1998), particularly through the interaction between its C-terminal MRE11-binding domain, and the N-terminal FHA- and BRCT-domains of MRE11 (Desai-Mehta, Cerosaletti *et al.* 2001; Tauchi, Kobayashi *et al.* 2001; Zhao, Renthal *et al.* 2002). In addition, it was reported that mutations of conserved residues in FHA- and BRCT-domains of NBS1 disrupted nuclear MRN focus formation (Cerosaletti and Concannon 2004; Hari, Spycher *et al.* 2010). We were thus not surprised that NBS1-deficient cells did not form any MRE11 foci, implicating that MRE11 had cytoplasmic localization in NBS1-deficient cells.

In addition, we reported here that DNA damage-dependent nuclear MRE11 protein accumulation in HT1080-YFP-MRE11 cells that express N-terminally tagged MRE11-YFP proteins was slower than in those cells with a C-terminal YFP-tag. Due to the fact that the relocation of MRE11 is dependent on the interaction between the N-terminal NBS1-binding domain of MRE11 and NBS1, we are speculating that the N-terminal protein tag could hinder NBS1 from effectively binding to MRE11 affecting thus its nuclear localization to damaged DNA sites. However, to confirm this hypothesis further investigations are required.

5.2 IR-induced MRN foci have different qualitative features

We observed that the formation of nuclear MRN foci was strictly dependent upon the prior induction of DSBs. Moreover, the analysis of MRE11 foci formation in all examined cell types after exposure to either low or high LET radiation showed different MRE11 foci patterns at different times post-irradiation (4.1.4). In general, small foci were observed after short recovery times and low doses (1-2Gy) of low LET radiation, whereas after high radiation doses (4-8Gy) or high LET radiation the early response diminished leaving large foci to dominate the late response.

As discussed above, MRN is a keystone complex, rather than a single component within a linear pathway, as it has different enzymatic activities important for DNA damage sensing, signaling and DSB repair. We inquired whether IR-induced MRN foci of different size might reflect different functions of MRN in DSB repair. The dynamic assembly of large foci may be required for the repair of particularly complex and difficult to repair lesions. Such lesions are induced with higher frequency after exposure to high LET radiation, which also explains the dominance of large foci under these conditions. Small foci on the other hand, may be associated with signaling emanating from a larger fraction of DSBs.

The Petrini group was the first to report distinct localization patterns for nuclear MRE11 that were depended on the radiation dose applied and recovery times (Maser, Monsen *et al.* 1997). Furthermore, the Bonner laboratory hypothesized that the IRIF occur at sites where the repair machinery has difficulty repairing the breaks as a result of multiple ionization events along a radiation track (Paull, Rogakou *et al.* 2000). In line with this, Mirzoeva and Petrini (Mirzoeva and Petrini 2001) suggested that the later type of IR-induced MRE11 foci might represent MRE11's accumulation at irreparable or slowly repairing lesions that corresponds to downstream roles of MRN in DSB repair. Further studies reported that in response to DSBs MRN formed two types of nuclear foci: the first MRE11 foci type developed rapidly, was ATM-independent, and probably reflected the sensor mode of MRN action, while the second type of IR-induced MRE11 foci was ATM-dependent and prolonged (Mirzoeva and Petrini 2001; Mirzoeva and Petrini 2003). Accordingly, Petrini and Stracker (Petrini and Stracker 2003) proposed that following the initial action of MRN as a sensor, the subsequent phosphorylation of NBS1 turns it into a mediator in further stages of DDR. In addition, it was shown that high LET ions produced clear and large MRE11 foci (Karlsson and Stenerlöw 2004), and that the radiation dose and the time post-irradiation strongly influenced the number and the size of individual foci (van Veelen, Cervelli *et al.* 2005). Similar results were obtained for IR-induced γ-H2AX, ATM and RAD51 foci respectively, demonstrating that in response to high LET irradiation, the size and frequency of IRIF varied as a function of radiation quality, dose and recovery time (Costes, Boissiere *et al.* 2006).

5.3 The DNA damage-dependent response of MRN is bimodal

We showed in several repair-proficient cell lines, using radiation modalities of different LET, a cell cycle-independent bimodal MRN IRIF response with a sub-linear dose-dependency (4.1.5, 4.1.6). In general, after low radiation doses, fast developing MRN foci were detected, whereas high radiation doses caused a slower formation of MRN foci. Similar kinetics was also observed for nuclear chromatin accretion of MRE11 after exposure to IR. Notably, we were able to demonstrate that the bimodal response of IR-induced MRN foci was neither due to technical limitations in detection nor due to intracellular MRE11 protein depletion (4.1.8, 4.1.9).

We were thus wondering whether the bimodal response of MRN to DNA damage reflects its different functions in DSB repair, as discussed above for the different IR-dependent MRN foci patterns. This seems possible, since there is strong evidence that MRN is a primary DNA damage sensor that activates ATM, and hence initiates the intracellular DNA damage signaling cascade (Nelms, Maser *et al.* 1998; Carson, Schwartz *et al.* 2003; Uziel, Lerenthal *et al.* 2003; Bekker-Jensen, Lukas *et al.* 2006), but that it is also essential for all major DSB repair pathways (Tauchi, Kobayashi *et al.* 2002; Dinkelmann, Spehalski *et al.* 2009; Xie, Kwok *et al.* 2009; Taylor, Cecillon *et al.* 2010) despite the fact that they operate with different half times (Iliakis, Wang *et al.* 2004). Accordingly, the fast formation of small MRN foci and the increase of MRE11 protein accretion could be associated with MRN's activity as a DNA damage sensor, upstream of ATM, whereas after exposure to high radiation doses the slow formation of big IR-induced MRN foci and the slow accumulation of MRE11 protein at DNA damage sites, might reflect MRN's involvement in DSB repair pathways. Why so many MRN molecules are necessary at the site of one or a few DSBs is not known and remains to be resolved.

Our results are in agreement with previous studies, where in response to high x-ray doses (12Gy) only a slow appearance of IR-induced RAD50 foci was observed, associated with gradually increasing total fluorescence intensity of the individual foci (Paull, Rogakou *et al.* 2000; Gerashchenko and Dynlacht 2009). Eva Lee's group demonstrated a cell cycle-independent formation of nuclear DNA damage-dependent NBS1 foci (Yuan, Chang *et al.* 2003), and the Kanaar laboratory showed that radiation dose influenced the number of foci per nucleus and that the post-irradiation

time influenced the size of the foci (van Veelen, Cervelli *et al.* 2005). Interestingly, association of MRN with chromatin *in vivo* was shown by Zhao *et al.* (Zhao, Renthal *et al.* 2002). These authors claimed that MRN chromatin association was not exclusively dependent on IR, but increased also when cells entered S-phase. In support of this notion, we were also able to show a radiation-independent association of MRE11 with chromatin. However, we observed chromatin-bound MRE11 protein maxima at different recovery times after exposure to different radiation doses, indicating a radiation dose-dependent association of MRE11 with damaged DNA (Fig. 30 B). Moreover, the association of MRE11 with chromatin mirrored the kinetics of nuclear MRE11 protein abundance as well as the bimodal MRN IRIF response, following IR exposure. These data in aggregate demonstrated an interaction of MRN with damaged DNA in a time- and dose-dependent manner.

Quantitative analysis of MRN IRIF revealed that in response to high LET radiation, repair-proficient cells presented with less foci initially, retained however more foci at later times. As discussed above, these persisting foci may represent particularly complex and difficult to repair lesions associated with the increase in LET of radiation. The lower MRN foci numbers, following high LET irradiation, could be explained by the energy deposition pattern of high LET radiation. It is well established that high LET radiation deposits a large amount of energy in a much more localized area and creates thus a more localized and clustered DNA damage, including complex DSBs with multiple lesions within a helical turn. This is in contrast to low LET irradiation, where a more even distribution of energy will induce more frequently a uniform distribution of DNA damage that is separated by rather large distances (Goodhead 1994; Terato and Ide 2004; Okayasu, Okada *et al.* 2006). As a result of these characteristics of high LET radiation, the distribution pattern of clustered and complex DNA damage several DSBs can be generated in close proximity that will be detected as a single focus. This will affect both focus appearance, as well as the kinetics of its development and decay.

Our observations are in agreement with previous reports, where it was shown that after high LET irradiation, less IRIF formed than after x-rays, reflecting a clustering of multiple foci along the high LET ion track (Karlsson and Stenerlöw 2004; Costes, Boissiere *et al.* 2006). Moreover, it was shown that MRN remained associated to the damaged site until the bulk of DSB repair was completed (Nelms, Maser *et al.* 1998). Other groups have shown a slower DSB rejoining in response to high LET radiation (Stenerlöw, Höglund *et al.* 2000), presumably correlating with difficulties in the repair of the induced DSBs (Karlsson and Stenerlöw 2004).

However, the slower decay of MRN foci after high LET irradiation might also be because high LET radiation seems only to inhibit the KU-dependent DSB repair pathway (D-NHEJ), but not HRR or B-NHEJ. This hypothesis was postulated by the Ya Wang laboratory, demonstrating that high LET IR might induce small (<40bp) DSB fragments, which prevent KU from binding efficiently to the DNA ends, resulting in a delayed KU-dependent repair (Wang, Wang *et al.* 2008).

We concluded that persisting MRN foci represented DNA damage sites, which were difficult to repair and moreover suggested that with increasing lesion complexity, associated with an increase in LET, more DSBs were repaired slowly and recruited HRR for their removal from the genome.

In summary, while our results confirmed published data, they also extended the available information in several important ways, including highly sensitive detection methodology. Thus, previous studies used very high and very few radiation doses with only very few repair time points (Maser, Monsen *et al.* 1997). Therefore, important facts concerning the DNA damage-dependent response of MRN were missed. This study is the first to present full MRN IRIF formation and decay dynamics in several human cell lines at different LETs. The bimodal cell cycle-independent response of MRN foci formation and decay was shown here for the first time.

5.4 The MRN complex has different functions in DDR

The investigation of functional relationships between γ-H2AX and MRE11 IRIF revealed that following IR exposure, MRE11 co-localized with γ-H2AX to nuclear foci in a strongly dose- and time-dependent manner (4.1.11). There was no one-to-one colocalization between γ-H2AX and MRE11, indicating temporally and possibly also functionally distinct modes of operation of MRE11 in DDR. Generally, the early function of MRE11 was not overly DNA damage signaling-dependent, as only a small proportion of MRE11 foci colocalized with γ-H2AX foci (Fig. 33 A). On the other hand, γ-H2AX foci that were still present at later recovery times, when the vast majority of DSB repair was completed, showed a high colocalization with IR-induced MRE11 foci, implicating MRE11's involvement in DSB repair (Fig. 33 B). Hence, we speculated that these structures represent MRE11's accumulation at irreparable or slowly repairing lesions.

This is in keeping with several other studies, where a colocalization of γ-H2AX and MRN IRIF was shown (Paull, Rogakou *et al.* 2000; Mirzoeva and Petrini 2003; Karlsson and Stenerlöw 2004; Bekker-Jensen, Lukas *et al.* 2006; Hari, Spycher *et al.* 2010; Nakamura, Rao *et al.* 2010). Moreover, it was reported that the intensity of individual foci gradually increased over time, as did the extent of colocalization within individual cells (Paull, Rogakou *et al.* 2000). However, in previous sections (5.2, 5.3) we have postulated that the fast response of small MRN IRIF might reflect MRN's involvement in DNA damage sensing and signaling, whereas the slow response of big IR-induced MRN foci could reflect its contribution in the course of DSB repair. Indeed, there are several studies indicating that MRN acts as a primary DNA damage sensor, but is also involved in DNA damage signaling and DSB repair (Maser, Monsen *et al.* 1997; Nelms, Maser *et al.* 1998; Tauchi, Kobayashi *et al.* 2002; Carson, Schwartz *et al.* 2003; Uziel, Lerenthal *et al.* 2003; Taylor, Cecillon *et al.* 2010). Nevertheless, if one MRN focus represented a DNA damage sensing event, a larger MRN-γ-H2AX colocalization would be expected at early time points post-irradiation.

Taken together, while we could not exclude that the small, rapidly induced MRN foci did not reflect MRN's participation in DNA damage sensing and signaling, it seemed more reasonable to postulate that they reflect the involvement of MRN to DSB repair – presumably by HRR and/or B-NHEJ that operate with slower kinetics than NHEJ (Iliakis, Wang *et al.* 2004). It was hypothesized by several groups that the IRIF occur at sites where the repair machinery has difficulty repairing the breaks that are present (Paull, Rogakou *et al.* 2000; Petrini and Stracker 2003; Karlsson and Stenerlöw 2004). However, it remains to be solved, why so many proteins molecules are necessary at one DSB site and how MRN contributes to DDR.

5.5 The MRN complex acts as a factor in DSB repair

Our investigations confirmed that MRN acts as a repair factor in DSB repair. Moreover, we unveiled the contribution of MRN to different DSB repair pathways (4.2). Specifically, we could demonstrate a clear inter-dependent function of MRN and ATM in DSB repair by HRR. Interestingly, in MRN- and ATM-deficient cells respectively, DNA end resection was initiated, as visualized by RAD51 foci, but the DSB repair by HRR was incomplete as RAD51 foci did not decayed over time (4.2.1). Thus, HRR was impaired in cells without a functional MRN or ATM. We could thus conclude that MRN and ATM play an important role in HRR.

On the other hand, we could not detect a contribution of MRN to DSB repair by D-NHEJ, as measured by PFGE (4.2.2). But we were able to demonstrate that MRN has a role in DSB repair by B-NHEJ (4.2.3). These results allowed the important conclusion that MRN was not involved in all DSB repair pathways – it functioned specifically in HRR and B-NHEJ.

The above results are consistent with findings of other groups. It is well documented that the functions of MRN and ATM are intertwined (Maser, Monsen *et al.* 1997; Gatei, Young *et al.* 2000; Uziel, Lerenthal *et al.* 2003; Lee and Paull 2004; Difilippantonio, Celeste *et al.* 2005; Jazayeri, Balestrini *et al.* 2008; Di Virgilio, Ying *et al.* 2009). Moreover, the clinical presentation of human AT, ATLD and NBS patients is similar (Carney, Maser *et al.* 1998; Stewart, Maser *et al.* 1999; Shiloh and Kastan 2001).

It was hence not surprising that the MRE11 IRIF formation was severely reduced in ATM-deficient cells, which developed only 1/3 of the MRE11 foci scored in ATM-proficient cells and *vice versa* (4.1.10). There are some studies showing that in response to DSBs, MRN forms two types of nuclear foci: the first MRE11 foci type is rapid and ATM-independent, and probably reflects its sensor mode of action, while the second type of IR-induced MRE11 foci is ATM-dependent and prolonged (Mirzoeva and Petrini 2001; Mirzoeva and Petrini 2003). We might thus speculate that MRN IRIF-types reflected the independent function between MRN and ATM in focus formation.

Regarding MRN's function in recombinational repair, there are many studies showing that MRN is involved in DSB repair by HRR. This repair pathway requires architectural, structural and enzymatic components that can be provided by MRN. The DNA-tethering architectures of MRN implicate it as linker for homologous stretches of DNA and for tethering DNA ends in close proximity to facilitate repair using the sister chromatid. On the other hand, the end-resecting ability of MRE11 is implicated in DNA end processing that is essential for the formation of RAD51 nucleoprotein filament during the presynapsis step of recombination (Paull and Gellert 1998; Yamaguchi-Iwai, Sonoda *et al.* 1999; Tauchi, Kobayashi *et al.* 2002; de Jager, Trujillo *et al.* 2004; Yang, Saidi *et al.* 2006; Hopkins and Paull 2008; Budd and Campbell 2009; Cejka, Cannavo *et al.* 2010; Nimonkar, Genschel *et al.* 2011; Liao, Guay *et al.* 2012). Other groups showed that ATM defects impaired HR-mediated DSB repair (Golding, Rosenberg *et al.* 2004; Beucher, Birraux *et al.* 2009), particularly as *ATM*$^{-/-}$ cells showed altered kinetics of IR-induced RAD51 foci formation (Haaf, Golub *et al.* 1995; Maser, Monsen *et al.* 1997; Chen, Yuan *et al.* 1999; Morrison, Sonoda *et al.* 2000; Yuan, Chang *et al.* 2003). This is in agreement with our results, where we could clearly demonstrate that MRN and ATM had a strong impact on DSB repair by HRR, as documented by RAD51 IRIF. IR-induced RAD51 foci formed more rapidly in wild-type cells than in MRN- and ATM-deficient cells, although many more RAD51 foci accumulated in deficient cells (4.2.1), probably reflecting increased numbers of unrepaired breaks. We interpreted these findings to mean that the initial stages of recombination repair, mediated principally by RAD51 were disrupted by MRN and ATM deficiency.

Overall, these observations confirmed that MRN and ATM are major players in HRR and function in an inter-dependent manner. Notably, this study is the first to show detailed MRN and ATM foci formation and decay dynamics.

Whereas, it is well established that MRN participates in DSB repair by HRR, it is less clear how these proteins are involved in D-NHEJ or B-NHEJ. It is anticipated that MRN does contribute to both, D-NHEJ and B-NHEJ. However, published data is contradictory. Several studies claim that MRE11 is not important for accurate D-NHEJ (Moreau, Ferguson *et al.* 1999; Yamaguchi-Iwai, Sonoda *et al.* 1999; Di Virgilio and Gautier 2005; Taylor, Cecillon *et al.* 2010), and that it does not affect end-joining frequencies in plasmid based assays (Tauchi, Kobayashi *et al.* 2002; Yang, Saidi *et al.* 2006). In support of this notion, one group found the overall rates of DSB-rejoining in NBS cells, as measured by PFGE, to be very similar to those of wild-type cells (Kraakman-van der Zwet, Overkamp *et al.* 1999). On the other hand, other groups reported that MRN deficiency confers a strong defect in DSB repair by D-NHEJ, because MRE11 could control end-joining through both, ATM-dependent and ATM-independent pathways (Rass, Grabarz *et al.* 2009). The notion of MRN's involvement in D-NHEJ is supported by its ability to stabilize distant breaks (Fig. 16 A-B) (Hopfner, Craig *et al.* 2002), and by its DNA end recognition potential that implies a role in the early stage of NHEJ (Daley, Palmbos *et al.* 2005).

In addition, there is also strong evidence that MRN is involved in B-NHEJ (Xie, Kwok *et al.* 2009; Davies and Chen 2010; Della-Maria, Zhou *et al.* 2011). A likely function in this pathway is the processing by MRE11 of the DNA termini that seem to facilitate repair of DSBs by B-NHEJ (Deriano, Stracker *et al.* 2009; Rass, Grabarz *et al.* 2009; Lamarche, Orazio *et al.* 2010; Rahal, Henricksen *et al.* 2010; Taylor, Cecillon *et al.* 2010). In line with this postulate, several groups demonstrated that MRN deficiency was associated with strong defects in end-joining pathways involved in isotype class switching, and in the repair of chromosomal RAG-mediated DSBs generated during V(D)J recombination, affecting both B-NHEJ and D-NHEJ (Dinkelmann, Spehalski *et al.* 2009; Helmink, Bredemeyer *et al.* 2009; Saidi, Li *et al.* 2010). Overall, the precise functional significance of MRN in D-NHEJ and B-NHEJ requires further investigations.

However, in this study we provided further insights into how MRN contributed to different DSB repair pathways. We demonstrated that MRN deficiency had a dramatic impact on HRR. However, we also presented strong evidence that MRN was **not** required for D-NHEJ, although it played a substantial role in B-NHEJ. We concluded that MRN acted as a repair factor only in DSB repair pathways, where DNA end processing is an essential or a likely step, like HRR and B-NHEJ.

5.6 The DNA-PK has a regulatory function in DSB repair

As discussed above (1.4.3), the regulation of DSB repair pathway choice is still unknown. Thus, it is not clear how and when a cell selects which pathway to use for the repair of a given DSB, and whether the decision is affected by the nature of the DSB, or by a global regulatory network involving key regulatory proteins. Within this study we attempted to uncover such regulatory proteins by examining the putative role of DNA-PK in DSB repair pathway choice. This protein complex is one of the central components of D-NHEJ, and has been implicated in DDR signaling as a member of the PI3KK family. Moreover, DNA-PK is considered as one of the most important players in the maintenance of genomic stability (Chen, Trujillo *et al.* 2000; Meek, Gupta *et al.* 2004).

To investigate the role of DNA-PK in DSB repair, we used different DNA-PK-deficient cell lines and showed that DNA-PKcs contributes to DDR, as measured by MRE11 IRIF (4.3.1). Human DNA-PKcs-deficient M059J cells presented an altered response to DNA damage, irrespective of radiation dose or LET. Remarkably, these cells retained more MRE11 foci at later time points than their repair-proficient counterpart, M059K cells. This observation suggested a slower completion of the overall repair, probably because in D-NHEJ mutants a larger number of DSBs is handled by HRR or B-NHEJ, which operate with slower half-times (Wang, Zeng *et al.* 2001). This is in agreement with previous studies showing that MRE11 IRIF response was increased in D-NHEJ mutants (Maser, Monsen *et al.* 1997), and that DNA-PKcs-deficient cells were not capable of repairing DSBs with fast kinetics (Stiff, O'Driscoll *et al.* 2004). Moreover, Karlsson and Stenerloew (Karlsson and Stenerlöw 2004) reported that after high LET radiation exposure a high level of remaining foci correlated with the

lack of apparent DSB rejoining in M059J cells. Thus, functional DNA-PKcs seems also to be critical for DSB rejoining of breaks produced by radiation of high LET.

Furthermore, we detected a higher initiation of HRR in KU-deficient cells – although DSB repair appeared incomplete since IR-induced RAD51 foci did not decay over time (4.3.2). Increased HRR in cells with D-NHEJ defects was previously shown by several other groups, and can be explained by a passive competition model between D-NHEJ and HRR repair proteins (Pierce, Hu *et al.* 2001; Allen, Kurimasa *et al.* 2002; Delacote, Han *et al.* 2002; Barlow, Lisby *et al.* 2008; Taylor, Cecillon *et al.* 2010). However, the fact that higher eukaryotes predominantly use NHEJ for DSB repair makes a simple competition model difficult to accommodate as key determinant of DSB repair pathway choice.

Several lines of evidence suggest that DNA-PKcs is an active regulator of DSB repair. First there was the puzzling finding that inactivation of NHEJ by elimination of DNA-PKcs indeed increased HRR, but chemical inhibition of DNA-PKcs had the opposite effect (Perrault, Wang *et al.* 2004). These results suggested a model in which chemically inhibited DNA-PKcs fails to dissociate from DNA ends, and thereby blocks access to other NHEJ and HRR repair factors. The idea that DNA-PKcs actively regulates DSB repair pathway choice gained additional support when the Meek laboratory identified DNA-PKcs splice variants that lack the kinase domain and which surprisingly had dominant negative effects on DSB repair by HRR (Convery, Shin *et al.* 2005). Thus, the group of Jack Nickoloff reported more persistent IR-induced RAD51 foci formation in DNA-PKcs null cells, and proposed an active regulation of DSB repair by DNA-PKcs, despite an existing passive shunt to HRR (Shrivastav, Miller *et al.* 2009). These results strongly support the notion that DNA-PKcs is a key regulator of DSB repair pathway choice in higher eukaryotes and moreover indicate that DNA-PKcs is not only involved in DSB repair by D-NHEJ but also seems to have an effect on HRR. The latter function may contribute to DSB repair pathway choice, perhaps through a complex regulatory network that may involve crosstalk with ATM, and the regulation of other proteins involved in HRR, which are phosphorylated by DNA-PKcs and/or ATM.

However, based on the competition model between D-NHEJ and HRR, we were stunned about the DSB repair phenotype detected in *DNA-PKcs*$^{-/-}$ (PK33N) and *DNA-PKcs*$^{-/-}$*KU80*$^{-/-}$ double mutant mouse embryonic fibroblasts (Fig. 39 B, D). Those cells presented a RAD51 IRIF response comparable to that of wild-type cells (Fig. 39 A). We were thus wondering, whether the RAD51 IRIF response in *DNA-PKcs*$^{-/-}$ and *DNA-PKcs*$^{-/-}$*KU80*$^{-/-}$ cells was the expression of a regulatory network involving DNA-PKcs, KU and MRN proteins. It is well established that KU is the first factor of D-NHEJ to interact with DSB ends, and which may help to bring and hold the DNA ends together (Feldmann, Schmiemann *et al.* 2000; Walker, Corpina *et al.* 2001), and for recruiting DNA-PKcs to the DNA ends (Lees-Miller and Meek 2003). As discussed above, DNA-PKcs seems to regulate HRR. Additionally, KU and MRN are known to interact with each other in somatic and yeast cells, respectively (Goedecke, Eijpe *et al.* 1999; Wu, Topper *et al.* 2008). Thus, we hypothesized that the response of IR-induced RAD51 foci in *DNA-PKcs*$^{-/-}$ cells (Fig. 39 B) was mediated by the KU heterodimer that was binding to DNA ends, hence preventing DNA end processing by MRN; a function required for efficient HRR. The response observed in the double DNA-PKcs and KU mutant might be due to the fact that the active HRR regulator – DNA-PKcs – acts in a KU-dependent manner. Hence, even though KU is not there to block the DNA ends for processing by MRN, DNA-PKcs is missing to regulate repair by HRR.

6 Summary and prospects

In summary, our results confirmed that following IR, MRN forms, in fixed and live cells, nuclear foci, which comprised the entire MRE11-RAD50-NBS1 protein complex, and which localized at the sites of DSBs. However, the results obtained also provided new insights. To date, we are the first to show a bimodal cell cycle-independent MRN IRIF response with different MRE11 foci patterns, using different radiation modalities. We documented small MRE11 IRIF mainly forming at early time points and which later developed to larger MRE11 foci. Notably, after high LET irradiation the initial MRE11 IRIF response mostly included large MRE11 foci.

These observations indicated that the dynamic assembly of large MRE11 foci may be required for the repair of particularly complex and difficult to repair DSBs induced by high LET irradiation or by high doses of low LET radiation. We concluded that complex DSBs induced by high LET radiation changed the accretion characteristics of MRE11. Moreover, we confirmed an inter-dependent function of MRE11 and ATM to IR, as ATM influenced MRN's ability to localize to nuclear foci and *vice versa*. However, the colocalization analysis of γ-H2AX and MRE11 IRIF suggested functionally distinct modes of MRE11's activity in DDR, as MRE11 clearly localized to sites of γ-H2AX but could be found only at a subset of DSBs.

In addition, our results unveiled the contribution of MRN to different DSB repair pathways, and confirmed that MRN acts as a repair factor in several of them. Specifically, we showed that MRN and ATM deficiency had a dramatic impact on HRR. Thus, in cells with defective MRN or ATM, DNA end resection was initiated but repair remained incomplete. On the other hand, we could not detect a contribution of MRE11 to DSB repair by D-NHEJ. However, we were able to show that MRN plays a major role in DSB repair by B-NHEJ. These results in aggregate provided strong evidence that MRN is not involved in **all** DSB repair pathways, as it is occasionally anticipated in published reports. The MRN complex seems to specifically function in HRR and B-NHEJ, where DNA end processing is an essential or a likely step.

In addition, we demonstrated a clear effect of DNA-PKcs in DDR, as higher and longer persisting MRE11 foci numbers were detected in DNA-PKcs-deficient cells. In addition, we showed that DNA-PK not only plays a role in D-NHEJ but also has a function in HRR. Specifically, we detected a higher initiation of HRR in KU-deficient cells and, more interestingly, incomplete HRR in DNA-PK-deficient cells.

Still many questions remain unanswered. It remains to be elucidated what exactly a small and a large MRN focus represents. Does a small and rapidly forming MRN focus represent MRN's participation in DNA damages sensing and signaling, or do all MRN IRIF reflect its involvement in DSB repair, independently of their size. It remains also unknown why so many protein molecules are necessary at one DSB site. How MRN contributes to DDR and why MRN IRIF do form in a bimodal and cell cycle-independent mode certainly requires further investigation.

Although we were able to unveil MRN's contribution to different DSB repair pathways, its precise role and exact mechanistic contribution to HRR and B-NHEJ remains unknown. Moreover, it remains to be solved how the different DSB repair pathways are controlled. Is it just a simple competition between the different DSB repair pathways or are there regulatory proteins, like MRN or DNA-PK, which actively regulate this choice. Is DNA end processing the key step in DSB pathway choice? Addressing these questions is certain to be the focus of numerous future studies.

7 Bibliography

Ajimura, M., S.-H. Leem, *et al.* (1993). "Identification of new genes required for meiotic recombination in *Saccharomyces cerevisiae.*" Genetics **133**: 51-66.

Alani, E., S. Subbiah, *et al.* (1989). "The yeast RAD50 gene encodes a predicted 153-kD protein containing a purine nucleotide-binding domain and two large heptad-repeat regions." Genetics **122**: 47-57.

Alberts, B., A. Johnson, *et al.* (2008). Molecular Biology of The Cell. New York, Garland Science, Taylor & Francis Group.

Allen, C., A. Kurimasa, *et al.* (2002). "DNA-dependent protein kinase suppresses double-strand break-induced and spontaneous homologous recombination." Proceedings of the National Academy of Sciences of the United States of America **99**: 3758-3763.

Anderson, L., C. Henderson, *et al.* (2001). "Phosphorylation and Rapid Relocalization of 53BP1 to Nuclear Foci upon DNA Damage." Molecular and Cellular Biology **21**(5): 1719-1508.

Arnaudeau, C., C. Lundin, *et al.* (2001). "DNA double-strand breaks associated with replication forks are predominantly repaired by homologous recombination involving an exchange mechanism in mammalian cells." Journal of Molecular Biology **307**(5): 1235-1245.

Audebert, M., B. Salles, *et al.* (2004). "Involvement of Poly(ADP-ribose) Polymerase-1 and XRCC1/DNA Ligase III in an Alternative Route for DNA Double-strand Breaks Rejoining." Journal of Biological Chemistry **279**: 55117-55126.

Aylon, Y., B. Liefshitz, *et al.* (2004). "The CDK regulates repair of double-strand breaks by homologous recombination during the cell cycle." EMBO Journal **23**(24): 4868-4875.

Bakkenist, C. J. and M. B. Kastan (2003). "DNA damage activates ATM through intermolecular autophosphorylation and dimer dissociation." Nature **421**: 499-506.

Balajee, A. S. and C. R. Geard (2004). "Replication protein A and γ-H2AX foci assembly is triggered by cellular response to DNA double-strand breaks." Experimental Cell Research **300**: 320-334.

Ballarini, F., D. Alloni, *et al.* (2008). "Heavy-ion effects: from track structure to DNA and chromosome damage." New Journal of Physics **10**: doi:10.1088/1367-2630/1010/1087/075008.

Banin, S., L. Moyal, *et al.* (1998). "Enhanced phosphorylation of p53 by ATM in response to DNA damage." Science **281**: 1674-1677.

Barlow, J. H., M. Lisby, *et al.* (2008). "Differential Regulation of the Cellular Response to DNA Double-Strand Breaks in G1." Molecular Cell **30**(1): 73-85.

Bekker-Jensen, S., C. Lukas, *et al.* (2006). "Spatial organization of the mammalian genome surveillance machinery in response to DNA strand breaks." Journal of Cell Biology **173**(2): 195-206.

Bennetzen, M. V., D. H. Larsen, *et al.* (2010). "Site-specific Phosphorylation Dynamics of the Nuclear Proteome during the DNA Damage Response." Molecular & Cellular Proteomics **9**: 1314-1323.

Berkovich, E., R. J. Monnat Jr., *et al.* (2007). "Roles of ATM and NBS1 in chromatin structure modulation and DNA double-strand break repair." Nature Cell Biology **9**(6): 683-690.

Berns, M. W., Z. Wang, *et al.* (2000). "Gene inactivation by multiphoton-targeted photochemistry." Proceedings of the National Academy of Sciences of the United States of America **97**(17): 9504-9507.

Beucher, A., J. Birraux, *et al.* (2009). "ATM and Artemis promote homologous recombination of radiation-induced DNA double-strand breaks in G2." EMBO Journal **28in press**: 3413-3427.

Bhaskara, V., A. Dupre, *et al.* (2007). "Rad50 Adenylate Kinase Activity Regulates DNA Tethering by Mre11/Rad50 Complexes." Molecular Cell **25**: 647-661.

Bolderson, E., N. Tomimatsu, *et al.* (2010). "Phosphorylation of Exo1 modulates homologous recombination repair of DNA double-strand breaks." Nucleic Acids Research **38**(6): 1821-1831.

Borde, V. and J. Cobb (2009). "Double functions for the Mre11 complex during DNA double-strand break repair and replication." International Journal of Biochemistry & Cell Biology **41**(6): 1249-1253.

Budd, M. E. and J. L. Campbell (2009). "Interplay of Mre11 Nuclease with Dna2 plus Sgs1 in Rad51-Dependent Recombinational Repair." PLoS ONE **4**(1): e4267.

Buis, J., Y. Wu, *et al.* (2008). "Mre11 Nuclease Activity Has Essential Roles in DNA Repair and Genomic Stability Distinct from ATM Activation." Cell **135**(1): 85-96.

Burma, S., B. P. Chen, *et al.* (2001). "ATM phosphorylates histone H2AX in response to DNA double-strand breaks." Journal of Biological Chemistry **276**: 42462-42467.

Calmettes, P. P. and M. W. Berns (1983). "Laser-induced multiphoton processes in living cells." Proceedings of the National Academy of Sciences of the United States of America **80**: 7197-7199.

Canman, C. E., D.-S. Lim, *et al.* (1998). "Activation of the ATM kinase by ionizing radiation and phosphorylation of p53." Science **281**: 1677-1679.

Capp, J.-P., F. Boudsocq, *et al.* (2006). "The DNA polymerase {lambda} is required for the repair of non-compatible DNA double strand breaks by NHEJ in mammalian cells." Nucleic Acids Research **34**(10): 2998-3007.

Carney, J. P., R. S. Maser, *et al.* (1998). "The hMre 11/hRad50 protein complex and Nijmegen breakage syndrome: Linkage of double-strand break repair." Cell **93**: 477-486.

Carson, C. T., R. A. Schwartz, *et al.* (2003). "The Mre11 complex is required for ATM activation and the G_2/M checkpoint." EMBO Journal **22**: 6610-6620.

Cejka, P., E. Cannavo, *et al.* (2010). "DNA end resection by Dna2-Sgs1-RPA and its stimulation by Top3-Rmi1 and Mre11-Rad50-Xrs2." Nature **467**(7311): 112-116.

Celeste, A., O. Fernandez-Capetillo, *et al.* (2003). "Histone H2AX phosphorylation is dispensable for the initial recognition of DNA breaks." Nature Cell Biology **5**: 675-679.

Cerosaletti, K. and P. Concannon (2004). "Independent Roles for Nibrin and Mre11-Rad50 in the Activation and Function of Atm." Journal of Biological Chemistry **279**: 38813-38819.

Chaturvedi, P., W. K. Eng, *et al.* (1999). "Mammalian Chk2 is a downstream effector of the ATM-dependent DNA damage checkpoint pathway." Oncogene **18**: 4047-4054.

Chen, G., S.-S. F. Yuan, *et al.* (1999). "Radiation-induced assembly of Rad51 and Rad52 recombination complex requires ATM and c-Abl." Journal of Biological Chemistry **274**: 12748-12752.

Chen, H. T., A. Bhandoola, *et al.* (2000). "Response to RAG-Mediated V(D)J Cleavage by NBS1 and γ-H2AX." Science **290**: 1962-1964.

Chen, L., K. Trujillo, *et al.* (2000). "Interactions of the DNA Ligase IV-XRCC4 Complex with DNA Ends and the DNA-dependent Protein Kinase." Journal of Biological Chemistry **275**(34): 26196-26205.

Claxton, N. S., T. J. Fellers, *et al.*

Convery, E., E. K. Shin, *et al.* (2005). "Inhibition of homologous recombination by variants of the catalytic subunit of the DNA-dependent protein kinase (DNA-PKcs)." Proceedings of the National Academy of Sciences of the United States of America **102**(5): 1345-1350.

Cortez, D., Y. Wang, *et al.* (1999). "Requirement of ATM-Dependent Phosphorylation of Brca1 in the DNA Damage Response to Double-Strand Breaks." Science **286**: 1162-1166.

Costes, S. V., A. Boissiere, *et al.* (2006). "Imaging Features that Discriminate between Foci Induced by High- and Low-LET Radiation in Human Fibroblasts." Radiation Research **165**: 505-515.

Couedel, C., K. D. Mills, *et al.* (2004). "Collaboration of homologous recombination and nonhomologous end-joining factors for the survival and integrity of mice and cells." Genes & Development **18**: 1293-1304.

Critchlow, S. E. and S. P. Jackson (1998). "DNA end-joining: from yeast to man." Trends in Biochemical Sciences **23**: 394-398.

Cruet-Hennequart, S., M. T. Glynn, *et al.* (2008). "Enhanced DNA-PK-mediated RPA2 hyperphosphorylation in DNA polymerase [eta]-deficient human cells treated with cisplatin and oxaliplatin." DNA Repair **7**(4): 582-596.

Cui, X. and K. Meek (2007). "Linking double-stranded DNA breaks to the recombination activating gene complex directs repair to the nonhomologous end-joining pathway." Proceedings of the National Academy of Sciences of the United States of America **104**(43): 17046-17051.

Cui, X., Y. Yu, *et al.* (2005). "Autophosphorylation of DNA-Dependent Protein Kinase Regulates DNA End Processing and May Also Alter Double-Strand Break Repair Pathway Choice." Molecular and Cellular Biology **25**(24): 10842-10852.

d'Adda di Fagagna, F., P. M. Reaper, *et al.* (2003). "A DNA damage checkpoint response in telomere-initiated senescence." Nature **426**: 194-198.

D'Amours, D. and S. P. Jackson (2002). "The Mre11 Complex: At the Crossroads of DNA Repair and Checkpoint Signalling." Nature Reviews **3**: 317-327.

Daboussi, F., A. Dumay, *et al.* (2002). "DNA double-strand break repair signalling: The case of RAD51 post-translational regulation." Cellular Signalling **14**: 969-975.

Daley, J. M., P. L. Palmbos, *et al.* (2005). "Nonhomologous End Joining in Yeast." Annual Review of Genetics **39**: 431-451.

Davies, A. J. and D. J. Chen (2010). "A role for ATM kinase activity and Mre11 in microhomology-mediated end-joining." Cell Cycle **9**(16): 3147-3148.

de Jager, M., K. M. Trujillo, *et al.* (2004). "Differential Arrangements of Conserved Building Blocks among Homologs of the Rad50/Mre11 DNA Repair Protein Complex." Journal of Molecular Biology **339**: 937-949.

de Jager, M., J. van Noort, *et al.* (2001). "Human Rad50/Mre11 Is a Flexible Complex that Can Tether DNA Ends." Molecular Cell **8**: 1129-1135.

Delacote, F., M. Han, *et al.* (2002). "An xrcc4 defect or Wortmannin stimulates homologous recombination specifically induced by double-strand breaks in mammalian cells." Nucleic Acids Research **30**: 3454-3463.

Della-Maria, J., Y. Zhou, *et al.* (2011). "Human Mre11/Human Rad50/Nbs1 and DNA Ligase IIIα/XRCC1 Protein Complexes Act Together in an Alternative Nonhomologous End Joining Pathway." Journal of Biological Chemistry **286**(39): 33845-33853.

Dellaire, G., R. Kepkay, *et al.* (2009). "High resolution imaging of changes in the structure and spatial organization of chromatin, γ-H2A.X and the MRN complex within etoposide-induced DNA repair foci." Cell Cycle **8**(22): 3750-3769.

Demuth, I., P.-O. Frappart, *et al.* (2004). "An inducible null mutant murine model of Nijmegen breakage syndrome proves the essential function of NBS1 in chromosomal stability and cell viability." Human Molecular Genetics **13**: 2385-2397.

Deriano, L., T. H. Stracker, *et al.* (2009). "Roles for NBS1 in Alternative Nonhomologous End-Joining of V(D)J Recombination Intermediates." Molecular Cell **34**(1): 13-25.

Desai-Mehta, A., K. M. Cerosaletti, *et al.* (2001). "Distinct Functional Domains of Nibrin Mediate Mre11 Binding, Focus Formation, and Nuclear Localization." Molecular and Cellular Biology **21**(6): 2184-2025.

Di Virgilio, M. and J. Gautier (2005). "Repair of double-strand breaks by nonhomologous end joining in the absence of Mre11." Journal of Cell Biology **171**(5): 765-771.

Di Virgilio, M., C. Y. Ying, *et al.* (2009). "PIKK-dependent phosphorylation of Mre11 induces MRN complex inactivation by disassembly from chromatin." DNA Repair **8**(11): 1311-1320.

DiBiase, S. J., Z.-C. Zeng, *et al.* (2000). "DNA-dependent protein kinase stimulates an independently active, nonhomologous, end-joining apparatus." Cancer Research **60**: 1245-1253.

Difilippantonio, S., A. Celeste, *et al.* (2005). "Role of Nbs1 in the activation of the Atm kinase revealed in humanized mouse models." Nature Cell Biology **7**(7): 675-685.

Dimitrova, N. and T. de Lange (2009). "Cell Cycle-Dependent Role of MRN at Dysfunctional Telomeres: ATM Signaling-Dependent Induction of Nonhomologous End Joining (NHEJ) in G1 and Resection-Mediated Inhibition of NHEJ in G2." Molecular and Cellular Biology **29**(20): 5552-5563.

Dinkelmann, M., E. Spehalski, *et al.* (2009). "Multiple functions of MRN in end-joining pathways during isotype class switching." Nature Structural & Molecular Biology **16**(8): 808-813.

Dong, Z., Q. Zhong, *et al.* (1999). "The Nijmegen breakage syndrome protein is essential for Mre11 phosphorylation upon DNA damage." Journal of Biological Chemistry **274**: 19513-19516.

Esashi, F., N. Christ, *et al.* (2005). "CDK-dependent phosphorylation of BRCA2 as a regulatory mechanism for recombinational repair." Nature **434**: 598-604.

Essers, J., H. van Steeg, *et al.* (2000). "Homologous and non-homologous recombination differentially affect DNA damage repair in mice." EMBO Journal **19**: 1703-1710.

Fanning, E., V. Klimovich, *et al.* (2006). "A dynamic model for replication protein A (RPA) function in DNA processing pathways." Nucleic Acids Research **34**(15): 4126-4137.

Fattah, F., E. H. Lee, *et al.* (2010). "Ku Regulates the Non-Homologous End Joining Pathway Choice of DNA Double-Strand Break Repair in Human Somatic Cells." PLoS Genetics **6**(2): e1000855.

Fattah, F. J., N. F. Lichter, *et al.* (2008). "Ku70, an essential gene, modulates the frequency of rAAV-mediated gene targeting in human somatic cells." Proceedings of the National Academy of Sciences of the United States of America **105**(25): 8703-8708.

Feldmann, E., V. Schmiemann, *et al.* (2000). "DNA double-strand break repair in cell-free extracts from Ku80-deficient cells: implications for Ku serving as an alignment factor in non-homologous DNA end joining." Nucleic Acids Research **28**: 2585-2596.

Fernandez-Capetillo, O., A. Celeste, *et al.* (2003). "Focusing on foci: H2AX and the recruitment of DNA-damage response factors." Cell Cycle **2**(5): 426-427.

Fukushima, T., M. Takata, *et al.* (2001). "Genetic Analysis of the DNA-dependent Protein Kinase Reveals an Inhibitory Role of Ku in Late S-G_2 Phase DNA Double-strand Break Repair." Journal of Biological Chemistry **276**: 44413-44418.

Gatei, M., D. Young, *et al.* (2000). "ATM-dependent phosphorylation of nibrin in response to radiation exposure." Nature Genetics **25**: 115-119.

Gately, D. P., J. C. Hittle, *et al.* (1998). "Characterization of ATM expression, localization, and associated DNA-dependent protein kinase activity." Molecular Biology of the Cell **9**: 2361-2374.

Gerashchenko, B. I. and J. R. Dynlacht (2009). "A tool for enhancement and scoring of DNA repair foci." Cytometry Part A **75A**(3): 245-252.

Giesen, U., F. Langner, *et al.* (2011). "Online imaging of initial DNA damages at the PTB microbeam." Radiation Protection Dosimetry **143**(2-4): 349-352.

Girard, P.-M., N. Foray, *et al.* (2000). "Radiosensitivity in Nijmegen breakage syndrome cells is attributable to a repair defect and not cell cycle checkpoint defects." Cancer Research **60**: 4881-4888.

Goedecke, W., M. Eijpe, *et al.* (1999). "Mre11 and Ku70 interact in somatic cells, but are differentially expressed in early meiosis." Nature Genetics **23**: 194-198.

Goldberg, M., M. Stucki, *et al.* (2003). "MDC1 is required for the intra-S-phase DNA damage checkpoint." Nature **421**: 952-956.

Golding, S. E., E. Rosenberg, *et al.* (2004). "Double Strand Break Repair by Homologous Recombination Is Regulated by Cell Cycle-independent Signaling via ATM in Human Glioma Cells." Journal of Biological Chemistry **279**: 15402-15410.

Goodhead, D. T. (1994). "Initial events in the cellular effects of ionizing radiations: clustered damage in DNA." International Journal of Radiation Biology **65**(1): 7-17.

Goodhead, D. T. (1995). "Molecular and cell models of biological effects of heavy ion radiation." Radiation and Environmental Biophysics **34**: 67-72.

Goodhead, D. T. (2006). "Energy deposition stochastics and track structure: what about the target?" Radiation Protection Dosimetry **122**(1-4): 3-15.

Goodhead, D. T. and H. Nikjoo (1989). "Track structure analysis of ultrasoft X-rays compared to high- and low-LET radiations." International Journal of Radiation Biology **55**(4): 513-529.

Griffin, C. S., P. J. Simpson, *et al.* (2000). "Mammalian recombination-repair genes XRCC2 and XRCC3 promote correct chromosome segregation." Nature Cell Biology **2**: 757-761.

Haaf, T., E. I. Golub, *et al.* (1995). "Nuclear foci of mammalian Rad51 recombination protein in somatic cells after DNA damage and its localization in synaptonemal complexes." Proceedings of the National Academy of Sciences of the United States of America **92**: 2298-2302.

Hada, M. and A. G. Georgakilas (2008). "Formation of Clustered DNA Damage after High-LET Irradiation: A Review." Journal of Radiation Research **49**(3): 203-210.

Haince, J.-F., D. McDonald, *et al.* (2008). "PARP1-dependent Kinetics of Recruitment of MRE11 and NBS1 Proteins to Multiple DNA Damage Sites." Journal of Biological Chemistry **283**(2): 1197-1208.

Hall, E. J. and A. J. Giaccia (2006). Radiobiology for the Radiologist. Philadelphia, Baltimore, New York, London, Buenos Aires, Hong Kong, Sydney, Tokyo, Lippincott Williams & Wilkins.

Hari, F. J., C. Spycher, *et al.* (2010). "A divalent FHA/BRCT-binding mechanism couples the MRE11-RAD50-NBS1 complex to damaged chromatin." EMBO Reports **11**(5): 387-392.

Hartwell, L. H. and T. A. Weinert (1989). "Checkpoints: Controls that ensure the order of cell cycle events." Science **246**: 629-634.

Hashimoto, Y., A. R. Chaudhuri, *et al.* (2010). "Rad51 protects nascent DNA from Mre11-dependent degradation and promotes continuous DNA synthesis." Nature Structural & Molecular Biology **17**(11): 1305-1311.

Heikkinen, K., K. Rapakko, *et al.* (2006). "RAD50 and NBS1 are breast cancer susceptibility genes associated with genomic instability." Carcinogenesis **27**(8): 1593-1599.

Helleday, T., J. Lo, *et al.* (2007). "DNA double-strand break repair: From mechanistic understanding to cancer treatment." DNA Repair **6**(7): 923-935.

Helmink, B. A., A. L. Bredemeyer, *et al.* (2009). "MRN complex function in the repair of chromosomal Rag-mediated DNA double-strand breaks." Journal of Experimental Medicine **206**(3): 669-679.

Helt, C. E., W. A. Cliby, *et al.* (2005). "Ataxia Telangiectasia Mutated (ATM) and ATM and Rad3-related Protein Exhibit Selective Target Specificities in Response to Different Forms of DNA Damage." Journal of Biological Chemistry **280**(2): 1186-1192.

Holley, W. R. and A. Chatterjee (1996). "Clusters of DNA damage induced by ionizing radiation: Formation of short DNA fragments. 1. Theoretical modeling." Radiation Research **145**: 188-199.

Hopfner, K.-P., L. Craig, *et al.* (2002). "The Rad50 zinc-hook is a structure joining Mre11 complexes in DNA recombination and repair." Nature **418**: 562-566.

Hopfner, K.-P., A. Karcher, *et al.* (2001). "Structural biochemistry and interaction architecture of the dna double-strand break repair mre11 nuclease and rad50-atpase." Cell **105**(4): 473-485.

Hopfner, K.-P., A. Karcher, *et al.* (2000). "Structural biology of Rad50 ATPase: ATP-driven conformational control in DNA double-strand break repair and the ABC-ATPase superfamily." Cell **101**: 789-800.

Hopkins, B. B. and T. T. Paull (2008). "The P. furiosus Mre11/Rad50 Complex Promotes 5' Strand Resection at a DNA Double-Strand Break." Cell **135**(2): 250-260.

Huertas, P., F. Cortes-Ledesma, *et al.* (2008). "CDK targets Sae2 to control DNA-end resection and homologous recombination." Nature **455**: 689-692.

Iijima, K., M. Ohara, *et al.* (2008). "Dancing on Damaged Chromatin: Functions of ATM and the RAD50/MRE11/NBS1 Complex in Cellular Responses to DNA Damage." Journal of Radiation Research **49**: 451-464.

Iliakis, G. (2009). "Backup pathways of NHEJ in cells of higher eukaryotes: Cell cycle dependence." Radiotherapy and Oncology **92**: 310-315.

Iliakis, G., B. Rosidi, *et al.* (2005). Plasmid-Based Assays for DNA End-Joining In Vitro. Methods in Molecular Biology: DNA Repair Protocols: Mammalian Systems. D. S. Henderson. Totowa, N.M., Humana Press Inc.**:** 123-131.

Iliakis, G., H. Wang, *et al.* (2004). "Mechanisms of DNA double strand break repair and chromosome aberration formation." Cytogenetic and Genome Research **104**: 14-20.

Jackson, S. P. (2002). "Sensing and repairing DNA double-strand breaks." Carcinogenesis **23**: 687-696.

Jazayeri, A., A. Balestrini, *et al.* (2008). "Mre11-Rad50-Nbs1-dependent processing of DNA breaks generates oligonucleotides that stimulate ATM activity." EMBO Journal **27**(14): 1953-1962.

Jeggo, P. A. and L. M. Kemp (1983). "X-ray-sensitive mutants of Chinese hamster ovary cell line. Isolation and cross-sensitivity to other DNA-damaging agents." Mutation Research **112**: 313-327.

Jeggo, P. A. and M. Löbrich (2005). "Artemis Links ATM to Double Strand Break Rejoining." Cell Cycle **4**: e-42-e-44.

Jones, J. and C. Simkus (2009). "The roles of the RAG1 and RAG2 “non-core” regions in V(D)J recombination and lymphocyte development." Archivum Immunologiae et Therapiae Experimentalis **57**(2): 105-116.

Kadhim, M. A., M. A. Hill, *et al.* (2006). "Genomic instability and the role of radiation quality." Radiation Protection Dosimetry **122**(1-4): 221-227.

Kanaar, R., J. H. J. Hoeijmakers, *et al.* (1998). "Molecular mechanisms of DNA double-strand break repair." Trends in Cell Biology **8**: 483-489.

Karlsson, K. H. and B. Stenerlöw (2004). "Focus Formation of DNA Repair Proteins in Normal and Repair-Deficient Cells Irradiated with High-LET Ions." Radiation Research **161**: 517-527.

Karran, P. (2000). "DNA double strand break repair in mammalian cells." Current Opinion in Genetics & Development **10**: 144-150.

Kastan, M. B. (2001). "Checking two steps." Nature **410**: 766-767.

Kastan, M. B. and D.-S. Lim (2000). "The many substrates and functions of ATM." Nature Reviews. Molecular Cell Biology **1**: 179-186.

Khanna, K. K. and S. P. Jackson (2001). "DNA double-strand breaks: signaling, repair and the cancer connection." Nature Genetics **27**: 247-254.

Kim, J.-E., K. Minter-Dykhouse, *et al.* (2006). "Signaling Networks Controlled by the MRN Complex and MDC1 During Early DNA Damage Responses." Molecular Carcinogenesis **45**: 403-408.

Kim, J.-S., T. B. Krasieva, *et al.* (2005). "Independent and sequential recruitment of NHEJ and HR factors to DNA damage sites in mammalian cells." Journal of Cell Biology **170**(3): 341-347.

Kinner, A., W. Wu, *et al.* (2008). "γ-H2AX in recognition and signaling of DNA double-strand breaks in the context of chromatin." Nucleic Acids Research **36**(17): 5678-5694.

Kobayashi, J., H. Tauchi, *et al.* (2002). "NBS1 localizes to γ-H2AX foci through interaction with the FHA/BRCT domain." Current Biology **12**: 1846-1851.

Kraakman-van der Zwet, M., W. J. I. Overkamp, *et al.* (1999). "Immortalization and characterization of Nijmegen Breakage Syndrome fibroblasts." Mutation Research **434**: 17-27.

Krüger, I., K. Rothkamm, *et al.* (2004). "Enhanced fidelity for rejoining radiation-induced DNA double-strand breaks in the G_2 phase of Chinese hamster ovary cells." Nucleic Acids Research **32**(9): 2677-2684.

Kurimasa, A., H. Ouyang, *et al.* (1999). "Catalytic subunit of DNA-dependent protein kinase: Impact on lymphocyte development and tumorigenesis." Proceedings of the National Academy of Sciences of the United States of America **96**: 1403-1408.

Lafleur, M. V. M., J. Woldhuis, *et al.* (1979). "Alkali-labile sites and post-irradiation effects in gamma-irradiated biologically active double-stranded DNA in aqueous solution." International Journal of Radiation Biology **36**(3): 241-247.

Lamarche, B. J., N. I. Orazio, *et al.* (2010). "The MRN complex in double-strand break repair and telomere maintenance." FEBS Letters **584**(17): 3682-3695.

Lavin, M. F. (2007). "ATM and the Mre11 complex combine to recognize and signal DNA double-strand breaks." Oncogene **26**(56): 7749-7758.

Lee, A. C., O. Fernandez-Capetillo, *et al.* (2005). "Specific Association of Mouse MDC1/NFBD1 with NBS1 at Sites of DNA-Damage." Cell Cycle **4**(1): 177-182.

Lee, G. S., M. B. Neiditch, *et al.* (2004). "RAG Proteins Shepherd Double-Strand Breaks to a Specific Pathway, Suppressing Error-Prone Repair, but RAG Nicking Initiates Homologous Recombination." Cell **117**: 171-184.

Lee, J.-H., R. Ghirlando, *et al.* (2003). "Regulation of Mre11/Rad50 by Nbs1." Journal of Biological Chemistry **278**(46): 45171-45181.

Lee, J.-H. and T. T. Paull (2004). "Direct Activation of the ATM Protein Kinase by the Mre11/Rad50/Nbs1 Complex." Science **304**: 93-100.

Lee, J.-H. and T. T. Paull (2005). "ATM Activation by DNA Double-Strand Breaks Through the Mre11-Rad50-Nbs1 Complex." Science **308**(5721): 551-554.

Lee, J. H. and T. T. Paull (2007). "Activation and regulation of ATM kinase activity in response to DNA double-strand breaks." Oncogene **26**(56): 7741-7748.

Lee, S. E., R. A. Mitchell, *et al.* (1997). "Evidence for DNA-PK-dependent and -independent DNA double-strand break repair pathways in mammalian cells as a function of the cell cycle." Molecular and Cellular Biology **17**: 1425-1433.

Lees-Miller, S. P., R. Godbout, *et al.* (1995). "Absence of p350 subunit of DNA-activated protein kinase from a radiosensitive human cell line." Science **267**: 1183-1185.

Lees-Miller, S. P. and K. Meek (2003). "Repair of DNA double strand breaks by non-homologous end joining." Biochimie **85**: 1161-1173.

Liao, S., C. Guay, *et al.* (2012). "Analysis of MRE11's function in the 5′→3′ processing of DNA double-strand breaks." Nucleic Acids Research **in press**.

Lieber, M. R. (2010). "The Mechanism of Double-Strand DNA Break Repair by the Nonhomologous DNA End-Joining Pathway." Annual Review of Biochemistry **79**: 1.1-1.31.

Lieber, M. R., U. Grawunder, *et al.* (1997). "Tying loose ends: roles of Ku and DNA-dependent protein kinase in the repair of double-strand breaks." Current Opinion in Genetics & Development **7**: 99-104.

Lieber, M. R. and T. E. Wilson (2010). "SnapShot: Nonhomologous DNA End Joining (NHEJ)." Cell **142**(3): 496-496.e491.

Lisby, M., J. H. Barlow, *et al.* (2004). "Choreography of the DNA Damage Response: Spatiotemporal Relationships among Checkpoint and Repair Proteins." Cell **118**: 699-713.

Llorente, B. and L. S. Symington (2004). "The Mre11 Nuclease Is Not Required for 5' to 3' Resection at Multiple HO-Induced Double-Strand Breaks." Molecular and Cellular Biology **24**(21): 9682-9694.

Lloyd, J., J. R. Chapman, *et al.* (2009). "A Supramodular FHA/BRCT-Repeat Architecture Mediates Nbs1 Adaptor Function in Response to DNA Damage." Cell **139**(1): 100-111.

Lou, Z., K. Minter-Dykhouse, *et al.* (2006). "MDC1 maintains genomic stability by participating in the amplification of ATM-dependent DNA damage signals." Molecular Cell **21**(2): 187-200.

Luo, C.-M., W. Tang, *et al.* (1996). "High frequency and error-prone DNA recombination in ataxia telangiectasia cell lines." Journal of Biological Chemistry **271**: 4497-4503.

Mahajan, K. N., S. A. N. McElhinny, *et al.* (2002). "Association of DNA Polymerase μ (pol μ) with Ku and Ligase IV: Role for pol μ in End-Joining Double-Strand Break Repair." Molecular and Cellular Biology **22**: 5194-5202.

Mari, P.-O., B. I. Florea, *et al.* (2006). "Dynamic assembly of end-joining complexes requires interaction between Ku70/80 and XRCC4." Proceedings of the National Academy of Sciences of the United States of America **103**(49): 18597-18602.

Maser, R. S., K. J. Monsen, *et al.* (1997). "hMre11 and hRad50 nuclear foci are induced during the normal cellular response to DNA double-strand breaks." Molecular and Cellular Biology **1997**: 6087-6096.

Matsuoka, S., G. Rotman, *et al.* (2000). "Ataxia telangiectasia-mutated phosphorylates chk2 in vivo and in vitro." Proceedings of the National Academy of Sciences of the United States of America **97**: 10389-10394.

Matsuura, S., H. Tauchi, *et al.* (1998). "Positional cloning of the gene for Nijmegen breakage syndrome." Nature Genetics **19**: 179-181.

Mazin, A. V., O. M. Mazina, *et al.* (2010). "Rad54, the motor of homologous recombination." DNA Repair **9**(3): 286-302.

McKinnon, P. J. (2004). "ATM and ataxia telangiectasia." EMBO Reports **5**: 772-776.

Meek, K., S. Gupta, *et al.* (2004). "The DNA-dependent protein kinase: the director at the end." Immunological Reviews **200**(1): 132-141.

Meldrum, R. A., S. W. Botchway, *et al.* (2003). "Nanoscale spatial induction of ultraviolet photoproducts in cellular DNA by three-photon near-infrared absorption." EMBO Reports **4**(12): 1144-1149.

Mimitou, E. P. and L. S. Symington (2008). "Sae2, Exo1 and Sgs1 collaborate in DNA double-strand break processing." Nature **455**(7214): 770-774.

Mimitou, E. P. and L. S. Symington (2009). "DNA end resection: Many nucleases make light work." DNA Repair **8**(9): 983-995.

Mimitou, E. P. and L. S. Symington (2009). "Nucleases and helicases take center stage in homologous recombination." Trends in Biochemical Sciences **34**(5): 264-272.

Mimitou, E. P. and L. S. Symington (2010). "Ku prevents Exo1 and Sgs1-dependent resection of DNA ends in the absence of a functional MRX complex or Sae2." EMBO Journal **29**(19): 3358-3369.

Mirzoeva, O. K. and J. H. J. Petrini (2001). "DNA damage-dependent nuclear dynamics of the Mre11 complex." Molecular and Cellular Biology **21**(1): 281-288.

Mirzoeva, O. K. and J. H. J. Petrini (2003). "DNA Replication-Dependent Nuclear Dynamics of the Mre11 Complex." Molecular and Cancer Research **1**: 207-218.

Mladenov, E. and G. Iliakis (2011). "Induction and Repair of DNA Double Strand Breaks: The Increasing Spectrum of Non-homologous End Joining Pathways." Mutation Research/Fundamental and Molecular Mechanisms of Mutagenesis **711**: 61-72.

Moreau, S., J. R. Ferguson, *et al.* (1999). "The nuclease activity of Mre11 is required for meiosis but not for mating type switching, end joining, or telomere maintenance." Molecular and Cellular Biology **19**: 556-566.

Moreno-Herrero, F., M. de Jager, *et al.* (2005). "Mesoscale conformational changes in the DNA-repair complex Rad50/Mre11/Nbs1 upon binding DNA." Nature **437**: 440-443.

Morrison, C., E. Sonoda, *et al.* (2000). "The controlling role of ATM in homologous recombinational repair of DNA damage." EMBO Journal **19**: 463-471.

Mortusewicz, O., J.-C. Ame, *et al.* (2007). "Feedback-regulated poly(ADP-ribosyl)ation by PARP-1 is required for rapid response to DNA damage in living cells." Nucleic Acids Research **35**(22): 7665-7675.

Mothersill, C. and C. Seymour (2006). "Radiation-Induced Bystander Effects: Evidence for an Adaptive Response to Low Dose Exposures?" Dose-Response **4**(4): 283-290.

Moynahan, M. E. and M. Jasin (2010). "Mitotic homologous recombination maintains genomic stability and suppresses tumorigenesis." Nature Reviews. Molecular Cell Biology **11**(3): 196-207.

Nagaraju, G., S. Odate, *et al.* (2006). "Differential Regulation of Short- and Long-Tract Gene Conversion between Sister Chromatids by Rad51C." Molecular and Cellular Biology **26**(21): 8075-8086.

Nakamura, A. J., V. A. Rao, *et al.* (2010). "The complexity of phosphorylated H2AX foci formation and DNA repair assembly at DNA double-strand breaks." Cell Cycle **9**(2): 389-397.

Nelms, B. E., R. S. Maser, *et al.* (1998). "In situ visualization of DNA double strand break repair in human fibroblasts." Science **280**: 590-593.

Niida, H. and M. Nakanishi (2006). "DNA damage checkpoints in mammals." Mutagenesis **21**(1): 3-9.

Nikjoo, H., D. E. Charlton, *et al.* (1994). "Monte Carlo Track Structure Studies of Energy Deposition and Calculation of Initial DSB and RBE." Advances in Space Research **14**(10): 10161-10180.

Nikjoo, H. and D. T. Goodhead (1991). "Track structure analysis illustrating the prominent role of low-energy electrons in radiobiological effects of low-LET radiations." Physics in Medicine and Biology **36**(2): 229-238.

Nimonkar, A. V., J. Genschel, *et al.* (2011). "BLM-DNA2-RPA-MRN and EXO1-BLM-RPA-MRN constitute two DNA end resection machineries for human DNA break repair." Genes & Development **25**(4): 350-362.

Niu, H., S. Raynard, *et al.* (2009). "Multiplicity of DNA end resection machineries in chromosome break repair." Genes & Development **23**(13): 1481-1486.

Nussenzweig, A., C. Chen, *et al.* (1996). "Requirement for Ku80 in growth and immunoglobulin V(D)J recombination." Nature **382**: 551-555.

O'Neill, T., A. J. Dwyer, *et al.* (2000). "Utilization of Oriented Peptide Libraries to Identify Substrate Motifs Selected by ATM." Journal of Biological Chemistry **275**(30): 22719-22727.

Okayasu, R., M. Okada, *et al.* (2006). "Repair of DNA Damage Induced by Accelerated Heavy Ions in Mammalian Cells Proficient and Deficient in the Non-homologous End-Joining Pathway." Radiation Research **165**: 59-67.

Olive, P. L. (1998). "The Role of DNA Single- and Double-Strand Breaks in Cell Killing by Ionizing Radiation." Radiation Research **150 (Suppl.)**: S42-S51.

Olive, P. L. and J. P. Banath (1993). "Detection of DNA double-strand breaks through the cell cycle after exposure to X-rays, bleomycin, etoposide and ^{125}IDUrd." International Journal of Radiation Biology **64**: 349-358.

Olsen, J. V., M. Vermeulen, *et al.* (2010). "Quantitative Phosphoproteomics Reveals Widespread Full Phosphorylation Site Occupancy During Mitosis." Science Signaling **3**(104): ra3.

Olson, E., C. J. Nievera, *et al.* (2007). "The Mre11 Complex Mediates the S-Phase Checkpoint through an Interaction with Replication Protein A." Molecular and Cellular Biology **27**(17): 6053-6067.

Otsuki, M., M. Seki, *et al.* (2007). "WRN counteracts the NHEJ pathway upon camptothecin exposure." Biochemical and Biophysical Research Communications **355**(2): 477-482.

Paap, B., D. M. Wilson III, *et al.* (2008). "Human abasic endonuclease action on multilesion abasic clusters: implications for radaition-induced biological damage." Nucleic Acids Research **36**(8): 2717-2727.

Pardo, B., B. Gómez-González, *et al.* (2009). "DNA double-strand break repair: how to fix a broken relationship." Cellular and Molecular Life Sciences **66**(6): 1039-1056.

Paull, T. T. and M. Gellert (1998). "The 3' to 5' exonuclease activity of Mre11 facilitates repair of DNA double-strand breaks." Molecular Cell **1**: 969-979.

Paull, T. T. and M. Gellert (1999). "Nbs1 potentiates ATP-driven DNA unwinding and endonuclease cleavage by the Mre11/Rad50 complex." Genes & Development **13**: 1276-1288.

Paull, T. T., E. P. Rogakou, *et al.* (2000). "A critical role for histone H2AX in recruitment of repair factors to nuclear foci after DNA damage." Current Biology **10**: 886-895.

Perrault, R., H. Wang, *et al.* (2004). "Backup Pathways of NHEJ Are Suppressed by DNA-PK." Journal of Cellular Biochemistry **92**: 781-794.

Petrini, J. H. (2000). "The Mre11 complex and ATM: collaborating to navigate S phase." Current Opinion in Cell Biology **12**: 293-296.

Petrini, J. H. J. and T. H. Stracker (2003). "The cellular response to DNA double-strand breaks: defining the sensors and mediators." Trends in Cell Biology **13**: 458-462.

Pierce, A. J., P. Hu, *et al.* (2001). "Ku DNA end-binding protein modulates homologous repair of double-strand breaks in mammalian cells." Genes & Development **15**: 3237-3242.

Pierce, A. J., R. D. Johnson, *et al.* (1999). "XRCC3 promotes homology-directed repair of DNA damage in mammalian cells." Genes & Development **13**: 2633-2638.

Pierce, A. J., J. M. Stark, *et al.* (2001). "Double-strand breaks and tumorigenesis." Trends in Cell Biology **11**: S52-S59.

Rahal, E. A., L. A. Henricksen, *et al.* (2010). "ATM regulates Mre11-dependent DNA end-degradation and microhomology-mediated end joining." Cell Cycle **9**(14): 2866-2877.

Rai, R., H. Zheng, *et al.* (2010). "The function of classical and alternative non-homologous end-joining pathways in the fusion of dysfunctional telomeres." EMBO Journal **29**(15): 2598-2610.

Rass, E., A. Grabarz, *et al.* (2009). "Role of Mre11 in chromosomal nonhomologous end joining in mammalian cells." Nature Structural & Molecular Biology **16**(8): 819-825.

Riballo, E., M. Kühne, *et al.* (2004). "A pathway of double-strand break rejoining dependent upon ATM, artemis, and proteins locating to γ-H2AX foci." Molecular Cell **16**: 715-724.

Rich, T., R. L. Allen, *et al.* (2000). "Defying death after DNA damage." Nature **407**: 777-783.

Richardson, C., N. Horikoshi, *et al.* (2004). "The role of the DNA double-strand break response network in meiosis." DNA Repair **3**: 1149-1164.

Richardson, C., M. E. Moynahan, *et al.* (1998). "Double-strand break repair by interchromosomal recombination: suppression of chromosomal translocations." Genes & Development **12**: 3831-3842.

Robert, I., F. Dantzer, *et al.* (2009). "Parp1 facilitates alternative NHEJ, whereas Parp2 suppresses IgH/c-myc translocations during immunoglobulin class switch recombination." Journal of Experimental Medicine **206**(5): 1047-1056.

Robison, J. G., K. Dixon, *et al.* (2007). "Cell Cycle-and Proteasome-Dependent Formation of Etoposide-Induced Replication Protein A (RPA) or Mre11/Rad50/Nbs1 (MRN) Complex Repair Foci." Cell Cycle **6**(19): 2399-2407.

Rogakou, E. P., C. Boon, *et al.* (1999). "Megabase chromatin domains involved in DNA double-strand breaks *in vivo*." Journal of Cell Biology **146**: 905-915.

Rogakou, E. P., D. R. Pilch, *et al.* (1998). "DNA double-stranded breaks induce histone H2AX phosphorylation on serine 139." Journal of Biological Chemistry **273**: 5858-5868.

Rosidi, B., M. Wang, *et al.* (2008). "Histone H1 functions as a stimulatory factor in backup pathways of NHEJ." Nucleic Acids Research **36**(5): 1610-1623.

Rothkamm, K., I. Krüger, *et al.* (2003). "Pathways of DNA Double-Strand Break Repair during the Mammalian Cell Cycle." Molecular and Cellular Biology **23**: 5706-5715.

Rothkamm, K. and M. Löbrich (2003). "Evidence of a lack of DNA double-strand break repair in human cells exposed to very low X-ray doses." Proceedings of the National Academy of Sciences of the United States of America **100**: 5057-5062.

Rupnik, A., N. Lowndes, *et al.* (2009). "MRN and the race to the break." Chromosoma **in press**: doi:10.1007/s00412-00009-00242-00414.

Rupnik, A., N. Lowndes, *et al.* (2010). "MRN and the race to the break." Chromosoma **119**(2): 115-135.

Rydberg, B. (1996). "Clusters of DNA damage induced by ionizing radiation: Formation of short DNA fragments. 11. Experimental detection." Radiation Research **145**: 200-209.

Rydberg, B. (2001). "Radiation-induced DNA Damage and Chromatin Structure." Acta Oncologica **40**: 682-685.

Saidi, A., T. Li, *et al.* (2010). "Dual Functions of Nbs1 in the Repair of DNA Breaks and Proliferation Ensure Proper V(D)J Recombination and T-Cell Development." Molecular and Cellular Biology **30**(23): 5572-5581.

Sallmyr, A., A. E. Tomkinson, *et al.* (2008). "Up-regulation of WRN and DNA ligase IIIα in chronic myeloid leukemia: consequences for the repair of DNA double-strand breaks." Blood **112**(4): 1413-1423.

San Filippo, J., P. Sung, *et al.* (2008). "Mechanism of Eukaryotic Homologous Recombination." Annual Review of Biochemistry **77**: 229-257.

Sancar, A., L. A. Lindsey-Boltz, *et al.* (2004). "Molecular Mechanisms of Mammalian DNA Repair and the DNA Damage Checkpoints." Annual Review of Biochemistry **73**: 39-85.

Sartori, A. A., C. Lukas, *et al.* (2007). "Human CtIP promotes DNA end resection." Nature **450**: 509-514.

Schaetzlein, S., N. R. Kodandaramireddy, *et al.* (2007). "Exonuclease-1 Deletion Impairs DNA Damage Signaling and Prolongs Lifespan of Telomere-Dysfunctional Mice." Cell **130**(5): 863-877.

Sedelnikova, O., I. Horikawa, *et al.* (2004). "Senescing human cells and ageing mice accumulate DNA lesions with unrepairable double-strand breaks." Nature Cell Biology **6**(2): 168-170.

Sedelnikova, O. A., E. P. Rogakou, *et al.* (2002). "Quantitative detection of ^{125}IdU-induced DNA double-strand breaks with γ-H2AX antibody." Radiation Research **158**: 486-492.

Sherr, C. J. and J. M. Roberts (1995). "Inhibitors of mammalian G1 cyclin-dependent kinases. (Review)." Genes & Development **9**: 1149-1163.

Shiloh, Y. (2003). "ATM and related protein kinases: Safeguarding genome integrity." Nature Reviews. Cancer **3**: 155-168.

Shiloh, Y. and M. B. Kastan (2001). ATM: Genome stability, neuronal development, and cancer cross paths. Advances in Cancer Research, Academic Press. **Volume 83:** 209-254.

Shiloh, Y. and A. R. Lehmann (2004). "Maintaining integrity." Nature Cell Biology **6**: 923-928.

Shin, D. S., C. Chahwan, *et al.* (2004). "Structure and function of the double-strand break repair machinery." DNA Repair **3**: 863-873.

Shiotani, B. and L. Zou (2009). "Single-Stranded DNA Orchestrates an ATM-to-ATR Switch at DNA Breaks." Molecular Cell **33**(5): 547-558.

Shrivastav, M., C. A. Miller, *et al.* (2009). "DNA-PKcs and ATM co-regulate DNA double-strand break repair." DNA Repair **8**(8): 920-929.

Singh, S. K., W. Wu, *et al.* (2009). "Extensive Repair of DNA Double-Strand Breaks in Cells Deficient in the DNA-PK Dependent Pathway of NHEJ after Exclusion of Heat-Labile Sites." Radiation Research **172**: 152-164.

Smits, V. A. J., P. M. Reaper, *et al.* (2006). "Rapid PIKK-Dependent Release of Chk1 from Chromatin Promotes the DNA-Damage Checkpoint Response." Current Biology **16**(2): 150-159.

Sorensen, C. S., L. T. Hansen, *et al.* (2005). "The cell-cycle checkpoint kinase Chk1 is required for mammalian homologous recombination repair." Nature Cell Biology **7**: 195-201.

Soulas-Sprauel, P., G. Le Guyader, *et al.* (2007). "Role for DNA repair factor XRCC4 in immunoglobulin class switch recombination." Journal of Experimental Medicine **204**(7): 1717-1727.

Stamato, T. D. and N. Denko (1990). "Asymmetric field inversion gel electrophoresis: A new method for detecting DNA double-strand breaks in mammalian cells." Radiation Research **121**: 196-205.

Stenerlöw, B., E. Höglund, *et al.* (2000). "Rejoining of DNA fragments produced by radiations of different linear energy transfer." International Journal of Radiation Biology **76**(4): 549-557.

Stewart, G. S., R. S. Maser, *et al.* (1999). "The DNA double-strand break repair gene hMRE11 is mutated in individuals with an ataxia-telangiectasia-like disorder." Cell **99**(6): 577-587.

Stiff, T., M. O'Driscoll, *et al.* (2004). "ATM and DNA-PK function redundantly to phosphorylate H2AX after exposure to ionizing radiation." Cancer Research **64**: 2390-2396.

Stracker, T. H., M. Morales, *et al.* (2007). "The carboxy terminus of NBS1 is requireds for induction of apoptosis by the MRE11 complex." Nature **447**: 218-221.

Stucki, M., J. A. Clapperton, *et al.* (2005). "MDC1 directly binds phosphorylated histone H2AX to regulate cellular responses to DNA double-strand breaks." Cell **123**: 1213-1226.

Sutherland, B. M., P. V. Bennett, *et al.* (2000). "Clustered DNA damages induced in isolated DNA and in human cells by low doses of ionizing radiation." Proceedings of the National Academy of Sciences of the United States of America **97**: 103-108.

Sutherland, R. M., P. V. Bennett, *et al.* (2002). "Clustered DNA Damages Induced by X Rays in Human Cells." Radiation Research **157**: 611-616.

Sy, S. M. H., M. S. Y. Huen, *et al.* (2009). "PALB2 is an integral component of the BRCA complex required for homologous recombination repair." Proceedings of the National Academy of Sciences of the United States of America **106**: 7155-7160.

Symington, L. S. (2002). "Role of Rad52 epistasis group genes in homologous recombination and double-strand break repair." Microbiology and Molecular Biology Reviews:MMBR **66**: 630-670.

Takahashi, A., E. Mori, *et al.* (2010). "The Foci of DNA Double Strand Break-recognition Proteins Localize with γH2AX after Heat Treatment." Journal of Radiation Research **51**: 91-95.

Takeda, S., K. Nakamura, *et al.* (2007). "Ctp1/CtIP and the MRN Complex Collaborate in the Initial Steps of Homologous Recombination." Molecular Cell **28**(3): 351-352.

Tanaka, T., X. Huang, *et al.* (2007). "ATM activation accompanies histone H2AX phosphorylation in A549 cells upon exposure to tobacco smoke." BMC Cell Biology **8**: 26.

Tauchi, H., J. Kobayashi, *et al.* (2001). "The Forkhead-associated Domain of NBS1 Is Essential for Nuclear Foci Formation after Irradiation but Not Essential for hRAD50·hMRE11·NBS1 Complex DNA Repair Activity." Journal of Biological Chemistry **276**(1): 12-15.

Tauchi, H., J. Kobayashi, *et al.* (2002). "Nbs1 is essential for DNA repair by homologous recombination in higher vertebrate cells." Nature **420**: 93-98.

Tauchi, H., S. Matsuura, *et al.* (2002). "Nijmegen breakage syndrome gene, NBS1, and molecular links to factors for genome stability." Oncogene **21**: 8967-8980.

Taylor, A. M., A. Grom, *et al.* (2004). "Ataxia-telangiectasia-like disorder (ATLD) - its clinical presentation and molecular basis." DNA Repair **3**: 1219-1225.

Taylor, E. M., S. M. Cecillon, *et al.* (2009). "The Mre11/Rad50/Nbs1 complex functions in resection-based DNA end joining in Xenopus laevis." Nucleic Acids Research **in press**: gkp905.

Taylor, E. M., S. M. Cecillon, *et al.* (2010). "The Mre11/Rad50/Nbs1 complex functions in resection-based DNA end joining in Xenopus laevis." Nucleic Acids Research **38**(2): 441-454.

Terato, H. and H. Ide (2004). "Clustered DNA damage induced by heavy ion particles." Biological Sciences in Space **18**(4): 206-215.

Thompson, L. H. and D. Schild (2002). "Recombinational DNA repair and human disease." Mutation Research **509**: 49-78.

Tibbetts, R. S., D. Cortez, *et al.* (2000). "Functional interactions between BRCA1 and the checkpoint kinase ATR during genotoxic stress." Genes & Development **14**(23): 2989-3002.

Tittel-Elmer, M., C. Alabert, *et al.* (2009). "The MRX complex stabilizes the replisome independently of the S phase checkpoint during replication stress." EMBO Journal **28**: 1142-1156.

Tommiska, J., S. Seal, *et al.* (2006). "Evaluation of *RAD50* in familial breast cancer predisposition." International Journal of Cancer **118**(11): 2911-2916.

Uchisaka, N., N. Takahashi, *et al.* (2009). "Two Brothers with Ataxia-Telangiectasia-like Disorder with Lung Adenocarcinoma." Journal of Pediatrics **155**: 435-438.

Ünsal-Kacmaz, K., A. M. Makhov, *et al.* (2002). "Preferential binding of ATR protein to UV-damaged DNA." Proceedings of the National Academy of Sciences of the United States of America **99**: 6673-6678.

Uziel, T., Y. Lerenthal, *et al.* (2003). "Requirement of the MRN complex for ATM activation by DNA damage." EMBO Journal **22**: 5612-5621.

Valerie, K. and L. F. Povirk (2003). "Regulation and mechanisms of mammalian double-strand break repair." Oncogene **22**: 5792-5812.

van den Bosch, M., R. T. Bree, *et al.* (2003). "The MRN complex: coordinating and mediating the response to broken chromosomes." EMBO Reports **4**(9): 844-849.

van der Linden, E., H. Sanchez, *et al.* (2009). "RAD50 and NBS1 form a stable complex functional in DNA binding and tethering." Nucleic Acids Research **37**(5): 1580-1588.

van Gent, D. C., J. H. J. Hoeijmakers, *et al.* (2001). "Chromosomal stability and the DNA double-stranded break connection." Nature Reviews. Genetics **2**: 196-206.

van Veelen, L. R., T. Cervelli, *et al.* (2005). "Analysis of ionizing radiation-induced foci of DNA damage repair proteins." Mutation Research **574**: 22-33.

Varon, R., C. Vissinga, *et al.* (1998). "Nibrin, a novel DNA double-strand break repair protein, is mutated in Nijmegen breakage syndrome." Cell **93**: 467-476.

Virsik-Köpp, P., M. Rave-Fränk, *et al.* (2003). "Role of DNA-PK in the process of aberration formation as studied in irradiated human glioblastoma cell lines M059K and M059J." International Journal of Radiation Biology **79**: 61-68.

Walker, J. R., R. A. Corpina, *et al.* (2001). "Structure of the Ku heterodimer bound to DNA and its implications for double-strand break repair." Nature **412**: 607-614.

Waltes, R., R. Kalb, *et al.* (2009). "Human RAD50 Deficiency in a Nijmegen Breakage Syndrome-like Disorder." American Journal of Human Genetics **84**: 605-616.

Wang, H., J. Guan, *et al.* (2001). "Replication Protein A2 Phosphorylation after DNA Damage by the Coordinated Action of Ataxia Telangiectasia-Mutated and DNA-dependent Protein Kinase." Cancer Research **61**: 8554-8563.

Wang, H., A. R. Perrault, *et al.* (2003). "Biochemical evidence for Ku-independent backup pathways of NHEJ." Nucleic Acids Research **31**: 5377-5388.

Wang, H., B. Rosidi, *et al.* (2005). "DNA Ligase III as a Candidate Component of Backup Pathways of Nonhomologous End Joining." Cancer Research **65**(10): 4020-4030.

Wang, H., X. Wang, *et al.* (2008). "The Ku-dependent non-homologous end-joining but not other repair pathway is inhibited by high linear energy transfer ionizing radiation." DNA Repair **7**(5): 725-733.

Wang, H., Z.-C. Zeng, *et al.* (2001). "Efficient rejoining of radiation-induced DNA double-strand breaks in vertebrate cells deficient in genes of the RAD52 epistasis group." Oncogene **20**: 2212-2224.

Wang, H., X. Zhang, *et al.* (2010). "Characteristics of DNA-binding proteins determine the biological sensitivity to high-linear energy transfer radiation." Nucleic Acids Research **38**(10): 3245-3251.

Wang, H., Z. Zhao-Chong, *et al.* (2001). "Genetic evidence for the involvement of DNA ligase IV in the DNA-PK-dependent pathway of non-homologous end joining in mammalian cells." Nucleic Acids Research **29**: 1653-1660.

Wang, M., W. Wu, *et al.* (2006). "PARP-1 and Ku compete for repair of DNA double strand breaks by distinct NHEJ pathways." Nucleic Acids Research **34**(21): 6170-6182.

Ward, J. F. (1988). "DNA damage produced by ionizing radiation in mammalian cells: Identities, mechanisms of formation, and reparability." Progress in Nucleic Acid Research **35**: 95-125.

Ward, J. F. (1990). "The yield of DNA double-strand breaks produced intracellularly by ionizing radiation: a review." International Journal of Radiation Biology **57**: 1141-1150.

Weaver, D. T. (1995). "V(D)J recombination and double-strand break repair." Advances in Immunology **58**: 29-85.

West, S. C. (2003). "Molecular views of recombination proteins and their control." Nature Reviews. Molecular Cell Biology **4**: 1-11.

Weterings, E. and D. J. Chen (2008). "The endless tale of non-homologous end-joining." Cell Research **18**(1): 114-124.

Whalen, M. K., S. K. Gurai, *et al.* (2008). "Specific ATM-Mediated Phosphorylation Dependent on Radiation Quality." Radiation Research **170**: 353-364.

Wilhelm, S., B. Gröbler, *et al.* (2009). Confocal Laser Scanning Microscopy. Microscopy from Carl Zeiss.

Williams, G. J., S. P. Lees-Miller, *et al.* (2010). "Mre11-Rad50-Nbs1 conformations and the control of sensing, signaling, and effector responses at DNA double-strand breaks." DNA Repair **9**(12): 1299-1306.

Williams, R. S., G. Moncalian, *et al.* (2008). "Mre11 Dimers Coordinate DNA End Bridging and Nuclease Processing in Double-Strand-Break Repair." Cell **135**(1): 97-109.

Williams, R. S., J. S. Williams, *et al.* (2007). "Mre11-Rad50-Nbs1 is a keystone complex connecting DNA repair machinery, double-strand break signaling, and the chromatin template." Biochemistry and Cell Biology **85**: 509-520.

Windhofer, F., W. Wu, *et al.* (2007). "Marked dependence on growth state of backup pathways of NHEJ." International Journal of Radiation Oncology Biology Physics **68**(5): 1462-1470.

Wold, M. S. (1997). "Replication Protein A: A heterotrimeric, single-stranded DNA-binding protein required for eukaryotic DNA metabolism." Annual Review of Biochemistry **66**: 61-92.

Wu, D., L. M. Topper, *et al.* (2008). "Recruitment and Dissociation of Nonhomologous End Joining Proteins at a DNA Double-Strand Break in Saccharomyces cerevisiae." Genetics **178**(3): 1237-1249.

Wu, P.-Y., P. Frit, *et al.* (2007). "Interplay between Cernunnos-XLF and Nonhomologous End-joining Proteins at DNA Ends in the Cell." Journal of Biological Chemistry **282**(44): 31937-31943.

Wu, W., M. Wang, *et al.* (2008). "Repair of radiation induced DNA double strand breaks by backup NHEJ is enhanced in G2." DNA Repair **7**(2): 329-338.

Xie, A., A. Kwok, *et al.* (2009). "Role of mammalian Mre11 in classical and alternative nonhomologous end joining." Nature Structural & Molecular Biology **16**(8): 814-818.

Yajima, H., K.-J. Lee, *et al.* (2006). "ATR-Dependent Phosphorylation of DNA-Dependent Protein Kinase Catalytic Subunit in Response to UV-Induced Replication Stress." Molecular and Cellular Biology **26**(20): 7520-7528.

Yamaguchi-Iwai, Y., E. Sonoda, *et al.* (1999). "Mre11 is essential for the maintenance of chromosomal DNA in vertebrate cells." EMBO Journal **18**(23): 6619-6629.

Yan, C. T., C. Boboila, *et al.* (2007). "IgH class switching and translocations use a robust non-classical end-joining pathway." Nature **449**: 478-482.

Yang, J., Y. Yu, *et al.* (2003). "ATM, ATR and DNA-PK: initiators of the cellular genotoxic stress responses." Carcinogenesis **24**: 1571-1580.

Yang, Y.-G., A. Saidi, *et al.* (2006). "Conditional deletion of Nbs1 in murine cells reveals its role in branching repair pathways of DNA double-strand breaks." EMBO Journal **25**: 5527-5538.

You, Z. and J. M. Bailis (2010). "DNA damage and decisions: CtIP coordinates DNA repair and cell cycle checkpoints." Trends in Cell Biology **20**(7): 402-409.

You, Z., J. M. Bailis, *et al.* (2007). "Rapid activation of ATM on DNA flanking double-strand breaks." Nature Cell Biology **9**(11): 1311-1318.

Young, D. B., J. Jonnalagadda, *et al.* (2005). "Identification of Domains of Ataxia-telangiectasia Mutated Required for Nuclear Localization and Chromatin Association." Journal of Biological Chemistry **280**(30): 27587-27594.

Yu, Y., B. L. Mahaney, *et al.* (2008). "DNA-PK and ATM phosphorylation sites in XLF/Cernunnos are not required for repair of DNA double strand breaks." DNA Repair **7**(10): 1680-1692.

Yuan, J. and J. Chen (2010). "MRE11-RAD50-NBS1 Complex Dictates DNA Repair Independent of H2AX." Journal of Biological Chemistry **285**(2): 1097-1104.

Yuan, S.-S. F., H.-L. Chang, *et al.* (2003). "Ionizing radiation-induced Rad51 nuclear focus formation is cell cycle-regulated and defective in both $ATM^{-/-}$ and $c\text{-}Abl^{-/-}$ cells." Mutation Research **525**: 85-92.

Yun, M. H. and K. Hiom (2009). "CtIP-BRCA1 modulates the choice of DNA double-strand-break repair pathway throughout the cell cycle." Nature **459**(7245): 460-463.

Zhao, S., W. Renthal, *et al.* (2002). "Functional analysis of FHA and BRCT domains of NBS1 in chromatin association and DNA damage responses." Nucleic Acids Research **30**(22): 4815-4822.

Zhou, B. B. and S. J. Elledge (2000). "The DNA damage response: putting checkpoints in perspective." Nature **408**: 433-439.

Zhu, Z., W.-H. Chung, *et al.* (2008). "Sgs1 Helicase and Two Nucleases Dna2 and Exo1 Resect DNA Double-Strand Break Ends." Cell **134**(6): 981-994.

Zhuang, J., G. Jiang, *et al.* (2009). "Exonuclease Function of Human Mre11 Promotes Deletional Nonhomologous End Joining." Journal of Biological Chemistry **284**(44): 30565-30573.

Declaration

Erklärung:

Hiermit erkläre ich, gem. § 6 Abs. (2) f) der Promotionsordnung der Fakultäten für Biologie, Chemie und Mathematik zur Erlangung des Dr. *rer. nat.*, dass ich das Arbeitsgebiet, dem das Thema *„Functions of the MRE11-RAD50-NBS1 complex in DNA double strand break repair“* zuzuordnen ist, in Forschung und Lehre vertrete und den Antrag von Frau Swetlana Konkow befürworte und die Betreuung, auch im Falle eines Weggangs, wenn nicht wichtige Gründe dem entgegenstehen, weiterführen werde.

Essen, _____ _____

Unterschrift eines Mitglieds der Universität Duisburg-Essen

Erklärung:

Hiermit erkläre ich, gem. § 7 Abs. (2) c) + e) der Promotionsordnung der Fakultäten für Biologie, Chemie und Mathematik zur Erlangung des Dr. *rer. nat.*, dass ich die vorliegende Dissertation selbständig verfasst und mich keiner anderen, als der angegebenen Hilfsmittel, bedient habe.

Essen, _____ _____

Unterschrift der Doktorandin

Erklärung:

Hiermit erkläre ich, gem. § 7 Abs. (2) d) + f) der Promotionsordnung der Fakultäten für Biologie, Chemie und Mathematik zur Erlangung des Dr. *rer. nat.*, dass ich keine anderen Promotionen bzw. Promotionsversuche in der Vergangenheit durchgeführt habe und dass diese Arbeit von keiner anderen Fakultät/Fachbereich abgelehnt worden ist.

Essen, _____ _____

Unterschrift der Doktorandin

The biography is not included in the online version for reasons of data protection

The biography is not included in the online version for reasons of data protection

The biography is not included in the online version for reasons of data protection

The biography is not included in the online version for reasons of data protection